EFFECTIVENESS FACTORS

AND PARAMETER IDENTIFICATION

MODELLING MICROBIAL GROWTH IN BIOREACTORS: EFFECTIVENESS FACTORS IN BIOFILMS AND BIOFLOCS, AND PARAMETER IDENTIFICATION FOR THE ANDREWS MODEL

By

JIACHENG SHEN, M.Sc.

A Thesis

Submitted to the School of Graduate Studies

In Partial Fulfilment of the Requirements

For the Degree

Master of Science

McMaster University

MASTER OF SCIENCE (2005) McMaster University

(Chemical Engineering) Hamilton, Ontario

TITLE: Modeling Microbial Growth in Bioreactors: Effectiveness Factors in Biofilms and Bioflocs, and Parameter Identification for the Andrews Model

AUTHOR: Jiacheng Shen, M.Sc. (University of Ottawa)

SUPERVISOR: Professor Carlos Filipe

NUMBER OF PAGES: XIV, 84

ABSTRACT

A novel mathematical model has been developed for biofilms and bioflocs. The model is based on the use of the effectiveness factor and the effect of cell density is included. The key assumption in the model is that cell density decreases in proportion to the substrate concentration within the biofilm or biofloc, reflecting lower rates of cellular metabolism. The equations given by the model were solved numerically for three types of reaction kinetics: Monod, Andrews (substrate inhibition), and multiple-Monod (two-limiting substrates), as well as for two geometries: a slab, as a representation of a biofilm and a sphere, as a representation of a biofloc. The simulations indicate that a decrease of the cell density in the biofilm and biofloc results in a decline of the effectiveness factor. Furthermore, the analytical solutions and approximate analytical versions of the effectiveness factor for the biofilm in two cell growth models: Monod and Andrews, have been derived. The effectiveness factors derived analytically are in agreement with those calculated numerically, and the approximate analytical versions are valid for the Thiele modulus greater than five. This new model was tested using operational data available in the literature, by including the effectiveness factor as a part of the design equations for an upflow anaerobic sludge blanket (UASB) reactor.

For any biologically mediated transformation, it is critical to uniquely identify the parameters associated with microbial growth models. In this study, it is proved that the parameters of the integrated Andrews model are identifiable if the experimental data does not contain any random noise based on a criterion proposed by Beck and Arnold [1977]. When noise is present, the parameters may or may not be identifiable, depending on noise levels. A new approach has been developed based on the calculation of dimensionless

sensitivity coefficients. Plotting these coefficients provides straightforward visualization of parameter identification. This method was used for quantitative evaluation of the noise level that can be associated with measurements, while still allowing parameter identification. It was demonstrated that an indirect cause of the parameter non-identification of the integrated Andrews model is the linearization of the Andrews model at a low or high substrate concentration. Robinson [1985] obtained a similar result with the Monod model.

TABLE OF CONTENTS

LIST OF FIGURES

LIST OF TABLES

NOMENCLATURE

Symbols

A cross section area of UASB

A_p surface area of the particle

C_i constant.

D_e effective diffusivity of substrate in the interior of particle

D_f phenol diffusivity

E allowed noisy level

F_S mass flow rate of substrate

K_I inhibition coefficient

K_M Michaelis constant

K_O oxygen saturation coefficient.

K_S saturation coefficient

K_{S1} substrate 1 saturation coefficient

K_{S2} substrate 2 saturation coefficient

k ratio of the maximum specific growth rate and yield coefficient

n number of replicated tests

O oxygen concentration in the bulk solution

p changed parameter value or model parameter

p_0 basic parameter value

Q volumetric flow rate

R linear correlation coefficient

R_p actual reaction rate expression for granular particles

R_s rate evaluated at outer surface conditions or reaction rate on the external surface of particles

r distance from the biofilm surface of supporting wall or the center of biofloc to a reaction site

r_m the maximum rate constant.

r_0 thickness of the biofilm or the radius of the biofloc

S substrate concentration

S_0 substrate concentration on the surface of bioparticles at the initial time

SC sensitivity coefficient at any time t

S^*_c dimensionless concentration on the biofilm surface of supporting wall and the center of the biofloc

SCM the maximum sensitivity coefficient in a variable range

S_e phenol concentration at the exit of the UASB

t retention time

t_m the maximum retention time.

u flow rate

V volume of the UASB

V_p surface volume of the particle

X_0 biomass density at the initial time

z height from the bottom of the UASB

Greek Symbols

η effectiveness factor

ϕ_l Thiele modulus for slab

ϕ_s Thiele modulus for sphere

μ_{av} average specific growth rate predicted by n replicated parameter sets

μ_m the maximum specific growth rate

Subscripts

ar arithmetic mean value for n experiments

i a replicated parameter estimate or the i-th experiment

P PRAMUS value

scm the maximum dimensionless sensitivity coefficient

μ the maximum specific growth rate

S saturation coefficient

I inhibition coefficient

Y yield coefficient

1 time t_1

2 time t_2,

Superscripts

* dimensionless quantity

' a different parameter at a constant time

ACKNOWLEGMENTS

I would like to express my deep gratitude to my supervisor Dr. Carlos Filipe, and my pre-supervisor Dr. Lisa Crossley, for their support, guidance and financial assistance throughout this project.

I would also like to express my gratitude to my colleagues Sherry Xie and Xin Ge for their help in the laboratory.

My sincere thanks to the research and technical staffs of the Department of Chemical Engineering: Dr. Xin Li, Doug Keller, and Gord Slater, for their technical assistance during the experiments.

Chapter One

Introduction

The effectiveness factor is an important concept in catalytic reaction engineering. It is used to estimate the efficiency of catalysts in chemical reactions and as a design parameter for solid-liquid reactors. The effectiveness factor is also applied to biochemical engineering in two areas: the immobilization enzyme and the immobilization cell [Shuler and Kargi, 2002]. In the former, the rate expressions in equations (2.4) and (2.5) (in Chapter 2) are represented by a Michaelis-Menten type kinetic equation. The original Michaelis-Menten equation is

$$R_s = \frac{r_m S}{K_M + S} \tag{1.1}$$

where R_s is the reaction rate on the external surface of particles, r_m is the maximum rate constant, and K_M is the Michaelis constant. Many researchers have calculated the effectiveness factor under Michaelis-Menten type kinetic equations. Moo-Young and Kobayaashi [1972] investigated the effectiveness factor of slab particles under various Michaelis-Menten type equations, including substrate inhibition and product inhibition for immobilization enzymes, and presented some typical graphs. Fink et al. [1973] presented a general numerical procedure to obtain the substrate concentration profile and effectiveness factor using a transformation method, and obtained generalized effectiveness factor charts. Chang [1982] suggested a numerical method for calculating the effectiveness factor for Michaelis-Menten type kinetics with high Thiele moduli, which represents the relative influence of reaction rate and intraparticle diffusion. Cano

and Cabanes [1994] made a generalized analysis of the effectiveness factor for immobilization enzyme in multi-enzyme reactions.

In the case of the immobilization cell, the earliest research was done by Atkinson and co-workers [1974]. They used both a numerical method and approximately analytic solution to compute the effectiveness factor in biofilms (slabs). Later [1978] they extended this method to bioflocs (spheres). Recently, Gheewala and Annachhatre [2003] studied more cases of Monod type equations with various conditions, such as substrate inhibition, secondary substrate inhibition, and product inhibition in biofilms. In these studies the Monod type equations replaced the Michaelis-Menten type equations in the rate expression. The Monod equation for the substrate reaction rate is

$$R_s = \frac{\mu_m S X}{Y_{X/S}(K_S + S)} \tag{1.2}$$

where $Y_{X/S}$ is the growth yield coefficient, X is the cell density, μ_m is the maximum specific growth rate coefficient, and K_S is the saturation coefficient. Note that there are two additional parameters $Y_{X/S}$ and X in equation (1.2) compared to equation (1.1). Generally, both parameters are considered constant, and are incorporated into the Thiele modulus, as the above researchers did. Therefore, in principle, all the methods used for the immobilized enzymes can be used for the immobilized cells. However, the difference between microbial and enzymatic reactions is that the number of microbial cells changes during the reaction process. Cells in biofilms and bioflocs rely on provision of substrates in a medium solution to maintain their life processes. At a steady state the cell density in biofilms and bioflocs depends on the growth-limiting substrate concentration in the medium solution. The lower the substrate concentration, the lower the cell density in biofilms and bioflocs. If no nutrient is provided, cells will gradually die once the nutrients

from the endogenous metabolism of the cells themselves are used up. When the substrate diffuses into the interior of biofilms and bioflocs, its concentration will decrease along the diffusion route, because of the cells' metabolism and mass transfer resistance. Therefore, the cell density of a biofilm or biofloc should also decrease with diffusion distance of the substrate. In particular, when the substrate in a biofilm or biofloc has a lower diffusivity and the cells have a faster reaction rate, *i.e.* a larger Thiele modulus, the substrate will be entirely consumed before it reaches the biofilm surface on the supporting wall or the center of the biofloc. Consequently, there are no living cells near the surface of a biofilm or the center of a biofloc. If the cell density is assumed to be constant in the entire biofilm thickness or biofloc radius as previous researchers did, it would change sharply from a constant to zero at a point of the interior of the biofilm or biofloc, respectively, at a large Thiele modulus. Such a situation is obviously impossible. A true profile of cell density in a biofilm or biofloc would be a smooth transition from an initial value at the bioparticle surface to zero in the interior.

For a rigorous description of bioprocesses, it is crucial to uniquely identify the parameters associated with microbial growth in the models commonly used to describe the relationship between the substrate concentration and the specific growth rate of microorganisms: the Monod and Andrews models. Both these models are nonlinear not only with respect to variation of growth-limiting substrate, but also with respect to the parameters: the maximum specific growth rate μ_m, the saturation coefficient K_S, and the inhibition coefficient K_I, because their sensitivity coefficients (*i.e.* first partial derivatives with respect to the parameters) involve two or more parameters [Robinson, 1985]. Nonlinear parameter estimation (NPE) deals in part with the estimation of parameters of

nonlinear equations. Holmberg [1982] proved that the parameters K_S and μ_m of the Monod model can be identified theoretically when the substrate and biomass concentrations are positive. However, he also pointed out that in practice both parameters cannot be determined with sufficient accuracy in situations with few and noise measurements. Robison and Tiedje [1983] studied the parameter identification of the Monod growth model using nonlinear least-square analysis. When the initial substrate concentration was in the mixed-order region, nonlinear estimation of simulated data sets containing known measurement errors provided accurate estimates of the μ_m, K_S, and $Y_{X/S}$ values. However, Robinson [1985] indicated that in the first order region the parameters V_{max} and K_m in the Michaelis-Menten model (equivalent to μ_m and K_S in the Monod model, respectively) are not estimated uniquely. Ellis et al. [1996] investigated the parameter identification of the Monod and Andrews models at various ratios of S_0/K_S, S_0/K_I, and K_S/K_I (S_0 is the initial substrate concentration). The lower the ratios of S_0/K_S and K_S/K_I, and the higher the ratio of S_0/K_I, the more difficult the identification of the parameters K_S, K_I, and K_I. Seagran et al. [2003] analyzed parameter identification in the Andrews model with variation of the biomass quantity, using visual inspection of the sensitivity equations. Their analysis showed that it was very difficult to simultaneously obtain a unique set of estimates of intrinsic kinetic parameters for the Andrews model using data from a single batch experiment. Berthouex and Brown [1994] concluded that it was impossible to estimate the parameters of the Monod and Andrews models independently as the parameters were correlated. However, experimental conditions could be selected to yield the greatest degree of independence among the parameters (Robinson, 1985; Ellis et al., 1996).

Our objectives in this study were:

1. To develop models of the effectiveness factor of biofilms and bioflocs, including the effect of cell density in the cases of various Monod type equations, to estimate the effectiveness factor in these cases under varying parameter values, and to compare the effects of the effectiveness factor on water quality in the effluent flow using the design equations of an upflow anaerobic sludge blanket bioreactor.

2. To develop a novel method for examining the parameter identification of the integrated Andrews model by plotting the dimensionless sensitivity coefficient, to apply this method to calculate the allowable noise levels for unique parameter estimation, and to examine the causes of parameter non-identification in the integrated Andrews model at low and high substrate concentrations.

Chapter Two

A Model of the Effectiveness Factor in Biofilms and Bioflocs Including the Effect of Cell Density

2.1 Development of the Effectiveness Factor Model Including Cell Density

The effectiveness factor is defined as [Smith, 1970]

$$\eta = \frac{actual\ rate\ for\ the\ whole\ pellet}{rate\ evaluated\ at\ outer\ surface\ conditions} = \frac{R_p}{R_s} \tag{2.1}$$

The difference between the rate expressions R_s and R_p is that the former uses the bulk substrate concentration in the solution, while the latter uses the concentration in the interior of the biofilm or biofloc, which usually decreases along the route of substrate diffusion. Based on the mass balance of a reactant in a particle, an expression for R_p is derived [Smith, 1970]:

$$R_p = \frac{A_p D_e}{V_p}\left(\frac{dS}{dr}\right)_{r=r_0} \tag{2.2}$$

where A_p and V_p are the surface area and volume of the particle, D_e is the effective diffusivity of the substrate in the interior of the particle, S is the substrate concentration, r is the distance from the biofilm surface on the supporting wall or the center of the biofloc to a reaction site, and r_0 is the thickness of the biofilm or the radius of the biofloc, respectively (Fig. 2.1). Therefore, the effectiveness factor can be expressed as

$$\eta = \frac{1}{R_s}\frac{A_p D_e}{V_p}\left(\frac{dS}{dr}\right)_{r=r_0}. \tag{2.3}$$

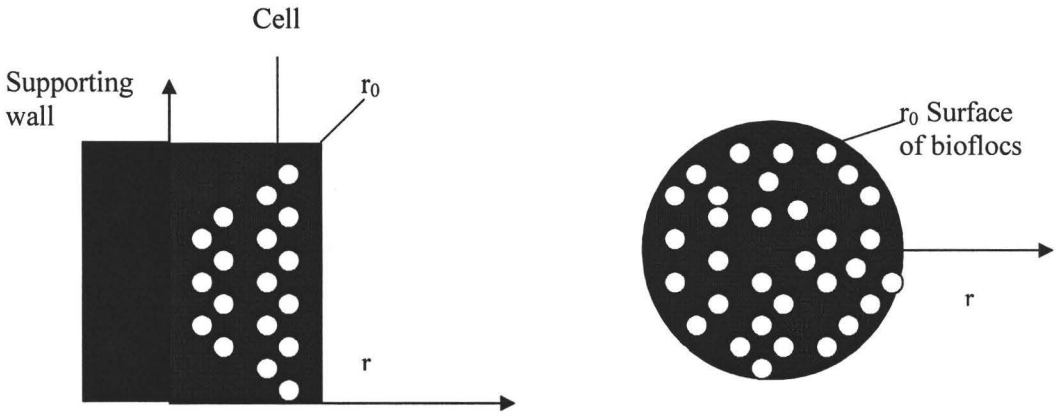

Fig. 2.1 The model of biofilms (A) and bioflocs (B)

The derivative dS/dr is determined by the following ordinary differential equations with respect to an intraparticle-reaction at the steady state (Eqs. (2.4) for the biofilm and (2.5) for the biofloc). Generally, a biofilm is taken to be a slab, for example, the attached biofilm in wastewater biological treatment, and a biofloc is taken to be a sphere, for example, the activated sludge in wastewater treatment process. Biofilms and bioflocs are referred to bioparticles. Therefore, two ordinary differential equations for the slab and sphere models can be expressed as

$$D_e \frac{d^2S}{dr^2} = R_s \text{ for a slab particle (biofilm)} \tag{2.4}$$

$$D_e\left(\frac{d^2S}{dr^2} + \frac{2}{r}\frac{dS}{dr}\right) = R_s \text{ for a spherical particle (biofloc)} \tag{2.5}$$

with boundary conditions

$$dS/dr = 0 \text{ at } r = 0 \tag{2.6}$$

$$S = S_0 \text{ at } r = r_0 \tag{2.7}$$

where S_0 is the substrate concentration on the surface of bioparticles. Some investigations have shown that the external diffusion is not significant compared to the internal diffusion [Chou and Huang, 2005]. If the external diffusion is eliminated, S_0 is equal to the substrate concentration in the bulk solution. The first boundary condition meets the requirement of no fluid flow in the biofilm surface on the supporting wall or in the center of the bioflocs [Hill, 1977].

2.2 Effectiveness Factor of Slab Particle (biofilm with length r)

Various Monod type kinetic models for cell growth have been proposed. Among these, the Monod, Andrews, and multiple-Monod equations are commonly used. These three models, including the effect of cell density, are studied below.

1. The Monod equation

The original Monod equation (1.2) is substituted into Eq. (2.4), to produce

$$D_e\left(\frac{d^2S}{dr^2}\right)=\frac{\mu_m SX}{Y_{X/S}\left(K_S+S\right)}. \tag{2.8}$$

Bailey and Ollis [1986] showed that the cell concentration was proportional to the substrate concentration when cells and substrate were added to the flow reactor at a steady state. Therefore, if the substrate entering the interior of a bioparticle is considered similarly to the feeding substrate in a bioreactor, then the cell density of bioparticles has a linear relationship to the substrate concentration, *i.e.*

$$dX = Y_{X/S}dS \tag{2.9}$$

Integrating Eq. (2.9) between the limits $X = X_0$ at $S = S_0$ and $X = X$ at $S = S$, produces

$$X = Y_{X/S}\left(S-S_0\right)+X_0, \tag{2.10}$$

where X_0 is the cell density on the surface of bioparticles.

Substituting Eq. (2.10) into Eq. (2.8), we have

$$D_e\left(\frac{d^2S}{dr^2}\right)=\frac{\mu_m S\left[Y_{X/S}(S-S_0)+X_0\right]}{Y_{X/S}(K_S+S)} \tag{2.11}$$

Note that when S = S_0, Eq. (2.11) reduces to Atkinson's model [1974]. The dimensionless substrate concentration S*, cell density X*, and length r* are defined by:

$$S^*=\frac{S}{S_0} \tag{2.12}$$

$$X^*=\frac{X}{X_0} \tag{2.13}$$

$$r^*=\frac{r}{r_0}. \tag{2.14}$$

Substituting these into Eq. (2.11) with boundary conditions (Eqs. (2.6) and (2.7)), yields the dimensionless expressions

$$\frac{d^2S^*}{dr^{*2}}=\frac{\phi_1^2 S^*\left[\alpha(S^*-1)+1\right]}{1+\beta S^*} \tag{2.15}$$

and

$$dS^*/dr^* = 0 \text{ at } r^* = 0 \tag{2.16}$$

$$S^* = 1 \text{ at } r^* = 1 \tag{2.17}$$

The parameters α, β, and ϕ_1 in Eq. (2.15) are defined by

$$\alpha=\frac{Y_{X/S}S_0}{X_0} \tag{2.18}$$

$$\beta=\frac{S_0}{K_S} \tag{2.19}$$

$$\phi_l = r_o \sqrt{\frac{\mu_m X_0}{Y_{X/S} D_e K_S}} \tag{2.20}$$

where ϕ_l is the Thiele modulus for a slab.

The effectiveness factor for a slab based on the dimensionless parameters is

$$\eta = \frac{1+\beta}{\phi_l^2}\left(\frac{dS^*}{dr^*}\right)_{r^*=1}. \tag{2.21}$$

Although it is impossible to obtain an analytic solution for the relationship between S^* and r^* in Eq. (2.15) because it is a non-linear boundary value equation, it is possible to get an expression for dS^*/dr^* and r^*, since Eq. (2.15) lacks the first order derivative term, and Eq. (2.15) can be re-written as:

$$\frac{1}{2}\frac{d\left(\frac{dS^*}{dr^*}\right)^2}{dS^*} = \frac{\phi_l^2 S^*\left[\alpha\left(S^*-1\right)+1\right]}{1+\beta S^*}. \tag{2.22}$$

Eq. (2.22) can be integrated between the limits $dS^*/dr^* = (dS^*/dr^*)_{r^*=1}$ and $S^* = 1$ at $r^* = 1$, and $dS^*/dr^* = (dS^*/dr^*)_{r^*=0} = 0$ and $S^* = S^*_c$ at $r^* = 0$, to produce

$$\left(\frac{dS^*}{dr^*}\right)_{r^*=1} = 2^{0.5}\phi_l \left\{ \begin{array}{l} \frac{1-\alpha}{\beta^2}\left[\beta\left(1-S_c^*\right) - \ln\frac{1+\beta}{1+S_c^*}\right] \\ +\frac{\alpha}{\beta^2}\left[\frac{1}{2}(1+\beta)^2 - \frac{1}{2}\left(1+\beta S_c^*\right)^2 - 2\beta\left(1-S_c^*\right) + \ln\frac{1+\beta}{1+\beta S_c^*}\right] \end{array} \right\}^{0.5} \tag{2.23}$$

Substituting Eq. (2.23) into Eq. (2.21), we obtain the effectiveness factor for a slab:

$$\eta = \frac{2^{0.5}(1+\beta)}{\phi_l} \left\{ \begin{array}{l} \frac{1-\alpha}{\beta^2}\left[\beta\left(1-S_c^*\right) - \ln\frac{1+\beta}{1+S_c^*}\right] \\ +\frac{\alpha}{\beta^2}\left[\frac{1}{2}(1+\beta)^2 - \frac{1}{2}\left(1+\beta S_c^*\right)^2 - 2\beta\left(1-S_c^*\right) + \ln\frac{1+\beta}{1+\beta S_c^*}\right] \end{array} \right\}^{0.5} \tag{2.24}$$

where S^*_c is the dimensionless substrate concentration on the biofilm surface on supporting wall or the center of the biofloc.

When the Thiele modulus ϕ_l is a large value, S^*_c is approximately equal to zero, and Eq. (2.24) reduces to

$$\eta = \frac{2^{0.5}(1+\beta)}{\phi_l}\left\{\frac{1-\alpha}{\beta^2}[\beta - \ln(1+\beta)] + \frac{\alpha}{\beta^2}\left[\frac{1}{2}(1+\beta)^2 - \frac{1}{2} - 2\beta + \ln(1+\beta)\right]\right\}^{0.5} \quad (2.25)$$

When $\alpha = 0$, Eq. (2.25) further reduces to the approximate analytic expression derived by Atkinson [1974].

2. The Andrews equation (substrate inhibition)

It was found that in some situations the specific growth rate of cells reaches a maximum, and then declines as the substrate concentration increases, which is different from the Monod growth pattern. This phenomenon is attributed to inhibition of cell growth due to the characteristics of the substrate. Andrews [1968] proposed the following equation to describe this phenomenon:

$$\mu = \frac{\mu_m S}{K_S + S + S^2/K_I} \quad (2.26)$$

where K_I is the inhibition coefficient.

The rate expression R_s for substrate consumption is

$$R_s = \frac{\mu_m S X}{Y_{X/S}\left(K_S + S + S^2/K_I\right)}. \quad (2.27)$$

Substituting Eqs. (2.10) and (2.27) into Eq. (2.4), yields

$$\frac{d^2S}{dr^2} = \frac{\mu_m S[Y_{X/S}(S - S_0) + X_0]}{Y_{X/S}\left(K_S + S + S^2/K_I\right)}. \quad (2.28)$$

As with the Monod model, there is a dimensionless version:

$$\frac{d^2S^*}{dr^{*2}} = \frac{\phi_l^2 S^*\left[\alpha\left(S^*-1\right)+1\right]}{1+\beta S^*+\delta S^{*2}} \tag{2.29}$$

with a new dimensionless parameter

$$\delta = \frac{S_0\beta}{K_I} = \frac{S_0^2}{K_S K_I}. \tag{2.30}$$

When $\delta = 0$, *i.e.* $K_I = \infty$, Eq. (2.29) reduces to Eq. (2.15).

The effectiveness factor for a slab, using the dimensionless parameters, is

$$\eta = \frac{1+\beta+\delta}{\phi_l^2}\left(\frac{dS^*}{dr^*}\right)_{r^*=1}. \tag{2.31}$$

Eq. (2.29) has two analytic expressions about dS^*/dr^* versus r^* for the condition of $\beta^2 - 4\delta \geq 0$ and $\beta^2 - 4\delta < 0$, respectively. Substituting these solutions to Eq. (2.31), when $\beta^2 - 4\delta \geq 0$, the effectiveness factor is

$$\eta = \frac{2^{0.5}\left(1+\alpha+\delta\right)}{\phi_l}\left\{\begin{array}{l}\dfrac{\alpha}{\delta}\left(1-S_c^*\right)+\dfrac{\left(\delta-\alpha\delta-\alpha\beta\right)}{2\delta^2}\ln\dfrac{1+\beta+\delta}{1+\beta S_c^*+\delta S_c^{*2}} \\ -\left(\dfrac{\alpha}{\delta}+\dfrac{\beta\left(\delta-\alpha\delta-\alpha\beta\right)}{2\delta^2}\right)\left(\beta^2-4\delta\right)^{-0.5} \\ \ln\left[\dfrac{2\delta+\beta-\left(\beta^2-4\delta\right)^{0.5}}{2\delta+\beta+\left(\beta^2-4\delta\right)^{0.5}}\right]\left[\dfrac{2\delta S_c^*+\beta+\left(\beta^2-4\delta\right)^{0.5}}{2\delta S_c^*+\beta-\left(\beta^2-4\delta\right)^{0.5}}\right]\end{array}\right\}. \tag{2.32}$$

and when $\beta^2 - 4\delta < 0$, it is

$$\eta = \frac{2^{0.5}\left(1+\alpha+\delta\right)}{\phi_l}\left\{\begin{array}{l}\dfrac{\alpha}{\delta}\left(1-S_c^*\right)+\dfrac{\left(\delta-\alpha\delta-\alpha\beta\right)}{2\delta^2}\ln\dfrac{1+\beta+\delta}{1+\beta S_c^*+\delta S_c^{*2}} \\ -\left(\dfrac{\alpha}{\delta}+\dfrac{\beta\left(\delta-\alpha\delta-\alpha\beta\right)}{2\delta^2}\right)\dfrac{2}{\left(4\delta-\beta^2\right)^{0.5}} \\ \left[\arctan\dfrac{2\delta+\beta}{\left(4\delta-\beta^2\right)^{0.5}}-\arctan\dfrac{2\delta S_c^*+\beta}{\left(4\delta-\beta^2\right)^{0.5}}\right]\end{array}\right\}. \tag{2.33}$$

When ϕ_l is large, $S^*_c \approx 0$, Eqs. (2.32) and (2.33) reduce, respectively, to

$$\eta = \frac{2^{0.5}(1+\alpha+\delta)}{\phi_l}\left\{\begin{array}{l}\dfrac{\alpha}{\delta}+\dfrac{(\delta-\alpha\delta-\alpha\beta)}{2\delta^2}\ln(1+\alpha+\delta) \\ -\left(\dfrac{\alpha}{\delta}+\dfrac{\beta(\delta-\alpha\delta-\alpha\beta)}{2\delta^2}\right)\left(\beta^2-4\delta\right)^{-0.5} \\ \ln\left[\dfrac{2\delta+\beta-\left(\beta^2-4\delta\right)^{0.5}}{2\delta+\beta+\left(\beta^2-4\delta\right)^{0.5}}\right]\left[\dfrac{\beta+\left(\beta^2-4\delta\right)^{0.5}}{\beta-\left(\beta^2-4\delta\right)^{0.5}}\right]\end{array}\right\} \tag{2.34}$$

$$\eta = \frac{2^{0.5}(1+\alpha+\delta)}{\phi_l}\left\{\begin{array}{l}\dfrac{\alpha}{\delta}+\dfrac{(\delta-\alpha\delta-\alpha\beta)}{2\delta^2}\ln(1+\beta+\delta) \\ -\left(\dfrac{\alpha}{\delta}+\dfrac{\beta(\delta-\alpha\delta-\alpha\beta)}{2\delta^2}\right)\dfrac{2}{\left(4\delta-\beta^2\right)^{0.5}} \\ \left[\arctan\dfrac{2\delta+\beta}{\left(4\delta-\beta^2\right)^{0.5}}-\arctan\dfrac{\beta}{\left(4\delta-\beta^2\right)^{0.5}}\right]\end{array}\right\}. \tag{2.35}$$

3. Multiple Monod equation (two-limiting substrates)

This equation, one of the interactive models, has been proposed to describe multiple limiting substrates. For two-limiting substrates, it is expressed as [Grady et al., 1999]

$$\mu = \frac{\mu_m S_1}{K_{S1}+S_1}\frac{S_2}{K_{S2}+S_2} \tag{2.36}$$

where S_1 and S_2 are the concentrations of the substrates 1 and 2 in the bulk solution, and K_{S1} and K_{S2} are their saturation coefficients, respectively.

In wastewater treatment, another common growth-limiting substrate apart from organic compounds often is oxygen. Therefore, for clarity, the rate equation can be expressed as

$$R_s = \frac{X}{Y_{X/S}}\frac{\mu_m S}{K_S+S}\frac{O}{K_O+O} \tag{2.37}$$

where O is the oxygen concentration in the bulk solution and K_O is the oxygen saturation coefficient.

Substituting Eq. (2.37) into Eq. (2.4), yields

$$\frac{d^2S}{dr^2} = \frac{X}{Y_{X/S}} \frac{\mu_m S}{K_S + S} \frac{O}{K_O + O}. \tag{2.38}$$

It is assumed that the substrate concentration is related linearly to the oxygen concentration:

$$dX = Y_{X/S} dS = Y_{X/O} dO. \tag{2.39}$$

Integrating Eq. (2.39) between the limits O = O_0, the oxygen concentration on the bioparticle surface, at S = S_0, and O = O at S = S, produces

$$O = \frac{Y_{X/O}(S - S_0)}{Y_{X/S}} + O_0. \tag{2.40}$$

Substituting Eqs. (2.10) and (2.40) into Eq. (2.4), produces

$$\frac{d^2S}{dr^2} = \left(\frac{\mu_m S}{K_S + S}\right)\left[\frac{\alpha(S - S_0) + X_0}{Y_{X/S}}\right]\left[\frac{Y_{X/O}(S - S_0)/Y_{X/S} + O_0}{K_O + Y_{X/O}(S - S_0)/Y_{X/S} + O_0}\right]. \tag{2.41}$$

Similarly to other models, there is a dimensionless version:

$$\frac{d^2S^*}{dr^{*2}} = \left(\frac{\phi_l^2 S^*}{1 + \beta S^*}\right)\frac{\left[\alpha(S^* - 1) + 1\right]\left[\gamma_1(S^* - 1) + 1\right]}{1 + \gamma_2\left[\gamma_1(S^* - 1) + 1\right]} \tag{2.42}$$

with the new parameters

$$\gamma_1 = \frac{Y_{X/S} S_0}{Y_{X/O} O_0} \tag{2.43}$$

$$\gamma_2 = \frac{O_0}{K_O} \tag{2.44}$$

$$\phi_l = r_0 \sqrt{\frac{\mu_m X_0 O_0}{Y_{X/S} D_e K_S K_O}}. \tag{2.45}$$

The effectiveness factor for a slab in this case is

$$\eta = \frac{(1+\beta)(1+\gamma_2)}{\phi_l^2}\left(\frac{dS^*}{dr^*}\right)_{r^*=1}. \tag{2.46}$$

Eq. (2.46) also has an analytic solution, for which we do not present because of its complexity.

2.3 The Effectiveness Factor of Spherical Particle (biofloc with radius r)

Similarly to the above derivations, the various expressions of the effectiveness factor for spherical particles (bioflocs) can be obtained. Unlike the case of biofilms, the effectiveness factor of bioflocs does not have an analytic solution.

1. Monod equation

$$\frac{d^2S^*}{dr^{*2}} + \frac{2}{r^*}\frac{dS^*}{dr^*} = \frac{9\phi_s^2 S^*}{1+\beta S^*}\left[\alpha\left(S^*-1\right)+1\right] \tag{2.47}$$

$$\phi_s = \frac{r_0}{3}\sqrt{\frac{\mu_m X_0}{Y_{X/S} D_e K_S}} \tag{2.48}$$

where the subscript s denotes the biofloc. The effectiveness factor for a sphere based on the dimensionless parameters is

$$\eta = \frac{1+\beta}{3\phi_s^2}\left(\frac{dS^*}{dr^*}\right)_{r^*=1}. \tag{2.49}$$

2. The Andrews equation (substrate inhibition)

$$\frac{d^2S^*}{dr^{*2}} + \frac{2}{r^*}\frac{dS^*}{dr^*} = \frac{9\phi_s^2 S^*}{1+\beta S^*+\delta S^{*2}}\left[\alpha\left(S^*-1\right)+1\right]. \tag{2.50}$$

The effectiveness factor for a sphere based on the dimensionless parameters is

$$\eta = \frac{1+\beta+\delta}{3\phi_s^2}\left(\frac{dS^*}{dr^*}\right)_{r^*=1}. \tag{2.51}$$

3. Multiple Monod equation (two-limiting substrates)

$$\frac{d^2S^*}{dr^{*2}}+\frac{2}{r^*}\frac{dS^*}{dr^*}=\left(\frac{9\phi^2S^*}{1+\beta S^*}\right)\frac{\left[\alpha\left(S^*-1\right)+1\right]\left[\gamma_1\left(S^*-1\right)+1\right]}{1+\gamma_2\left[\gamma_1\left(S^*-1\right)+1\right]} \tag{2.52}$$

$$\phi_s=\frac{r_0}{3}\sqrt{\frac{\mu_m X_0 O_0}{Y_{X/S}D_e K_S K_O}}\,. \tag{2.53}$$

The effectiveness factor for a sphere in this case is

$$\eta=\frac{(1+\beta)(1+\gamma_2)}{3\phi_s^2}\left(\frac{dS^*}{dr^*}\right)_{r^*=1}. \tag{2.54}$$

2. 4 The Calculated Results: the Effectiveness Factor Versus the Thiele Modulus and Parameters α, β, δ, γ_1, and γ_2

Using MATLAB [MathWorks, 2002], Eqs. (2.15), (2.29), (2.42), (2.47), (2.50), and (2.52) were solved to obtain dS^*/dr^* at $r^* = 1$ at various Thiele moduli, and parameters α, β, δ, γ_1, and γ_2. Thus the effectiveness factors can be calculated from Eqs. (2.21), (2.31), (2.46), (2.49), (2.51), and (2.54). Figs. 2.2-2.13 give these results.

2.5 The Effect of the Thiele Modulus on the Effectiveness Factor

All the graphs below show that the effectiveness factor will continuously decrease with increasing the Thiele modulus, except in the case of substrate inhibition (Figs. 2.6 and 2.8). This is because the Thiele modulus represents the relative influence of reaction rate and intraparticle diffusion. An increase of the Thiele modulus implies, from its definition, an increase of the reaction rate constant and a decrease of the substrate diffusivity.

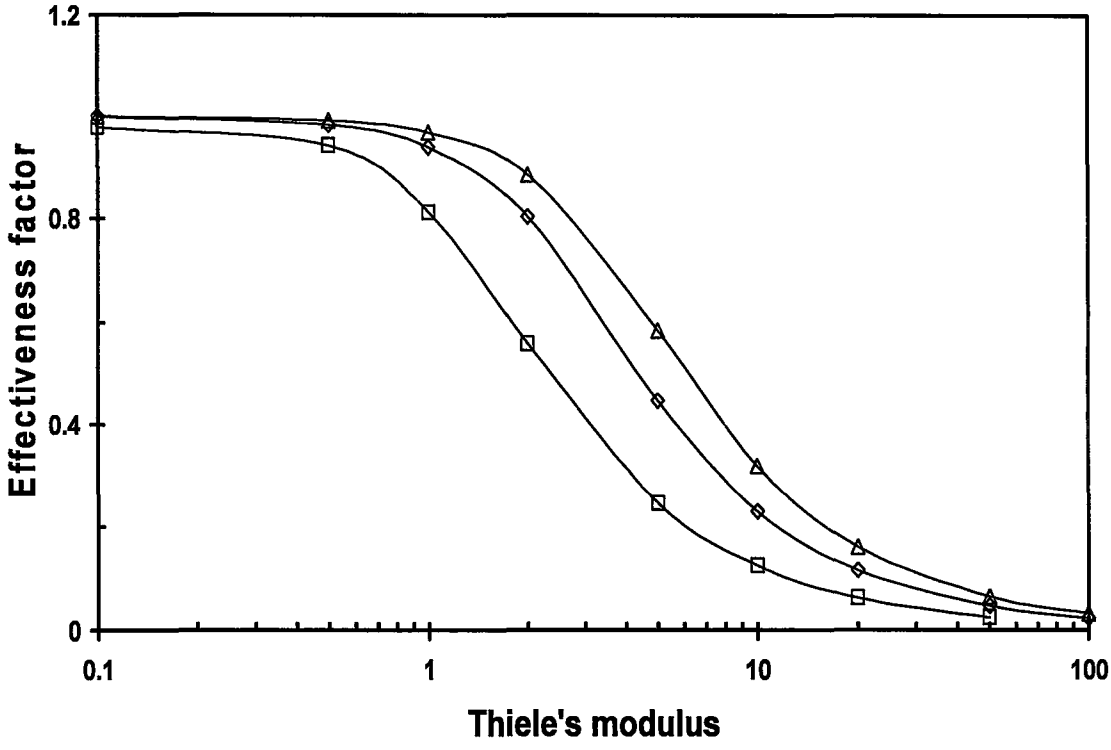

Fig. 2.2 Effects of Thiele's modulus and β on effectiveness factor in biofilms (Monod Eq.) □ β=1, ◊ β=5, Δ β=10 (α=1).

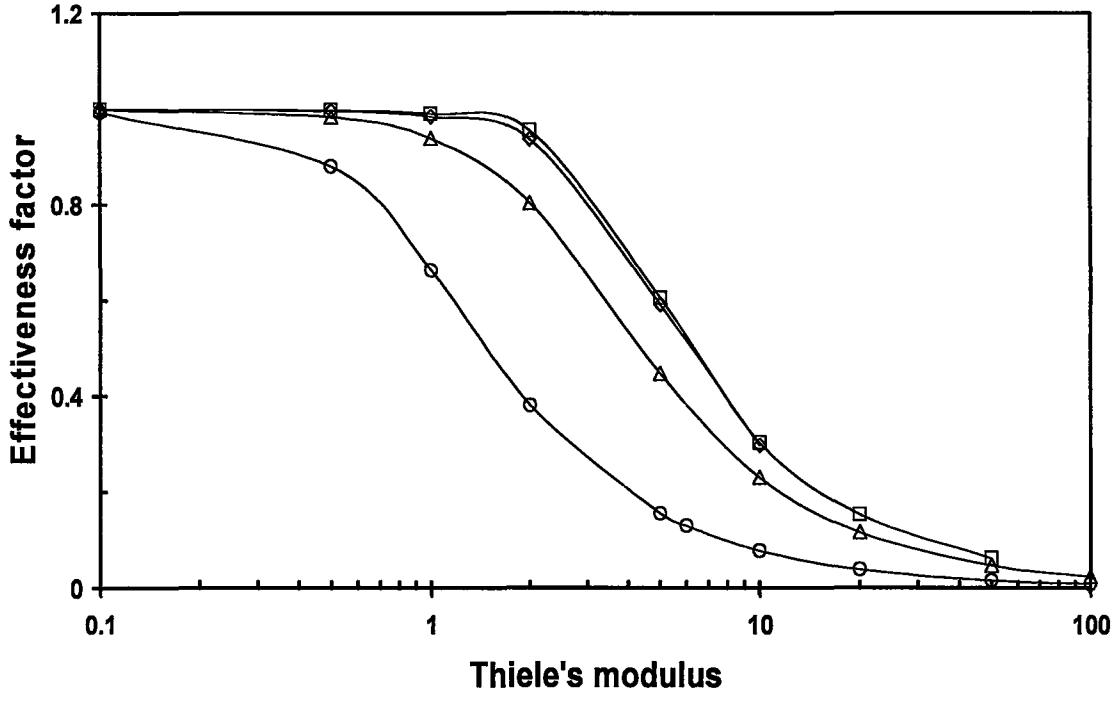

Fig. 2.3 Effects of Thiele's modulus and α on effectiveness factor of biofilms (Monod Eq.) □ α=0, ◊ α=0.1, Δ α=1, o α=10 (β=5).

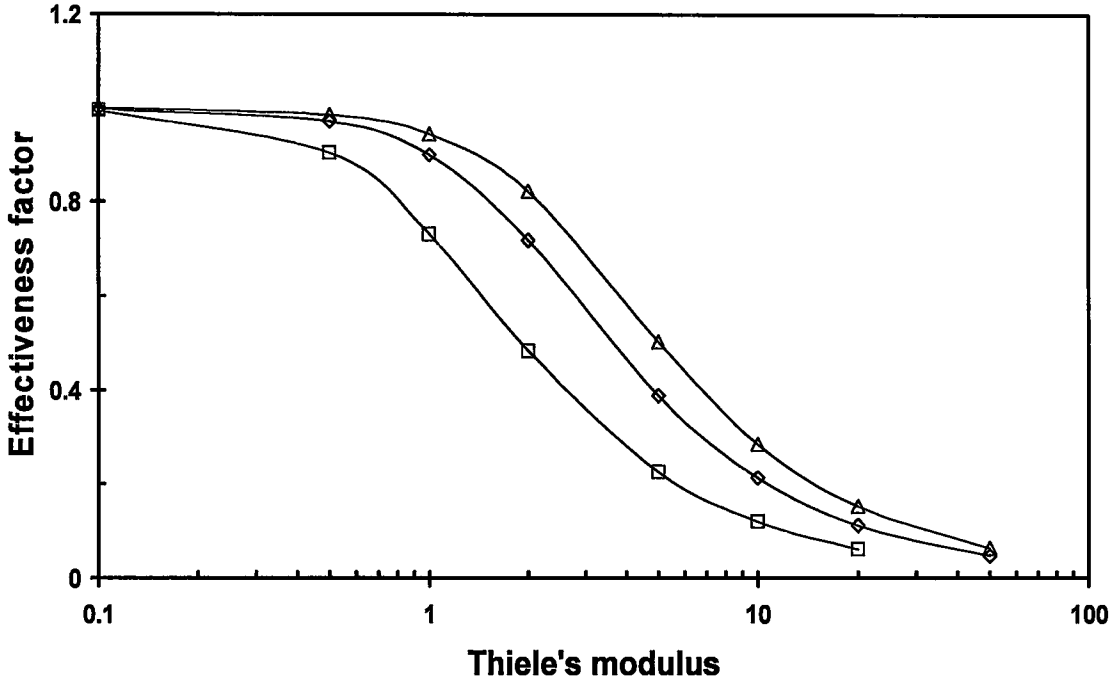

Fig. 2.4 Effects of Thiele's modulus and β on effectiveness factor in bioflocs (Monod Eq.) □ β=1, ◊ β=5, Δ β=10 (α=1).

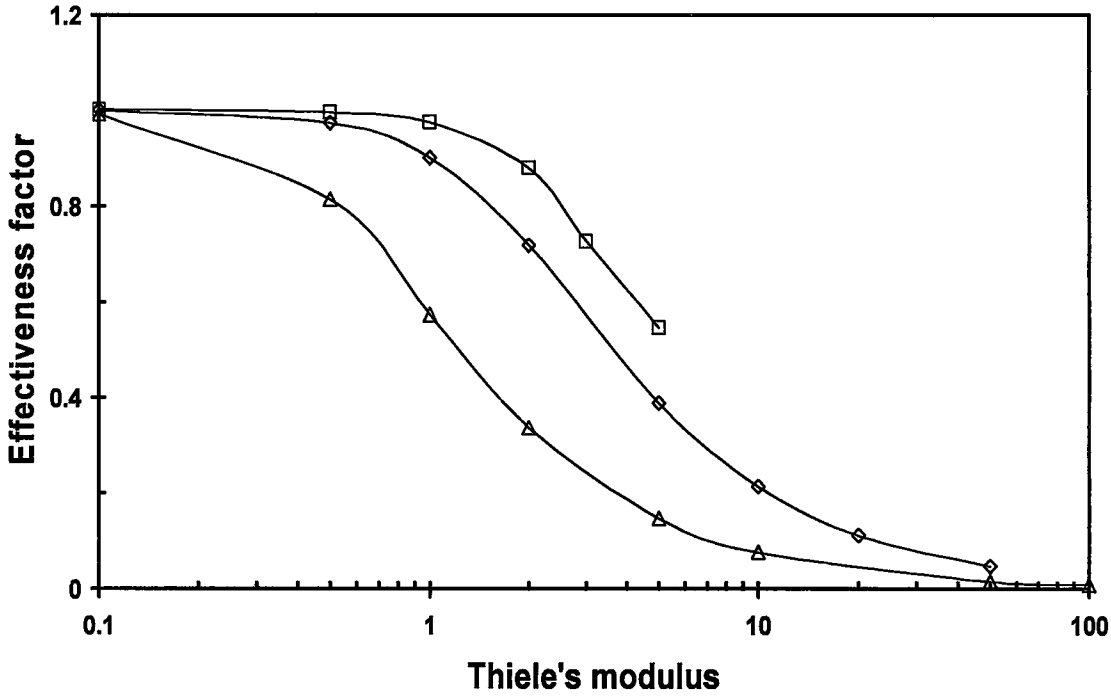

Fig. 2.5 Effects of Thiele's modulus and α on effectiveness factor in bioflocs (Monod Eq.) □ α=0.1, ◊ α=1, Δ α=10 (β=5).

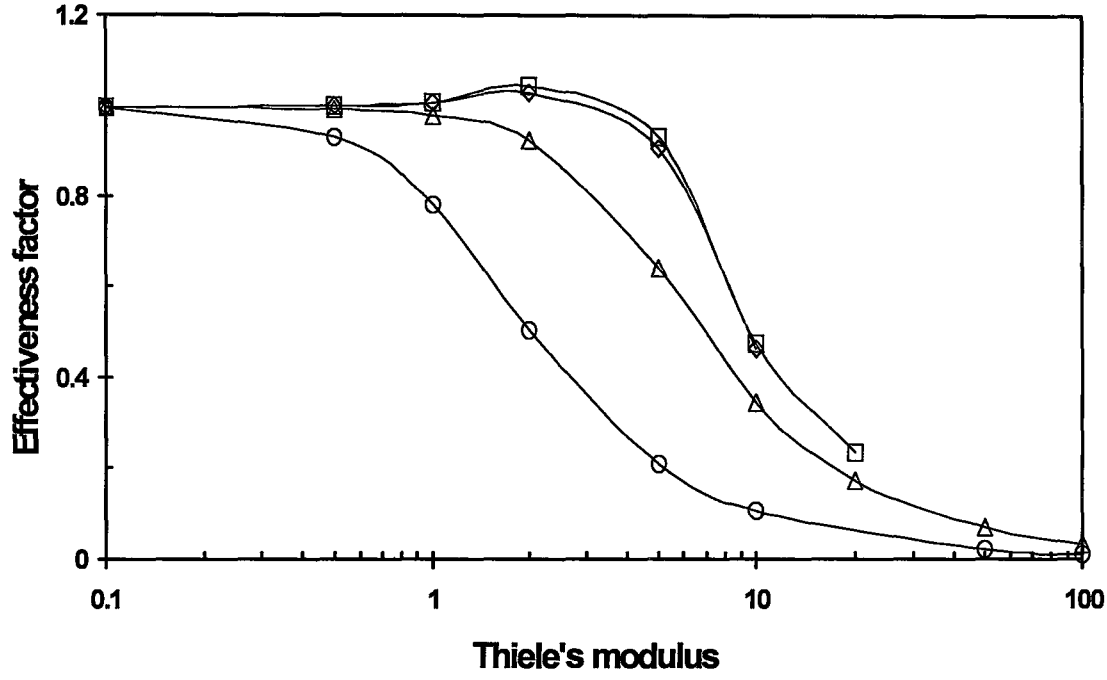

Fig. 2.6 Effects of Thiele's modulus and α on effectiveness factor in biofilms (Andrews Eq.) □ α=0, ◊ α=0.1, Δ α=1, o α=10 (β=5, δ=5).

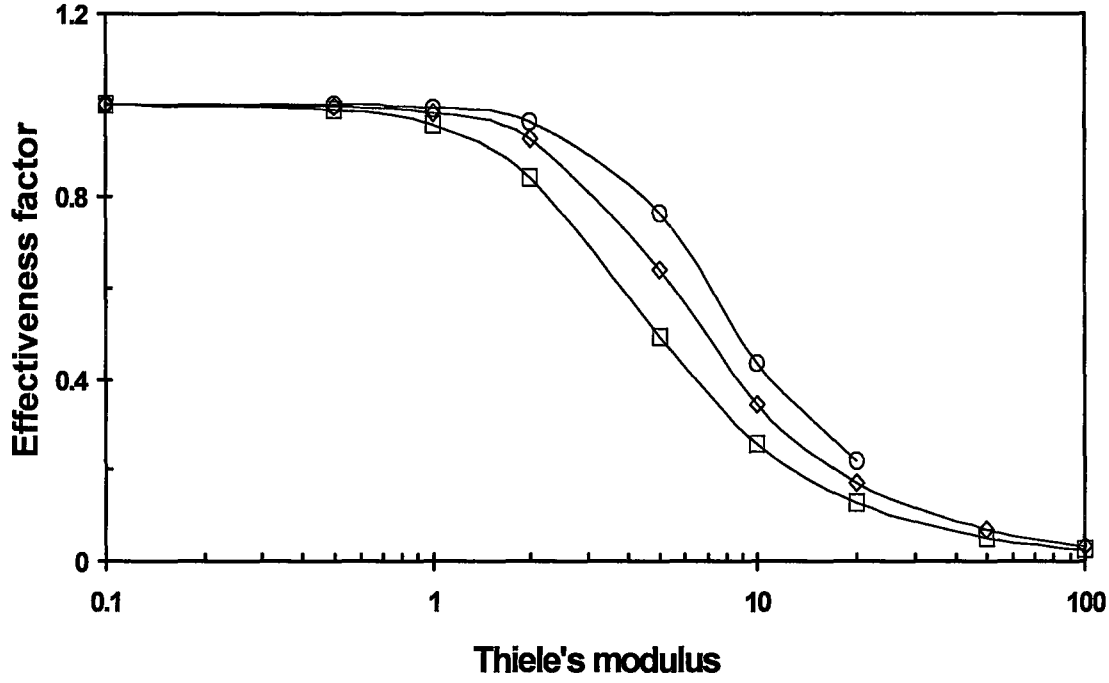

Fig. 2.7 Effects of Thiele's modulus and δ on effectiveness factor in biofilms (Andrews Eq.) □ δ =1, ◊ δ =5, Δ δ =10 (β=5, α=1).

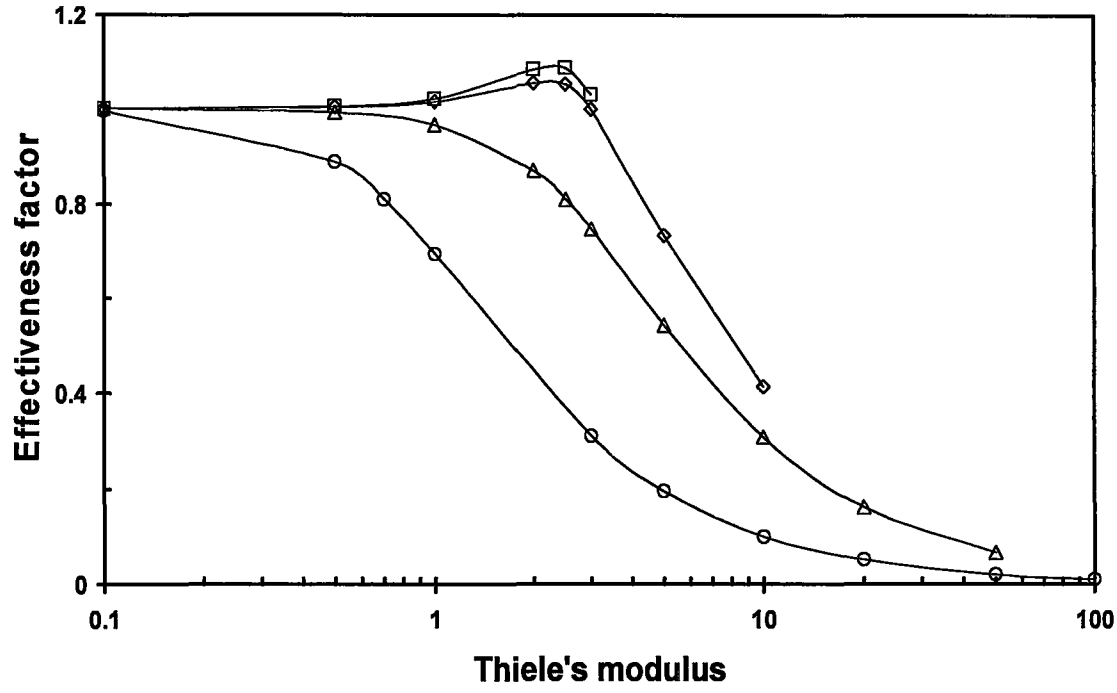

Fig. 2.8 Effects of Thiele's modulus and α on effectiveness factor in bioflocs (Andrews Eq.) □ α=0, ◊ α=0.1, Δ α=1, o α=10 (β=5, δ=5).

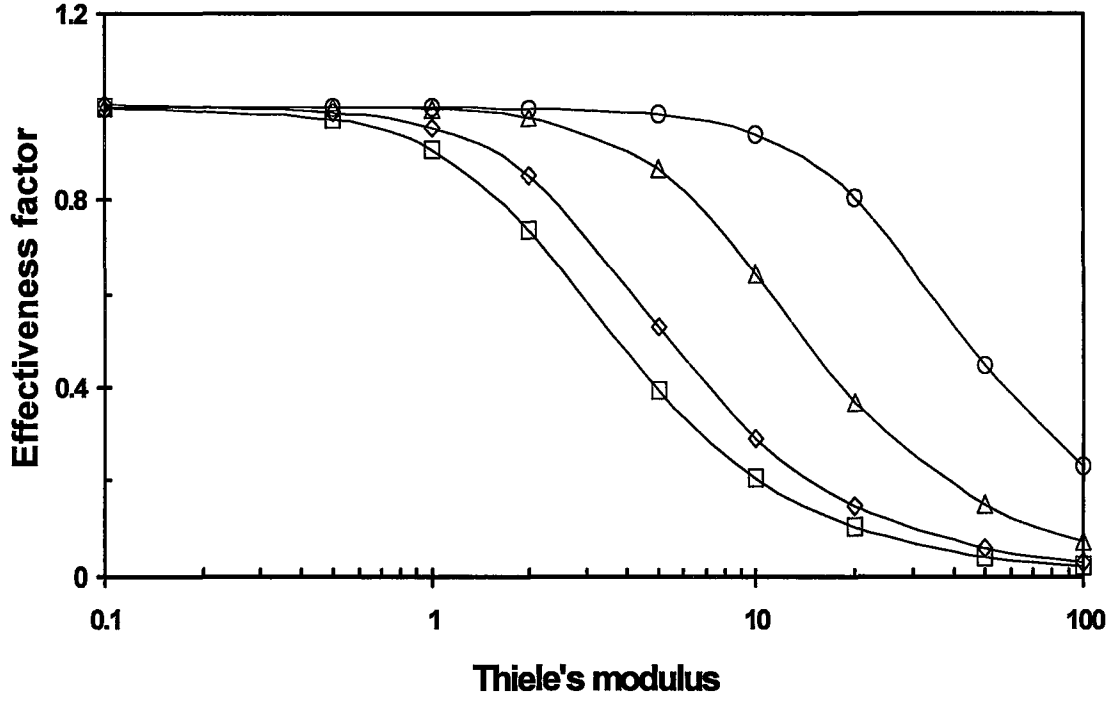

Fig. 2.9 Effects of Thiele's modulus and δ on effectiveness factor in bioflocs (Andrews Eq.) □ δ =1, ◊ δ =5, Δ δ =10 o δ=100 (β=5, α=1).

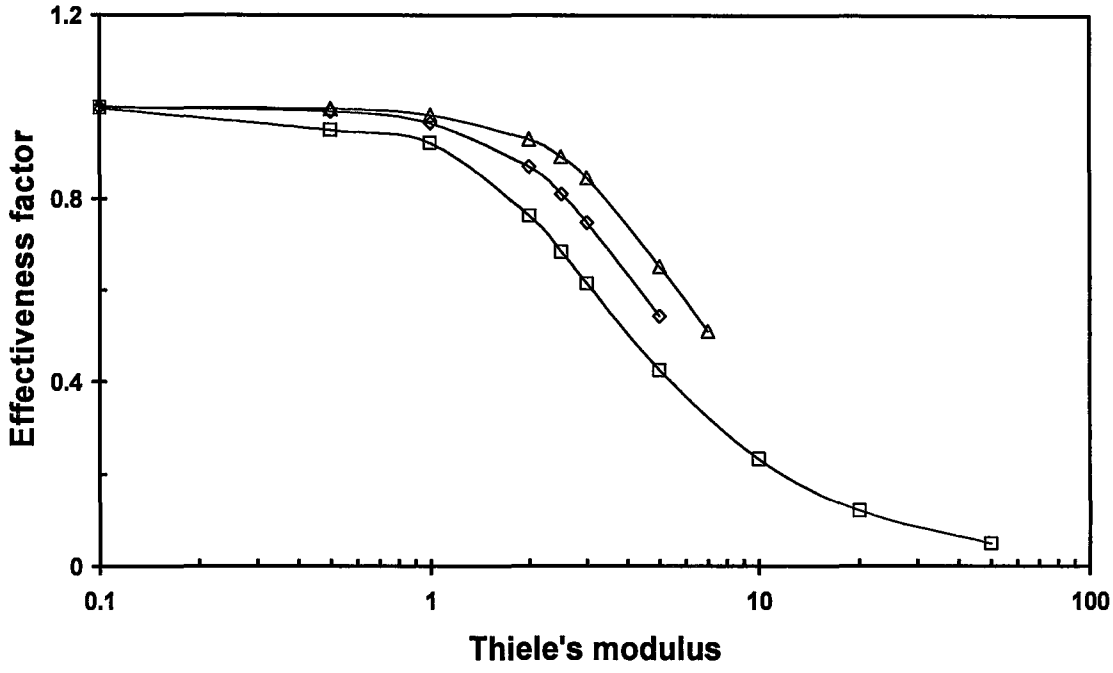

Fig. 2.10 Effects of Thiele's modulus and γ_2 on effectiveness factor in biofilms (two limiting substrate Eq.) □ γ_2=0.1, ◊ γ_2=1, Δ γ_2=10 (β=5, α=1, γ_1=1).

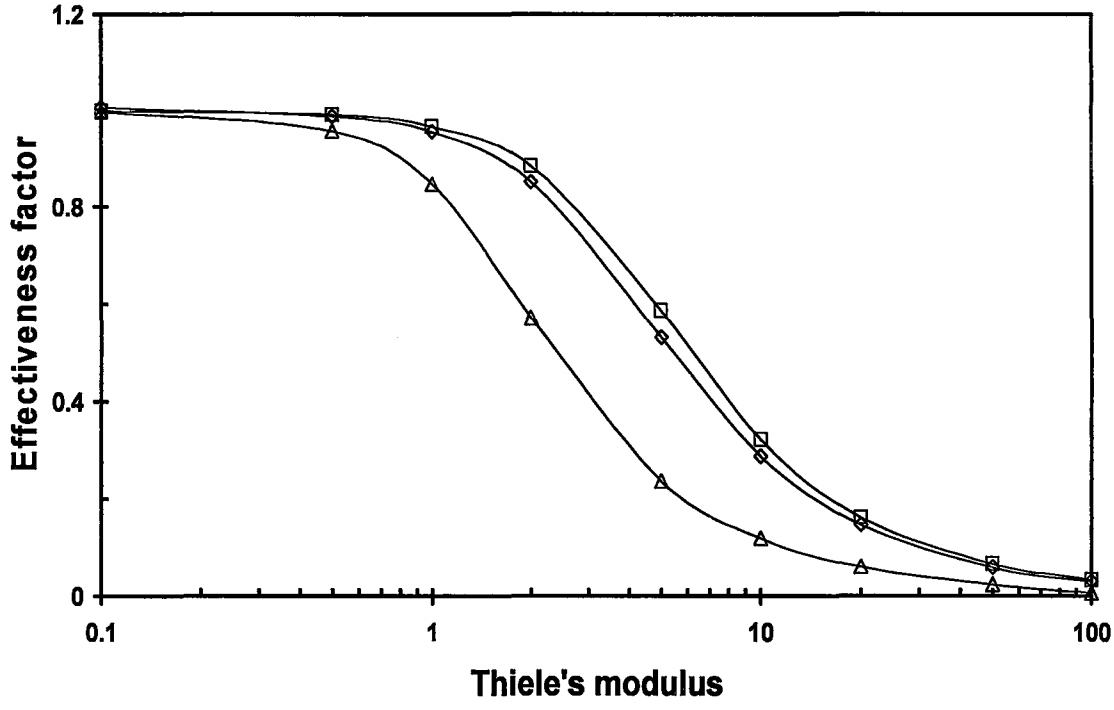

Fig. 2.11 Effects of Thiele's modulus and γ_1 on effectiveness factor in biofilms (two limiting substrate Eq.) □ γ_1=0.1, ◊ γ_1=1, Δ γ_1=10 (β=5, α=1, γ_2=1).

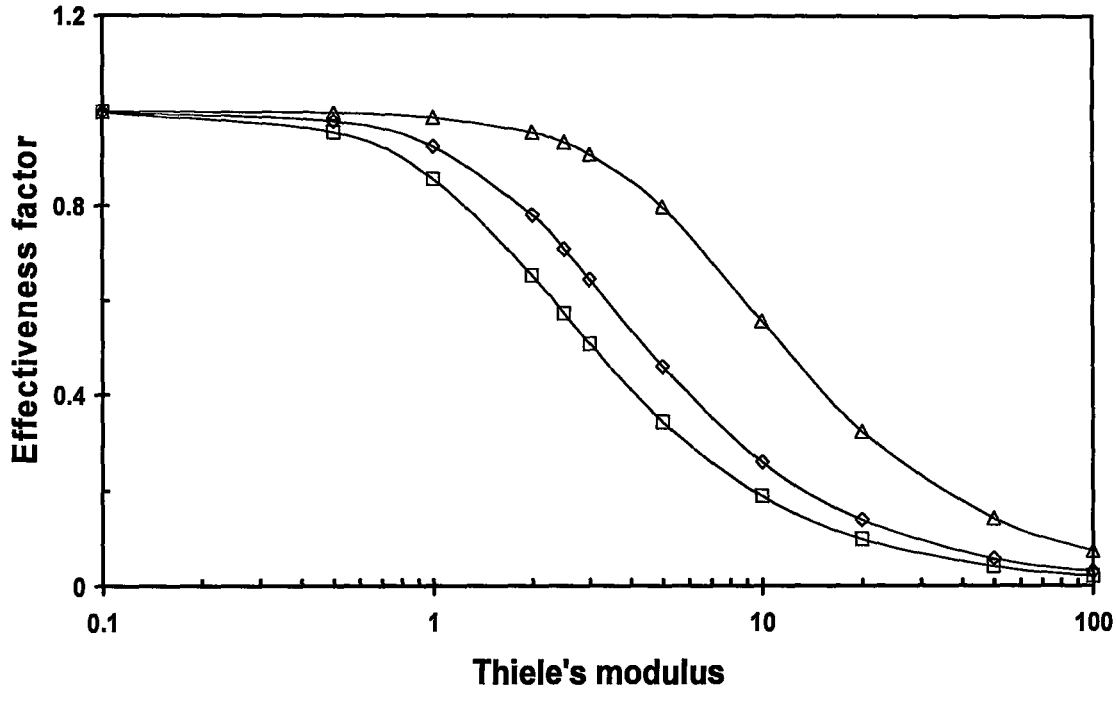

Fig. 2.12 Effects of Thiele's modulus and γ_2 on effectiveness factor in bioflocs (two limiting substrate Eq.) □ γ_2=0.1, ◊ γ_2=1, Δ γ_2=10 (β=5, α=1, γ_1=1).

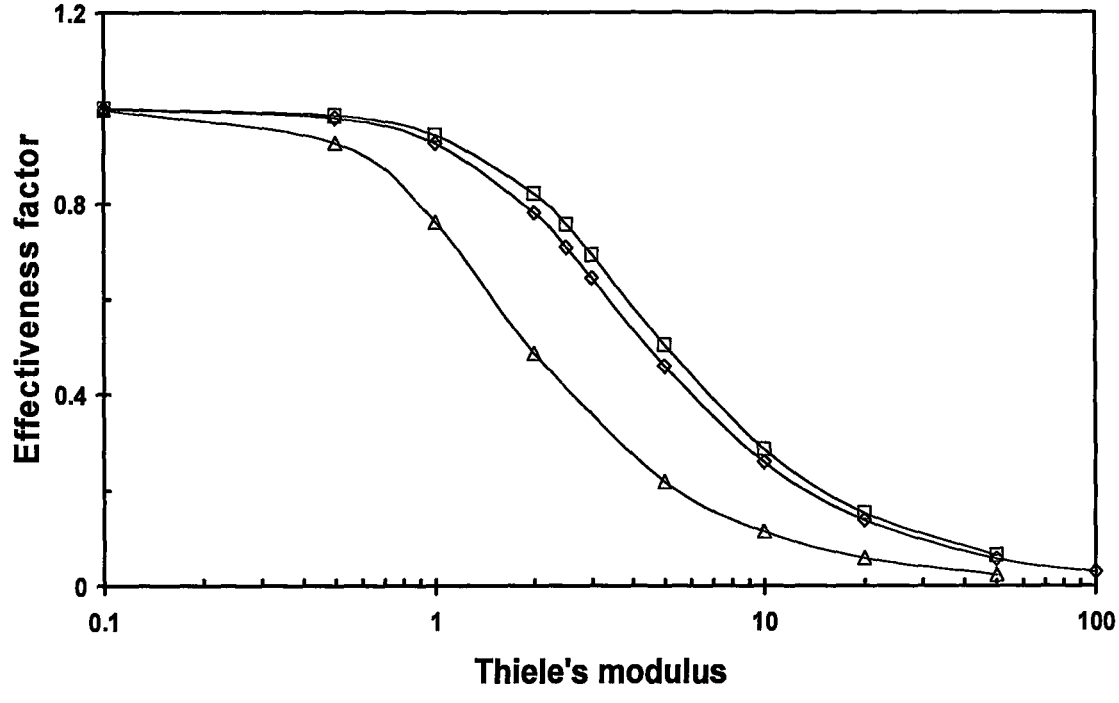

Fig. 2.13 Effects of Thiele's modulus and γ_1 on effectiveness factor in bioflocs (two limiting substrate Eq.) □ γ_1=0.1, ◊ γ_1=1, Δ γ_1=10 (β=5, α=1, γ_2=1).

Both changes enhance the importance of intraparticle diffusion and reduce the efficiency of the biofilm and biofloc in the bioprocess. In the case of substrate inhibition (Figs. 2.6 and 2.8) the effectiveness factor first increases a little, reaches a maximum greater than 1, and then decreases with increasing the Thiele modulus in the cases of the parameter α between 0 and 1. However, the substrate concentration gradients at the biofilm surface or at the center of the biofloc do not have the same shape as the effectiveness factors. They increase with the Thiele modulus (Figs. 2.14 and 2.15). Therefore, the maximum point of the effectiveness factor is determined by the relative weight of the Thiele modulus, whose increase causes a decrease of the effectiveness factor, and the substrate concentration gradient. The effectiveness factor being greater than 1 can be explained by assuming that the rate increase caused by substrate inhibition compensates for the rate decrease caused by the substrate concentration drop [Moo-Young and Kobayashi, 1972]. However, the increases of the effectiveness factor in the present study were very limited. The dramatic increase of effectiveness factor reported by Moo-Young and Kobayashi [1972] and Gheewala and Annachhatre [2003] was not observed.

2.6 The Effect of the Parameter α on the Effectiveness Factor

Figs 2.3, 2.5, 2.6, and 2.8 show the effect of the parameter α on the effectiveness factor in biofilms and bioflocs. With increasing α, the effectiveness factor decreases for a constant Thiele modulus. From the relationship between the dimensionless cell density and substrate concentration (the dimensionless version of Eq. (2.10)),

$$X^* = \alpha(S^* - 1) + 1 \tag{2.55}$$

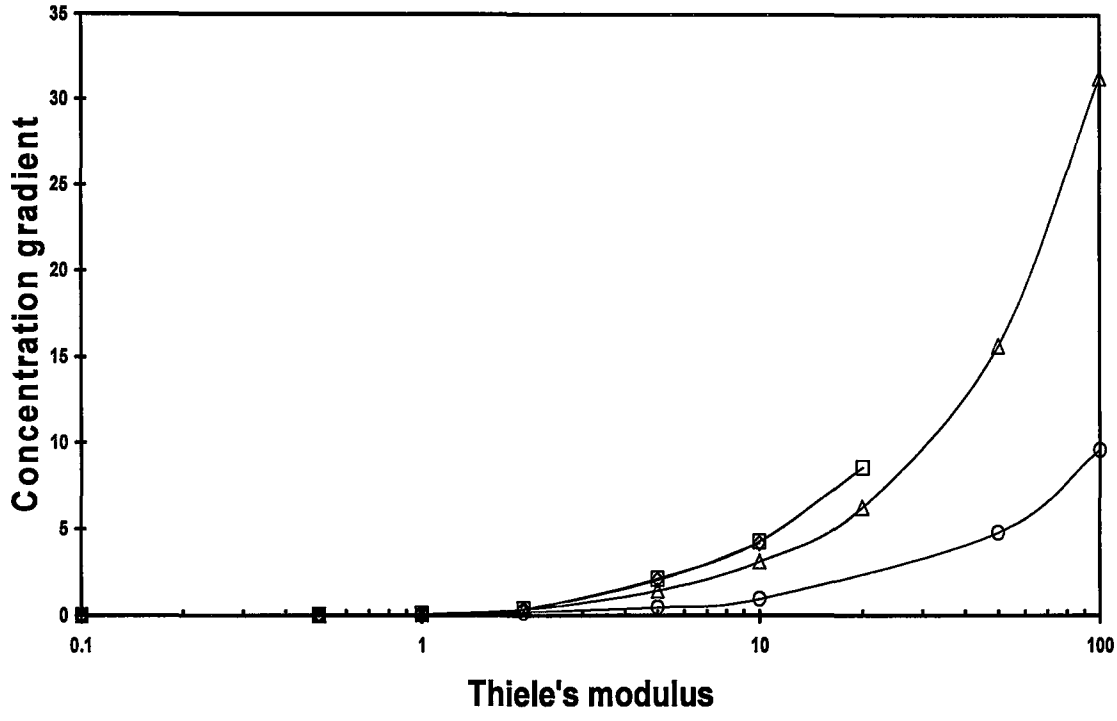

Fig. 2.14 Effects of Thiele's modulus and α on concentration gradient at r^*=1 in biofilms (Andrews Eq.) □ α=0, ◊ α=0.1, Δ α=1, ○ α=10 (Other conditions as Fig. 2.6 β=5, δ=5).

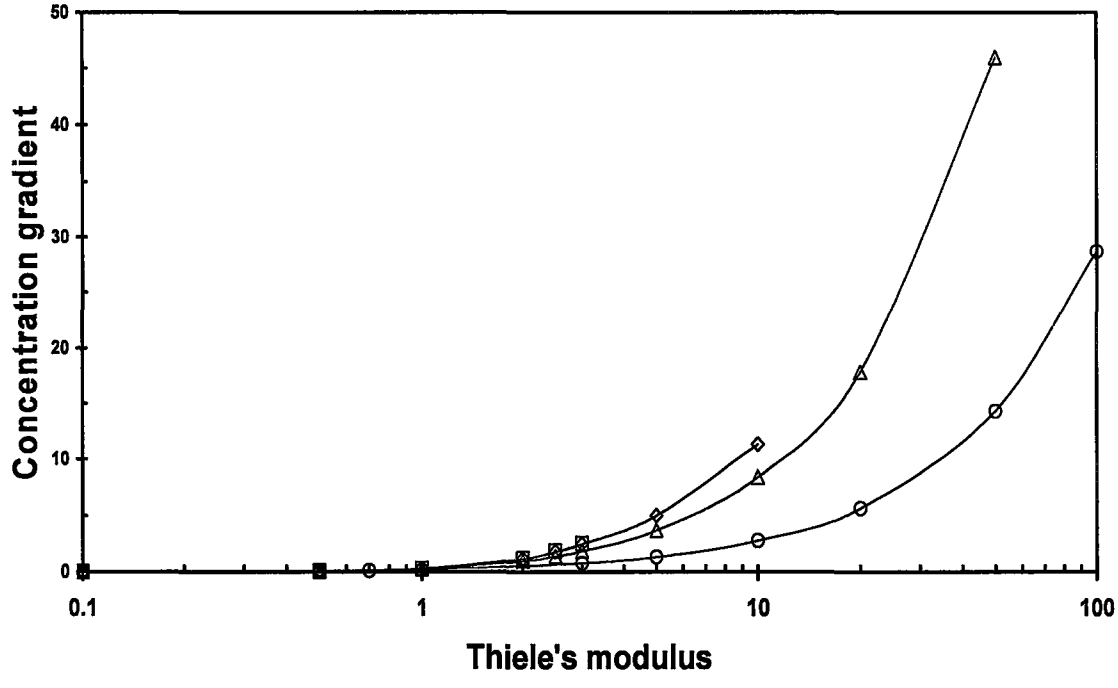

Fig. 2.15 Effects of Thiele's modulus and α on concentration gradient at r^*=1 in bioflocs (Andrew Eq.) □ α=0, ◊ α=0.1, Δ α=1, ○ α=10 (Other conditions as Fig. 2.8 β=5, δ=5).

we know that an increase of α results in a decrease of X^* because of $S^* \leq 1$, causing a drop of efficiency of biofilms or bioflocs. Note that when $\alpha > 1$, S^* will be greater than zero because $X^* \geq 0$. This suggests that the substrate concentration in the center of the biofloc or the biofilm surface is positive. The greater the parameter α is, the lower the substrate concentration in the biofilm surface or center of the biofloc is. For example, when $\alpha = 10$, the minimum dimensionless substrate concentration in the interior of the biofilm or biofloc is 0.9 for $X^* \geq 0$. On the other hand, note that when $\alpha > 1$ in Figs.2.6 and 2.8, the effectiveness factor is no longer greater than 1, because of the decrease of substrate concentration gradients with increasing α at a constant Thiele modulus (Fig. 14-15).

2.7 The Effect of the Parameter β on the Effectiveness Factor

The effects of the parameter β on the effectiveness factor in the biofilm and biofloc are shown in Figs. 2.2 and 2.4, respectively. An increase of β results in an enhancement of the effectiveness factor. This is because an increase of β is associated with an increase of the substrate concentration, which causes faster diffusion and reaction rate, and a decrease of the saturation constant, which accelerates reaction rate according to Eq. (1.2). However, since the reaction rate accelerates both on the surface and in the interior of bioparticles, the main effect should be enhancement of intraparticle diffusion. Fig. 2.16 shows a dimensionless concentration profile at the Thiele modulus 10 with the same conditions as Fig. 2.2. Form Fig. 2.16 it is seen that at a constant Thiele modulus the dimensionless concentration S^* has a greater value at a greater β for the entire dimensionless length. Therefore, the driving force for mass transfer in the interior of the

biofilm and biofloc at a greater β is greater than that at a smaller β. Consequently, the intraparticle diffusion rate and the effectiveness factor increase. On the other hand, although the concentration gradients at the surface $r^* = 1$ decrease with increasing β at a constant Thiele modulus (Fig. 2.17), the effectiveness factor still increases with the parameter β.

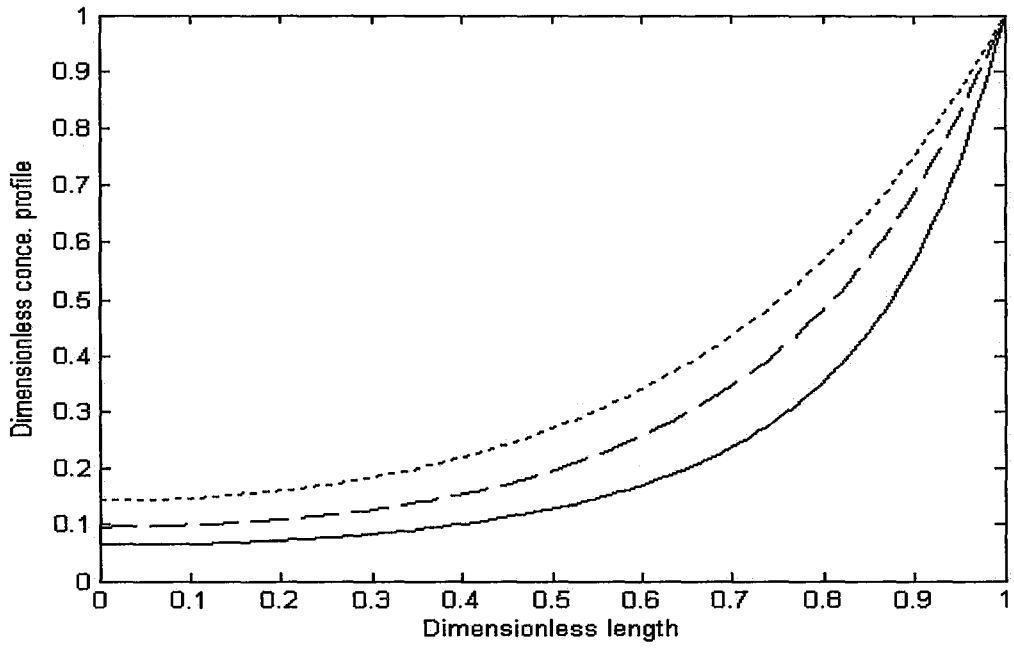

Fig. 2.16 Dimensionless concentration profile in biofilms and bioflocs. Solid line β =1, Dashed line β=5, Dotted line β=10 (α=1, ϕ_l=10).

2.8 The effects of particle geometry on the effectiveness factor

Referring to Fig. 2.18, it is found that the effectiveness factor for biofilms is greater than that for bioflocs. This is because a sphere has a smaller ratio of external area to volume than a slab. Note also that there are greater differences in the effectiveness factor for these two geometries in the middle range of the Thiele modulus. With increasing the

Thiele modulus, the two curves appear to converge asymptotically. This is similar to the result obtained for the first order solutions with the two geometries [Petersen, 1965].

2.9 Comparison of the Numerical and Approximate Solutions of Eqs. (2.15) and (2.29) for Biofilms

The approximate solutions of Eqs. (2.15) and (2.29) for the effectiveness factors in biofilms at $S^*_c = 0$ and $r^* = 0$ have been derived as Eqs. (2.25), (2.34), and (2.35). Their values have been plotted in Fig. 2.19 for a comparison with the corresponding numerical solutions. It can be seen that when the Thiele modulus is greater than 5, the approximate solutions are the same as the numerical solutions. But at smaller values of the Thiele modulus, there are larger differences between the two solutions. This error is caused by the assumption $S^*_c = 0$ at $r^* = 0$, which is only valid at large values of the Thiele modulus. In addition, to compare the results of the numerical solution of Eqs. (2.15) and (2.29) and the analytic solutions of Eqs. (2.24), (2.32) and (2.33) for the biofilm, we used the numerical method to solve Eqs. (2.15) and (2.29), and obtained the value of S^*_c at $r^* = 0$ so that the effectiveness factors in Eqs. (2.24), (2.32), and (2.33) can be calculated. The values from both methods were found to be the same.

2.10 Comparison of the Effectiveness Factors from Monod, Zero, and First Order Rate Expressions

It is well known that when the saturation coefficient K_S in the Monod equation is much larger than the substrate concentration, the Monod equation reduces to a first order rate expression; and when it is much smaller than a substrate concentration, the Monod

equation reduces to a zero order rate expression. Therefore, Eq. (2.15) can be expressed as follows for the first order rate and zero order rate, respectively:

$$\frac{d^2S^*}{dr^{*2}} = \phi_l^2 S^* \left[\alpha\left(S^* - 1\right) + 1\right] \tag{2.56}$$

$$\frac{d^2S^*}{dr^{*2}} = \frac{\phi_l^2}{\beta}\left[\alpha\left(S^* - 1\right) + 1\right]. \tag{2.57}$$

For Eq. (2.56) the substrate concentration gradient can be obtained by an integration method similar to that for Eq. (2.15), with integration limits $dS^*/dr^* = (dS^*/dr^*)_{r^*=1}$ and $S^* = 1$ at $r^* = 1$, and $dS^*/dr^* = (dS^*/dr^*)_{r^*=0} = 0$ and $S^* = S^*_c$ at $r^* = 0$, giving

$$\frac{dS^*}{dr^*} = 2^{0.5}\phi_l^2\left[\frac{\alpha}{3}\left(1 - S_c^{*3}\right) - \frac{\alpha}{2}\left(1 - S_c^{*2}\right) + 1 - S_c^*\right]. \tag{2.58}$$

The effectiveness factor is

$$\eta = \frac{1}{\phi_l^2}\left(\frac{dS^*}{dr^*}\right)_{r^*=1}. \tag{2.59}$$

Using MATLAB to solve Eq. (2.56) at $\alpha = 1$, the effectiveness factor can be obtained either directly or from S_c^* using Eqs. (2.58) and (2.59). The results are shown in Fig.2.20.

For Eq. (2.57) the substrate concentration gradient at $r^* = 1$, and the effectiveness factor are expressed as

$$\left(\frac{dS^*}{dr^*}\right)_{r^*=1} = \frac{2^{0.5}\phi_l}{\beta^{0.5}}\left[\frac{\alpha}{2} + 1 - \alpha - S_c^*\left(\frac{\alpha}{2}S_c^* + 1 - \alpha\right)\right]^{0.5} \tag{2.60}$$

$$\eta = \frac{\beta}{\phi_l^2}\left(\frac{dS^*}{dr^*}\right)_{r^*=1} \tag{2.61}$$

where S^*_c in Eq. (2.60) is determined by

$$\left(\frac{\beta}{2}\right)^{0.5}\phi_l \ln\left\{\frac{\alpha S_c^* + 1-\alpha}{1+(2\alpha)^{0.5}\left[\frac{\alpha}{2}+(1-\alpha)-S_c^*\left(\frac{\alpha}{2}S_c^*+1-\alpha\right)\right]^{0.5}}\right\}+1=0. \qquad (2.62)$$

When α =1, the effectiveness factor can be simply expressed as

$$\eta = \frac{\tanh\left(\frac{\phi_l}{\beta}\right)}{\frac{\phi_l}{\beta}} \qquad (2.63)$$

as shown in Fig. 2.20. From Fig. 2.20, it is found that all the curves representing the Monod equation are located between the two curves for the first order and zero order rates. With increasing or decreasing β, the effectiveness factor for the Monod model approaches those of the zero or first order model, respectively. This is because when β <<1 or β >> 1, Eq. (2.15) reduces to Eq. (2.56) or Eq. (2.57), respectively

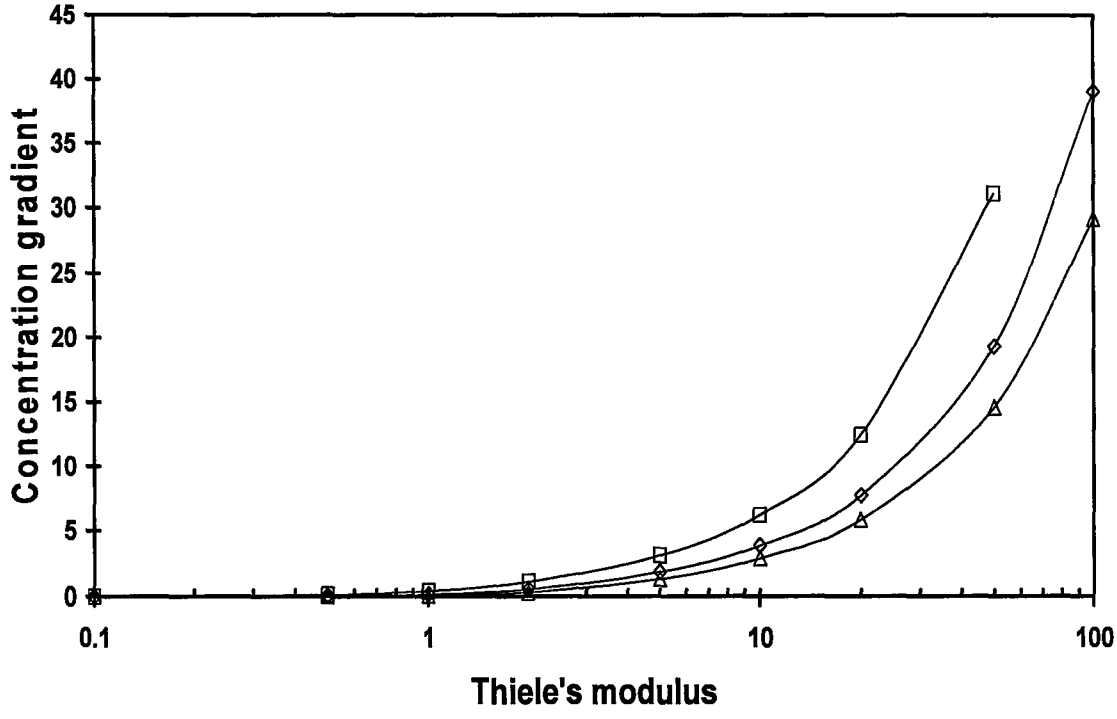

Fig. 2.17 Effects of Thiele's modulus and β on concentration gradient at $r^*=1$ in biofilms (Monod Eq.) □ β=1, ◊ β=5, Δ β=10 (other condition as Fig. 2.2 α=1).

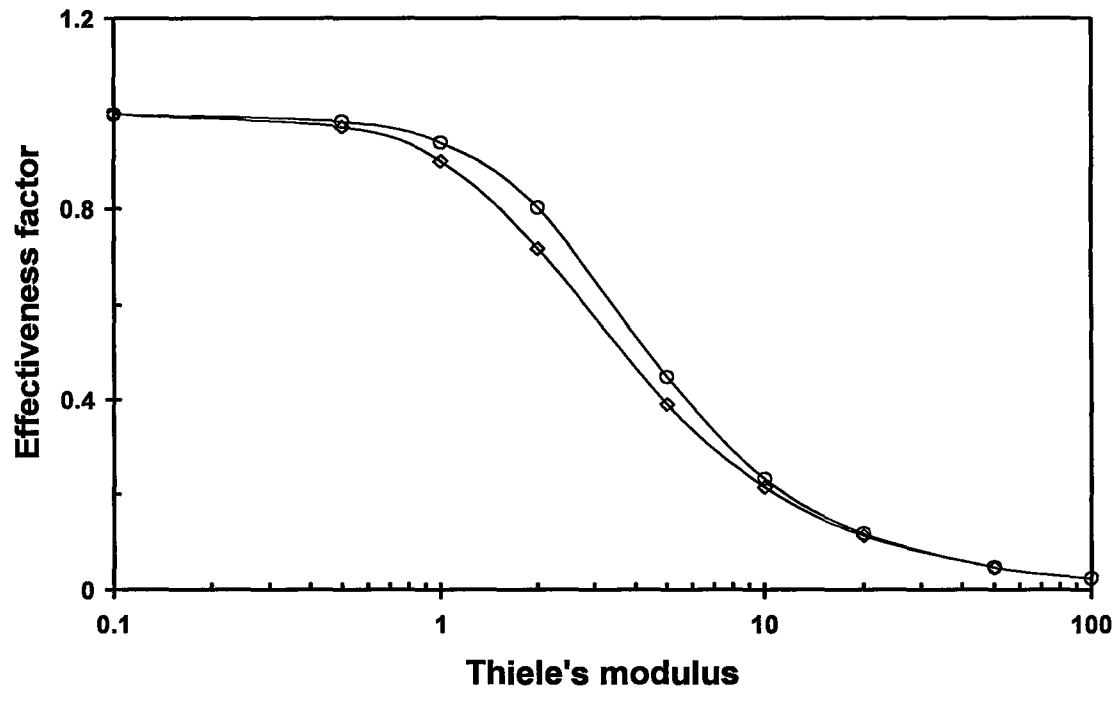

Fig. 2.18 Effect of particle geometry on effectiveness factor. ◊ biofilms, ○ bioflocs (α=1, β=5).

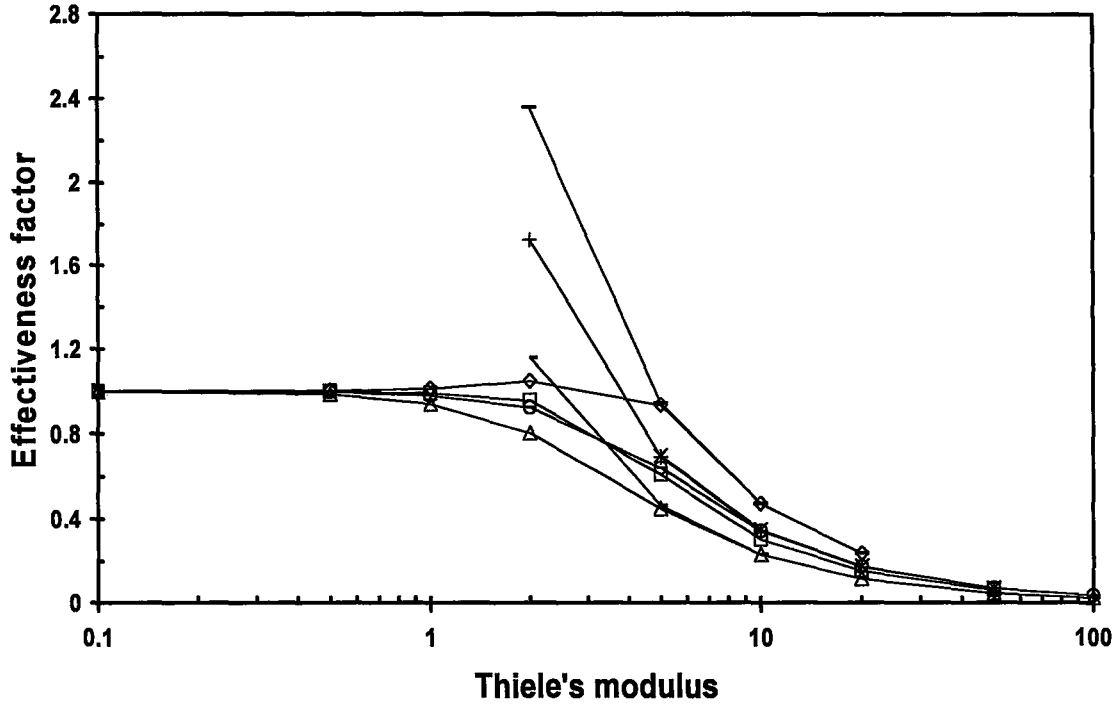

Fig. 2.19 Comparison of numerical solutions of Eqs. 2.15 and 2.29 and approximate solutions (Eqs. 2.25 and 2.34) for biofilms. □ Eq. 2.15, × Eq. 2.25, (α=0); Δ Eq. 2.15, - Eq. 2.25, (α=1); ◊ Eq. 2.29, – Eq. 2.34, (α=0); ○ Eq. 2.29, + Eq. 2.34, (α=1) (other conditions: β=5, δ=5).

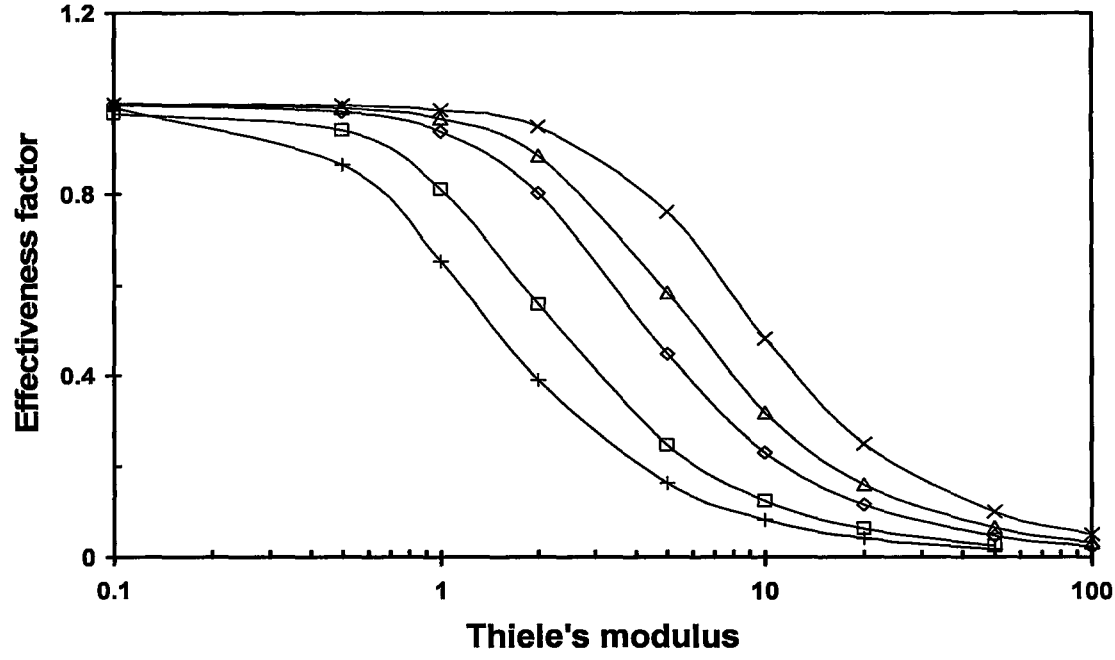

Fig. 2.20 Comparison of effectiveness factors for Monod, zero, and first order Eqs. Monod Eq. α=1: □ β=1, ◊ β=5, Δ β=10, zero order, α=1: × β=5, first order, α=1: +.

Chapter Three

Application of Effectiveness Factor to UASB Reactor Design

3.1 Microbial Aggregation

A common characteristic of microorganisms is a tendency to aggregate so as to develop bioflocs, or to attach themselves to available surfaces, thus forming biofilms with aid of extracellular polymeric matrices in many natural, industrial and medical environments [Costerton et al., 1987]. Therefore, a biofloc or biofilm can be considered as a community of microorganisms, including bacteria, fungi, yeasts, protozoa, and other microorganisms. The formation of bioflocs and biofilms is significant in our lives because they occur in nearly every industrial water-based process, including fermentation, water treatment and distribution, wastewater treatment, pulp and paper manufacturing, and operation of cooling towers.

In both natural and industrial environments, microorganism aggregation can be classified into two types: suspended bioflocs and attached biofilms. Bioflocs and biofilms differ in key ways: for example, biofilms adhere to a supporting wall, while bioflocs are formed without a supporting wall. However, they have one common characteristic that often needs to be considered explicitly in microbial kinetics: aggregation can create significant gradients in substrate concentrations. Because the mass transport of substrates from the outside of an aggregate to its inside is driven by concentration differences, microorganisms inside such aggregates are often exposed to substrate concentrations substantially lower than at the outer surface. Therefore, the rates of substrate utilization and cell growth are not uniform, but depend on the cell's location within the aggregate.

In the wastewater treatment process, two typical suspended biofloc processes are: activated sludge and upflow anaerobic sludge blanket (UASB), while the biofilm filter represents one of the attached growth biofilm processes. The functions of aggregated bioflocs and biofilms in wastewater treatment can be illustrated by an example of the activated sludge process. In this process, the microorganism's natural aggregation forms bioparticles which render them easily separable from the effluent water. Meanwhile, there is a large biomass concentration to be maintained in the treatment system, which enables it to bear a large COD (chemical oxygen demand) loading. Both functions provide good effluent quality for wastewater treatment.

In a manufacturing environment such as fermentation, the interaction between microorganisms and surfaces in the fermenter makes these surfaces become biologically active due to the adhesion of microorganisms, such that the isolated points of growth gradually form a continuous layer of microbial mass. The formation of biofilms and bioflocs affect the operating characteristics, the mass and heat transfer characteristics, the power requirements and the productivity of a fermenter. Some bioreactors are designed to promote biofilm growth to enhance production efficiency, because the productivity of growth-associated with fermentations depends on the quantity of biomass contained in the fermenter (microbial hold-up). In addition to an increase of microbial hold-up, the formation of bioflocs and biofilms also has other benefits: easier separation of biomass from the fermentation broth, and improvement of rheologic characteristics at high biomass concentrations [Atkinson et al., 1976]. One of the disadvantages of formation of bioflocs and biofilms during fermentation is that the overall specific substrate uptake is

likely to be reduced, because of diffusional limitations on the transfer of substrate through the bioflocs and biofilms.

3.2 Factors of Granular Formation in the UASB

Although bioflocs and biofilms are formed by various kinds of microorganisms, their formation mechanisms are similar. An example is granular formation by bacteria in an anaerobic culture. It was found that the various physical, chemical, and biological factors affect the granulation process. All known models for the above mechanisms, taken separately, seem unable to depict the entire anaerobic granulation process in a reasonable manner. All these factors should be considered in combination. Based on the existing mechanisms for the formation of anaerobic granules, a general four-step model for anaerobic granulation has been proposed as follows [Liu, et al., 2003].

Step 1: Bacterium-to-bacterium contact or bacterial attachment to nuclei by physical movement. The forces caused by physical movement are: hydrodynamic force, diffusion force, gravitation, thermodynamic forces, such as Brownian motion, and cell mobility due to flagella, cilia and pseudopods.

Step 2: Stable multicellular contacts by initial attractive forces. These attractive forces are 1) Physical forces such as Van der Waals forces, opposite charge attraction, thermodynamic forces including free surface energy (surface tension), and hydrophobicity. It follows from the thermodynamic theory that an increase in the hydrophobicity of cellular surfaces will lead to a corresponding decrease in the excess Gibbs energy of the surface, which in turn promotes cell-to-cell interaction and further serves as a driving force for bacterial aggregation out of the liquid phase (hydrophilic

phase). Therefore, the hydrophobicity of the bacterial surface plays a crucial role in the initiation of biofilms and anaerobic granules [Tay, et al., 2000; Teo, et al., 2000; Mahoney, et al., 1987; Van Loosdrecht, et al., 1987]. 2) Chemical forces such as hydrogen bonding, formation of ionic pairs and triplets, interparticulate bridges and so on. 3) Biochemical forces such as cellular surface dehydration, cellular membrane fusion, and signaling and collective action in bacterial communities.

Step 3: Cell aggregation matures by microbial forces. It was found that production of extracellular polymers, such as exopolysaccharides secreted by bacteria, could promote growth of cellular clusters. Further metabolic changes also promote the cell-cell interaction, and results in a highly organized microbial structure.

Step 4: A steady state three-dimensional structure of microbial aggregates shaped by hydrodynamic shear forces. The microbial aggregates will be finally shaped by hydrodynamic shear forces to form a certain structured community. The outer shape and size of the microbial aggregates are determined by the interactive strength and pattern between the aggregates and the hydrodynamic shear forces, microbial species and substrate loading rate.

This four-step mechanism is basic to the understanding of anaerobic granulation. It should be realized that the identification of gross phenomena in relation to anaerobic granulation is relatively easy, but understanding the mechanism responsible for anaerobic granulation at the molecular or genetic level is very difficult.

3.3 Simulation of Substrate Concentration Profile in the UASB

The UASB process was first developed in the late 1970s in the Netherlands by Lettinga and his coworkers [Lettinga et al., 1980]. In the past two decades it has been successfully used to treat various kinds of organic wastewaters. To design a UASB reactor, some important factors should be considered: 1) wastewater characteristics in terms of composition and solids contents, 2) volumetric organic load, 3) upflow velocity, 4) reactor volume, 5) physical features including the influent distribution system, and 6) the gas collection system [Metcalf & Eddy, 2003]. These factors need to be included in a design equation which is often based on a flow model and a reaction kinetic model. In operating reactors, hydraulics and chemical reactions occurring in the UASB often deviate from ideal behavior under the influence of various complicating factors. As with other designs of liquid-solid reactors, to correct these deviations, an effectiveness factor is introduced to the design equation in which the actual reactor volume is set equal to the ideal reactor volume divided by the effectiveness factor, which usually is less than one. The effectiveness factor is a combination of all the factors that cause the non-ideal behaviors in a reactor because it is difficult to consider these factors individually. The value of the effectiveness factor for a UASB reactor is recommended to be 0.8-0.9 [Metcalf & Eddy, 2003]. The granulation process occurring in a UASB greatly enhances biomass concentration in the reactor, and allows a higher organic loading rate than the conventional activated sludge process. However, the formation of granular bioparticles increases mass transfer resistance of the substrate for its transport into the interior of the bioparticles from the bulk solution, resulting in a decline of the effectiveness factor. This constitutes an important part affecting the effectiveness factor. Therefore, a study of the

mass transfer process of the substrate in the interior of the bioparticles can be used to reasonably estimate the effectiveness factor. For example, Chou and Huang [2005] used this approach to estimate the effectiveness factor of the bioparticles for phenol diffusion in a UASB process using a full mixing model plus a diffusion-reactor model. We will make a simulation of the substrate concentration profile along the height of the UASB column, using a plug flow model plus a diffusion-reactor model in which the Andrews model and the modified Andrews model including the effect of cell density were applied to the design equation of the UASB, and the effectiveness factors for the two models are estimated based on Chou and Huang's experimental data [2005].

1. Design parameter [Chou and Huang, 2005]

The following data are taken from Chou and Huang [2005].

Flow rate u = 0.5 m/h

Granular size (mm): lower section of the UASB = 1.52, middle section = 1.35, upper section = 0.71.

Biomass density (mg VSS/l): lower section of the UASB = 43110, middle section = 41650, upper section = 40470.

Height of the UASB column (m): 0.69

Cross section area of the UASB column (m × m): $0.06 \times 0.06 = 0.0036\ m^2$

Phenol concentration at entry of the UASB $S_0 = 1670$ mg/l

Phenol concentration at exit of the UASB $S_e = 28.3$ mg/l

Phenol diffusivity $D_f = 8.48 \times 10^{-5}\ m^2/d$

Parameters of the Andrews cell growth model

Saturation coefficient $K_S = 19.2$ mg/l

Inhibition coefficient K_I = 344 mg/l

Ratio k of the maximum specific growth rate and yield coefficient = 0.3

Using the assumption that:

Maximum specific growth rate μ_m = 0.4824 /d, the above gives a yield coefficient of

$Y_{X/S} = \mu_m/k$ = 1.608 mg phenol/mg VSS.

2. Design Equations

Making a mass balance of substrate (phenol) in the UASB, an ordinary differential equation can be obtained assuming plug flow in the UASB column:

$$\frac{dF_S}{dV} = -R_p \tag{3.1}$$

where F_S is the mass flow rate of substrate, V is the UASB volume, and R_p is the actual reaction rate for granular particles. Since

$$F_S = SQ \tag{3.2}$$

$$V = Az \tag{3.3}$$

and

$$u = \frac{Q}{A} \tag{3.4}$$

where S is the substrate concentration at a given height z from the bottom of the UASB, Q is the volumetric flow rate, A is the cross section area of the UASB, and u is the feeding flow rate. The reaction rates for the Andrews and the modified Andrews models (Chapter Two), respectively, are

$$R_p = \frac{\eta \mu_m S X_0}{Y_{X/S}\left(K_S + S + S^2/K_I\right)} \tag{3.5}$$

$$R_p = \frac{\eta \mu_m S}{Y_{X/S}\left(K_S + S + S^2 / K_I\right)}\left[Y_{X/S}\left(S - S_0\right) + X_0\right] \tag{3.6}$$

where η is the effectiveness factor, and X_0 is the biomass density at the UASB entry. Substituting Eqs. (3.5) and (3.6) into Eq. (3.1), yields

$$u\frac{dS}{dz} = \frac{\eta \mu_m S X_0}{Y_{X/S}\left(K_S + S + S^2 / K_I\right)} \tag{3.7}$$

$$u\frac{dS}{dz} = \frac{\eta \mu_m S}{Y_{X/S}\left(K_S + S + S^2 / K_I\right)}\left[Y_{X/S}\left(S - S_0\right) + X_0\right]. \tag{3.8}$$

From Eqs. (3.7) and (3.8), we know that the substrate concentration along the column height is a function of the effectiveness factor and the column height when μ_m, K_S, K_I, $Y_{X/S}$, u, and X_0 are constant. Furthermore, when the effectiveness factor is constant, the substrate concentration decreases along the column height, while at a constant column height, the substrate concentration increases with a decrease in the effectiveness factor. Using MATLAB [MathWorks, 2002], Eqs. (3.7) and (3.8) can be solved. We obtain the effectiveness factors 0.80 and 0.85 for the Andrews model and the modified Andrews model, respectively. The phenol concentration profiles along the UABS height for two cases are shown in Fig. 3.1. In Chou and Huang's paper [2005], the full mixing flow model was used. Therefore, no phenol concentration profile along the column height could be obtained. In fact, since the UASB reactor is a column, the plug flow model (Eqs. (3.7) and (3.8)) is a more reasonable description of the physical system. From Fig. 3.1, although the effectiveness factors are obviously different for the Andrews model (0.8) and the modified Andrews model (0.85), the two curves for the concentration profile along the column height are much closer.

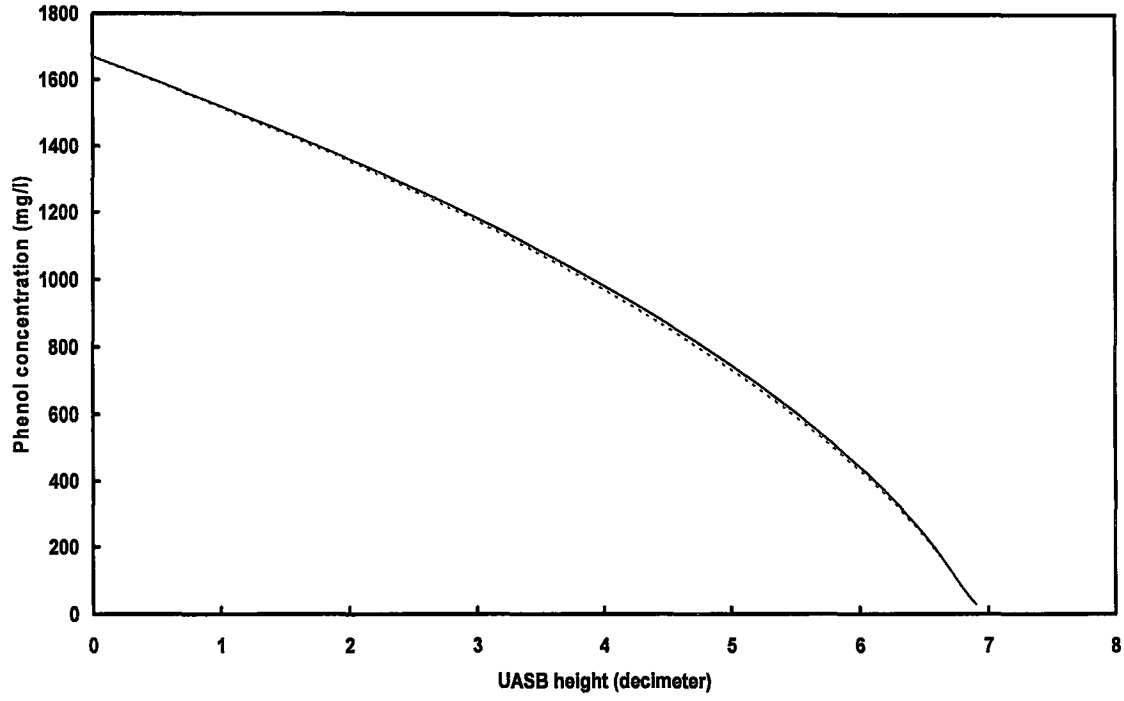

Fig. 3.1 Phenol concentration profiles along the height of UASB column. Solid line and dotted line denote the Andrews model (η=0.8) and modified Andrews model (η=0.85), respectively.

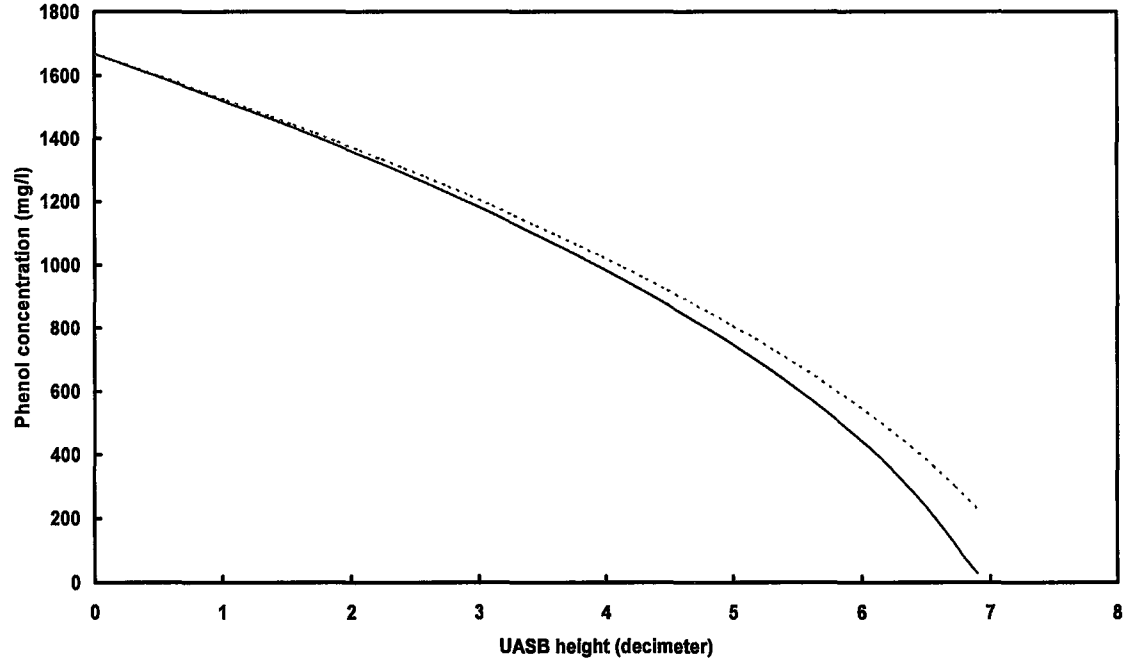

Fig. 3.2 Phenol concentration profiles along the height of UASB column for the effectiveness factor 0.8. Solid line and dotted line denote the Andrews model (phenol concentration at the exit is 28.3 mg/l) and modified Andrews model (phenol concentration at the exit is 228 mg/l), respectively.

This difference in the effectiveness factor will cause a greater difference in the substrate concentration at the column exit. For example, if we apply the effectiveness factor 0.8 to Eqs. (3.7) and (3.8), respectively, the two phenol concentration profiles along the column height are indicated in Fig. 3.2 in which the phenol concentration at the exit for Eq. (3.8) (228 mg/l) is much higher than that for Eq. (3.7) (28 mg/l). This is the accumulated effect of the small concentration difference along the height of the UASB. It is expected that the higher the column, the greater the difference in the substrate concentration at the column exit.

3.4 Sensitivity Analysis of the Parameters

To compare the effect of changes of the design parameters on the output substrate concentration from the UASB column, a sensitivity analysis was done for the Andrews parameters.

1. Initial values of the parameters

The six parameters u, K_S, K_I, $Y_{X/S}$, μ_m, and η in Eq. (3.7) were chosen. Their initial values are

Flow rate u = 0.5 m/h

K_S = 19.2 mg/l

K_I = 344 mg/l

Yield coefficient $Y_{X/S}$ = 1.608 mg phenol/mg VSS

Maximum specific growth rate μ_m = 0.4824 /d

Effectiveness factor η 0.8

2. Calculated procedure

The range in the values of most of the parameters was +/- 50 % of these initial values. The parameter K_S had a larger change range because of its insensitivity to substrate concentration. These ranges of the values were substituted into Eq. (3.7) and the substrate concentrations at the UASB column exit were calculated, yielding a relative change of the substrate concentration at the exit and entry of the UASB column:

$$\frac{\Delta S}{S_0} = \frac{S_0 - S_e}{S_0} \tag{3.9}$$

The parameter relative change is defined as

$$\frac{\Delta p}{p_0} = \frac{p_0 - p}{p_0} \tag{3.10}$$

where p_0 and p are the initial and changed parameter value, respectively. The calculated results are shown in Fig. 3.3.

The sensitivity order of the parameters is $\mu_m = \eta > K_I > u = Y_{X/S} > K_S$. This sensitivity order is different from that of Chou and Huang [2005]. Their calculation indicated that K_S was more sensitive than K_I to substrate concentration change. This difference may result from the different flow models (the plug model in our study and the full mixing model in theirs). In addition, the parameter sensitivity order is related to the initial substrate concentration. When the substrate concentration changes, the order may change correspondingly. An example, with detailed analysis and explanation, is given in Chapter Four. Note that for the sensitivity analysis $\mu_m = \eta$ and $u = Y_{X/S}$. This is because μ_m and η, and u and $Y_{X/S}$, can be combined, respectively, into two parameters in Eq. (3.7).

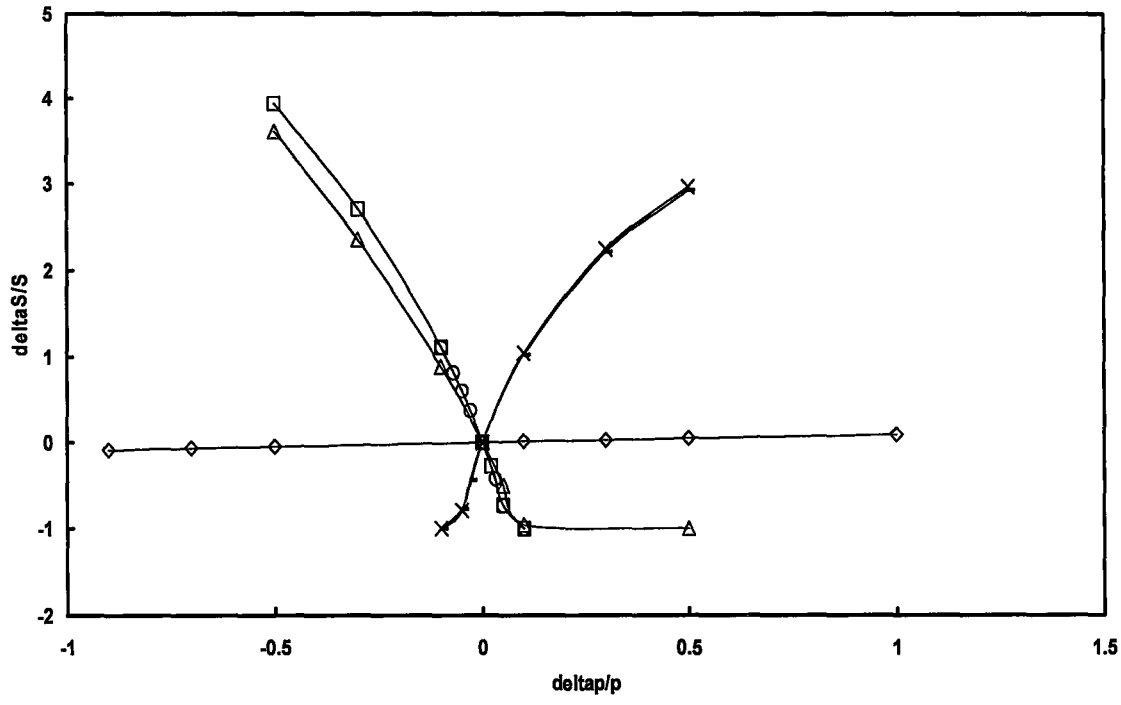

Fig. 3.3 Parameter sensitivity in the Andrews model. □ μ_m, ◊ K_S, Δ K_I, × $Y_{X/S}$, – u, O η.

Chapter Four

Parameter Identification and Estimation of the Integrated Andrews Model

4.1 PRAMUS and Arithmetic Mean Parameters in Replicated Experiments

In order to design a bioreactor or wastewater treatment process, it is necessary to accurately describe microorganism growth kinetics. This is because the productivity of a bioreactor is dependent on cell quantity, which in turn is proportional to product quantity in a manufacturing process. For a wastewater treatment process, microorganism growth reflects the ability for degradation of waste organic compounds. A number of cell growth models have been proposed. Among them, the most commonly used models are the Monod and Andrews equations. Both the Monod and the Andrews equations are similar to the classical Michaelis-Menten model and its inhibition type. Unlike the Michaelis-Menten model, which represents the enzyme reaction mechanism, the Monod and Andrews equations do not represent a specific mechanism or pathway for degradation. Both models indicate a correlation of the specific growth rate μ of the microorganism with an environmental variable, namely the growth-limiting substrate concentration S. The objective of a biokinetic experiment is to establish a quantitative relationship between the specific growth rate of the biomass and the growth-limiting substrate concentration, *i.e.* to determine the parameters in the biokinetic models. Generally, the parameters of the biokinetic models are often estimated based on measurements of concentration changes in the biomass and the substrate over time.

The general procedure for parameter estimation is as follows: first, a set of values for the specific growth rate of cells versus the growth-limiting substrate concentration is obtained from a batch or chemostat experiment; second, a set of initial trial values of

parameters are selected based on previous experience; third, the predicted specific growth rates are computed by substituting the experimental substrate concentrations and the trial parameters into the chosen model; fourth, the residual sum of squares (RSS, an objective function) between the observed and predicted specific growth rates is evaluated; and fifth, the optimized parameters are determined by changing the parameter values so as to minimize the RSS.

To ensure reliability of the experimental data, biokinetic experiments often include numerous replicated tests. If the experimental conditions are the same for all the replicated tests, the usual method is to take the arithmetic average values of these data, substitute them into the chosen model, and determine the model parameters. But if the experimental conditions vary, for example, with different initial substrate concentrations, or different experimental levels of noise, each set of experimental data should be fitted separately to the model, and sets of several model parameters will be obtained for these replicated tests. In order to combine a set of model parameters into a single parameter, two methods can be used. The first is called the Parameter values Representing the Average observed biokinetic (μ-S) response of the biomass (PRAMUS values) proposed by Magbanua et al. [1998]. It is defined as:

$$\mu_{av} = \frac{1}{n}\sum_{i=1}^{n}\frac{\mu_{mi}S}{K_{Si}+S+S^2/K_{Ii}} = \frac{\mu_{mP}S}{K_{SP}+S+S^2/K_{IP}} \tag{4.1}$$

where n is the number of replicated tests, μ_{av} is the average specific growth rate predicted by n replicated parameter sets at a given substrate concentration S, the subscript i refers to the i-th test, and the subscript P refers to PRAMUS value. The PRAMUS parameters are generally determined by the following procedure. 1) Each set of test data (μ-S) is substituted into the Andrews model, and the model parameters of μ_{mi}, K_{Si}, and K_{Ii} are

determined for each test, 2) the μ_{av} values for all experimental points are obtained through the left-hand term of Eq. (4.1), 3) the PRAMUS parameters μ_{mP}, K_{SP}, and K_{IP} are determined by a fitting process of μ_{av} and S at all the experimental points. The second method uses the arithmetic mean parameter for all replicated tests. It is defined as

$$p_{ar} = \frac{1}{n}\sum_{i=1}^{n} p_i \tag{4.2}$$

where p is the model parameter, which in particular denotes K_S, K_I, and μ_m in the Andrews model, and the subscript 'ar' denotes the arithmetic mean value for n tests. The first two steps to determine these parameters are the same as in the above procedure, but the third step uses Eq. (4.2) rather than Eq. (4.1).

4.2 A Comparison of PRAMUS and Mean Parameters of the Andrews Model

We fix a basic set of parameter values assuming that cell growth can be precisely described by the following the Andrews equation:

$$\mu = \frac{\mu_m S}{K_S + S + S^2 / K_I} \tag{4.3}$$

where μ_m is the maximum specific growth rate (0.15 /d), K_S is the saturation coefficient (19.2 mg/l), and K_I is the inhibition coefficient (344 mg/l) [Chou and Huang, 2005]. The noise levels associated with the determination of the substrate concentration for the various tests were taken to be +/- 5, 10, 20 30 % of the noise free values. For this noise ranges, the measured noise for each point was produced using a random number generator of Excel based on a uniform distribution. Each set of synthetic data containing noise were fitted for the Andrews equation (Eq. (4.3)), and the Andrews parameters μ_m, K_S, and K_I were determined (Table 4.1). These curves are presented in Fig. 4.1.

Table 4.1 The PRAMUS and arithmetic mean parameters of the Andrews model

	K_S (mg/l)	K_I (mg/l)	μ_m (/d)	$Y_{X/S}$	RSS (10^{-6})
Noise 0 %	19.2	344	0.150	0.5	0
Noise +/-5 %	18.2	360	0.147	0.5	4.289
Noise +/-10 %	18.9	342	0.149	0.5	37.50
Noise +/-20 %	14.8	374	0.142	0.5	73.73
Noise +/-30 %	13.0	419	0.135	0.5	332.5
PRAMUS	18.2	361	0.147	0.5	49.06
Mean	16.2	373	0.143	0.5	112.0

In order to compare the difference between the Andrews parameters obtained using the PRAMUS and arithmetic mean methods, the PRAMUS and arithmetic mean parameters of the Andrews model were calculated by Eqs. (4.1) and (4.2), respectively. The two curves are shown in Fig. 4.2, which also displays the arithmetic average specific growth rates μ_{av} (the left-hand term of Eq. (4.1)), which are the arithmetic average values of the specific biomass growth rate of the five curves at a constant substrate concentration shown in Fig. 4.1. From Fig. 4.2 it is seen that the curve of μ_{av} has the maximum deviation from that of the synthetic data that do not contain a noise component; the next highest deviation is associated with the arithmetic mean parameter from Eq. (4.2), while the PRAMUS curve show the lowest deviation from the noise free data. From the RSS column in Table 4.1, it can be seen that the RSS values (49.06) of PRAMUS are less than those (112.0) associated with the arithmetic mean parameter. This is because PRAMUS parameters are obtained by doing one additional parameter optimization as compared to the arithmetic mean parameters. From Eq. (4.2) a mean parameter is just the arithmetic

average value of n values of the same parameter, while a set of PRAMUS parameters is obtained by fitting these parameters to minimize the RSS between μ_{av} and S from the right-hand term of Eq. (4.1). It is clear that the PRAMUS parameters have been optimized one more time than the arithmetic mean parameters, resulting in the better simulated curve.

4.3 Sensitivity Coefficient and Parameter Identification

The influence of parameter perturbation on the response of the dependent variable can be indicated by a sensitivity coefficient [Beck and Arnold, 1977]. A sensitivity coefficient is the first partial derivative of the model function S with respect to a model parameter p_i, *i.e.*

$$Sensitivity\ \ Coefficient = \frac{\partial S}{\partial p_i} \tag{4.4}$$

One of the main functions of the sensitivity coefficient is to determine parameter identification of models, because in some cases not all the model parameters can be uniquely quantified for all possible conditions. A criterion of parameter identification has been demonstrated [Beck and Arnold, 1977]: parameters can be estimated if the sensitivity coefficients over the range of the observations are linearly independent. This criterion can be expressed by the following equation [Beck and Arnold, 1977].

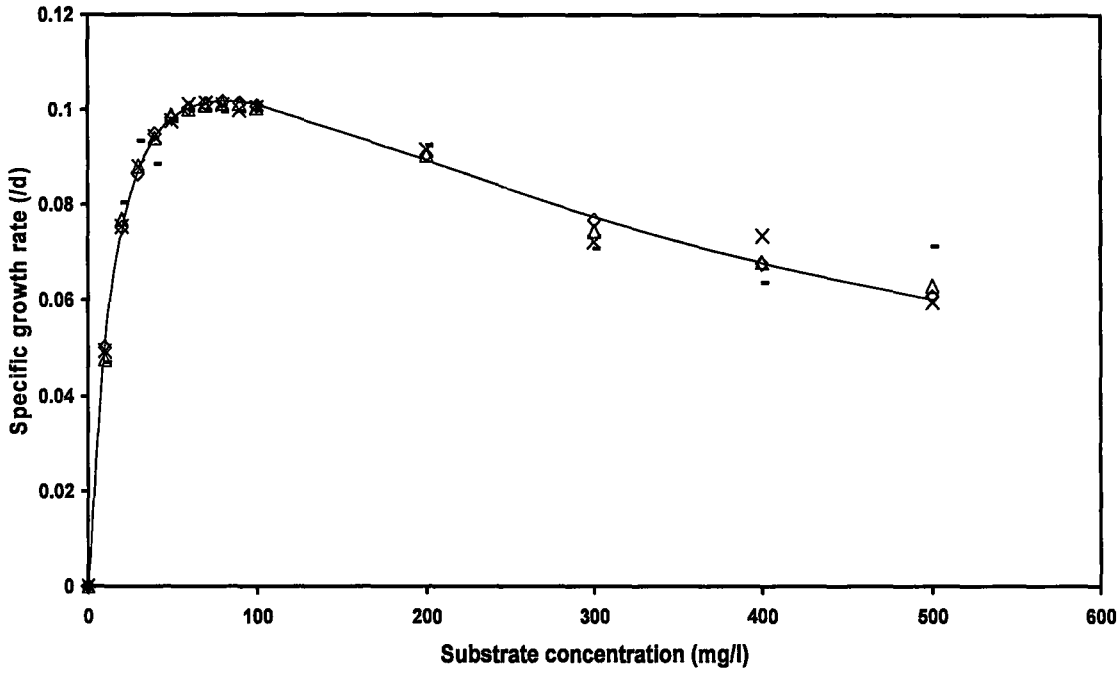

Fig. 4.1 Effect of noisy level on the Andrews model. Solid line 0 % noise, ◊ 5 % noise, Δ 10 % noise, × 20 % noise, - 30 % noise.

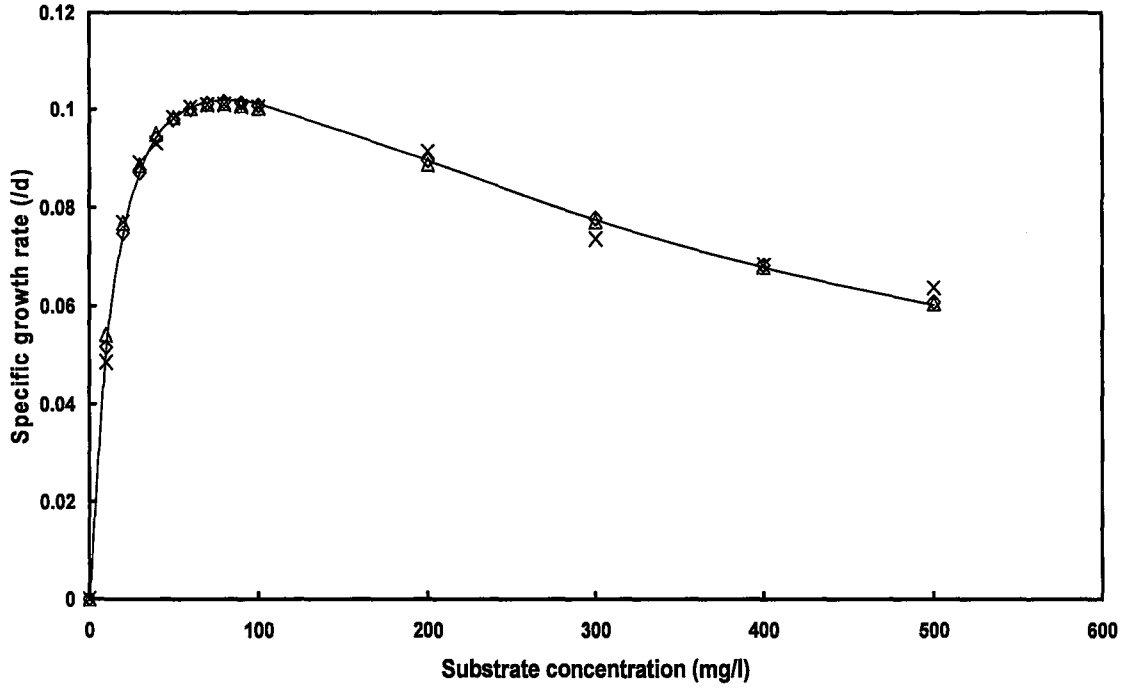

Fig. 4.2 A comparison of the parameters of PRAMUS, arithmetic mean and μ_{av}. Solid line 0 % noise, ◊ PRAMUS, Δ arithmetic mean, × $\mu_{av.}$

$$C_1 \frac{\partial S}{\partial p_1} + C_2 \frac{\partial S}{\partial p_2} + ... + C_i \frac{\partial S}{\partial p_i} + ... + C_n \frac{\partial S}{\partial p_n} = 0 \tag{4.5}$$

where C_i are constants. If the n constants C_i that are not all zero can satisfy Eq. (4.5), then the n parameters are linearly dependent, *i.e.* they cannot be estimated uniquely; otherwise, if the n constants in Eq. (4.5) are all zero, then the n parameters are linearly independent, *i.e.* they can be estimated uniquely [Haggard, 1972]. Furthermore, even if the n parameters are linearly dependent, it is still possible that n-1 of these parameters are linearly independent.

The following gives an example of sensitivity coefficients and parameter identification for the integrated Andrews model. Assuming that in a batch experiment, the change of substrate concentration as a function of time follows the Andrews model, and that the biomass is constant in the bioreactor (for example, in Chapter Four, the initial biomass concentration X_0 = 40470 mg/l, and the initial substrate concentration S_0 = 1670 mg/l. Because $X_0 >> S_0$, X_0 is considered constant), the substrate consumption rate can be expressed as

$$\frac{dS}{dt} = -\frac{\mu_m X_0 S}{Y_{X/S}\left(K_S + S + S^2 / K_I\right)} \tag{4.6}$$

which is called the differential Andrews equation. Integrating Eq. (4.6) with an initial condition $S = S_0$ at $t = t_0$, yields

$$K_S \ln\frac{S_0}{S} + S_0 - S + \frac{S_0^2 - S^2}{2K_I} = \frac{\mu_m}{Y_{X/S}} X_0 t \tag{4.7}$$

which is called the integrated Andrews equation. Rearranging Eq. (4.7) we can define the function f by

$$f(S,t) = K_S \ln\frac{S_0}{S} + S_0 - S + \frac{S_0^2 - S^2}{2K_I} - \frac{\mu_m}{Y_{X/S}} X_0 t \tag{4.8}$$

According to the definition of the sensitivity coefficient (Eq. (4.4)), the sensitivity coefficients for the parameters μ_m, K_S, K_I, and $Y_{X/S}$ are

$$\frac{\partial S}{\partial \mu_m} = -\frac{X_0 t}{Y_{X/S}\left(\frac{K_S}{S} + 1 + \frac{S}{K_I}\right)} \tag{4.9}$$

$$\frac{\partial S}{\partial K_S} = \frac{\ln\frac{S_0}{S}}{\left(\frac{K_S}{S} + 1 + \frac{S}{K_I}\right)} \tag{4.10}$$

$$\frac{\partial S}{\partial K_I} = -\frac{S_0^2 - S^2}{2K_I^2\left(\frac{K_S}{S} + 1 + \frac{S}{K_I}\right)} \tag{4.11}$$

$$\frac{\partial S}{\partial Y_{X/S}} = \frac{\mu_m X_0 t}{Y_{X/S}^2\left(\frac{K_S}{S} + 1 + \frac{S}{K_I}\right)}. \tag{4.12}$$

Considering the conditions required for parameter identification (Eq. (4.5)) for the sensitivity coefficients of μ_m, K_S, K_I, and $Y_{X/S}$ and substituting Eqs. (4.9)-(4.12) into Eq. (4.5), results in

$$C_1\frac{\partial S}{\partial \mu_m} + C_2\frac{\partial S}{\partial K_S} + C_3\frac{\partial S}{\partial K_I} + C_4\frac{\partial S}{\partial Y_{X/S}} = 0 \tag{4.13}$$

or

$$-C_1\frac{X_0 t}{Y_{X/S}\left(\frac{K_S}{S}+1+\frac{S}{K_I}\right)}+C_2\frac{\ln\frac{S_0}{S}}{\left(\frac{K_S}{S}+1+\frac{S}{K_I}\right)}$$
$$-C_3\frac{S_0^2-S^2}{2K_0^2\left(\frac{K_S}{S}+1+\frac{S}{K_I}\right)}+C_4\frac{\mu_m X_0 t}{Y_{X/S}^2\left(\frac{K_S}{S}+1+\frac{S}{K_I}\right)}=0 \qquad (4.14)$$

where C_1, C_2, C_3, and C_4 are constants. Clearly, when $C_1 = 1$, $C_2 = C_3 = 0$, and $C_4 = \frac{Y_{X/S}}{\mu_m}$ = constant, Eq. (4.14) is satisfied. Therefore, the parameters μ_m, K_S, K_I, and $Y_{X/S}$ of the integrated Andrews model (Eq. (4.7)) are linearly dependent, *i.e.* they cannot be identified theoretically. In fact, the parameters μ_m and $Y_{X/S}$ of Eq. (4.6) can be combined into a single parameter. Next we examine the identification of parameters μ_m, K_S, and K_I.

$$-C_1\frac{X_0 t}{Y_{X/S}\left(\frac{K_S}{S}+1+\frac{S}{K_I}\right)}+C_2\frac{\ln\frac{S_0}{S}}{\left(\frac{K_S}{S}+1+\frac{S}{K_I}\right)}-C_3\frac{S_0^2-S^2}{2K_0^2\left(\frac{K_S}{S}+1+\frac{S}{K_I}\right)}=0 \qquad (4.15)$$

It is impossible to find a set of constants (C_1, C_2, and C_3), not all zero, satisfying Eq. (4.15) over the entire variable range, because Eq. (4.15) involves three different functions X_0t, $\ln(S_0/S)$, and $(S_0^2 - S^2)$. Therefore, the parameters K_S, K_I, and μ_m of the integrated Andrews model are not linearly dependent, *i.e.* they are theoretically identifiable.

4.4 Parameter Identification Examination by Plotting Sensitivity Coefficients

In some situations the determination of linear dependence among the sensitivity coefficients may be difficult using the general Eq. (4.5). Also a direct observation may be convenient to examine parameter identification by plotting sensitivity coefficients against

time as suggested by Beck and Arnold [1977], Ellis et al. [1996], and Seagren et al. [2003]. If plotting the curves of two sensitivity coefficients as a function of time results in curves that are proportional to each other, *i.e.* they are multiples of one another, they are not identifiable theoretically. This method can be illustrated by the following two examples.

The first example (Case A) consists of a reactor operated with a large retention time (about 0.48 day). The parameters of Eq. (4.7) are μ_m = 0.15 /d, K_S = 19.2 mg/l, K_I = 344 mg/l, and $Y_{X/S}$ = 0.5 [Chou and Huang, 2005]. Two initial substrate concentrations of 1670 mg/l (S_0/K_S = 87) and 200 mg/l (S_0/K_S = 10.4) were studied. The other conditions are the same as those in Chapter Three. The second example (Case B) consists of a reactor operated with a short retention time (about 2.4 minutes). The parameters of Eq. (4.7) are μ_m = 0.15 /h, K_S = 0.07 mg/l, K_I = 11.1 mg/l, and $Y_{X/S}$ = 0.51 [Ellis et al., 1996]. Three initial substrate concentrations of 0.7 mg/l (S_0/K_S = 10), 0.07 mg/l (S_0/K_S = 1), and 0.007 mg/l (S_0/K_S = 0.1) were studied. The initial biomass concentration X_0 is 100 mg/l, and assumed to be constant [Ellis et al., 1996].

1. Solution of Eq. (4.7) for the initial substrate concentrations

Eq. (4.7) does not have an analytical solution and was solved numerically. Setting a series of decreasing substrate concentrations from the initial substrate concentration, five sets of numerical solutions for substrate concentration against time (the two sets for case A and the three sets for case B) were obtained by solving Eq. (4.7) using Excel. The results are shown in Figs. 4.3 and 4.4. It is found that the curve associated with a high initial substrate concentration (1670 mg/l of case A) is somewhat convex,

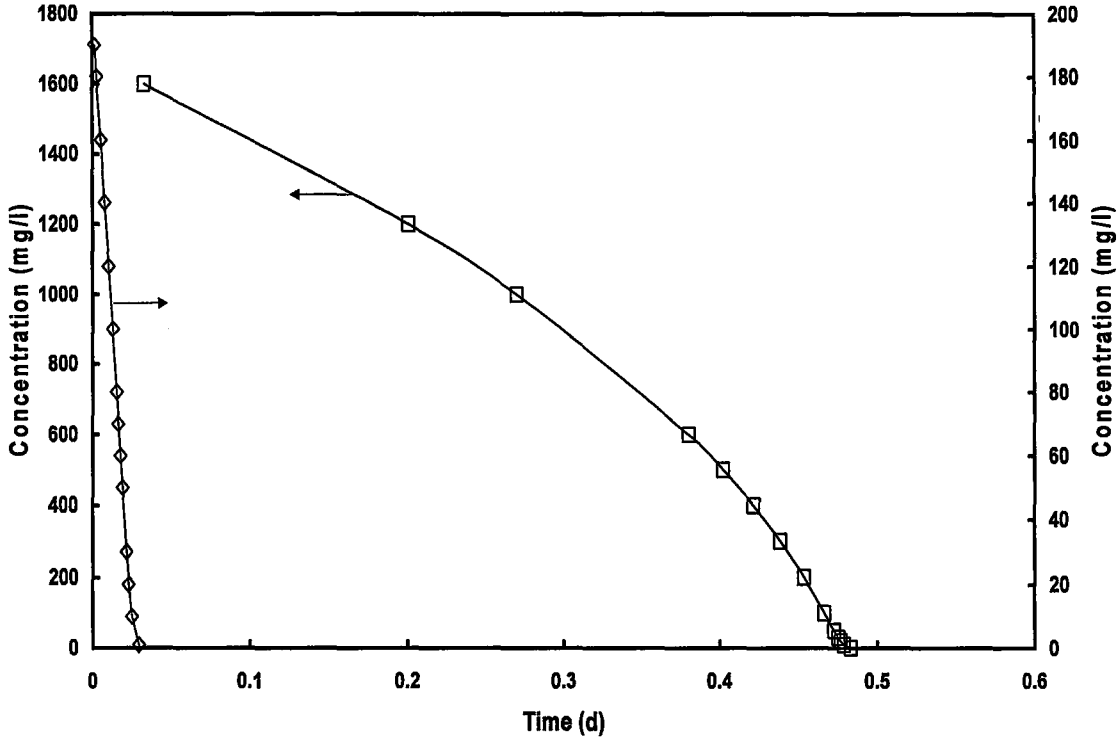

Fig. 4.3 The numerical solutions of concentration versus time of Eq. (4.7) □ 1670 mg/l, ◊ 200 mg/l.

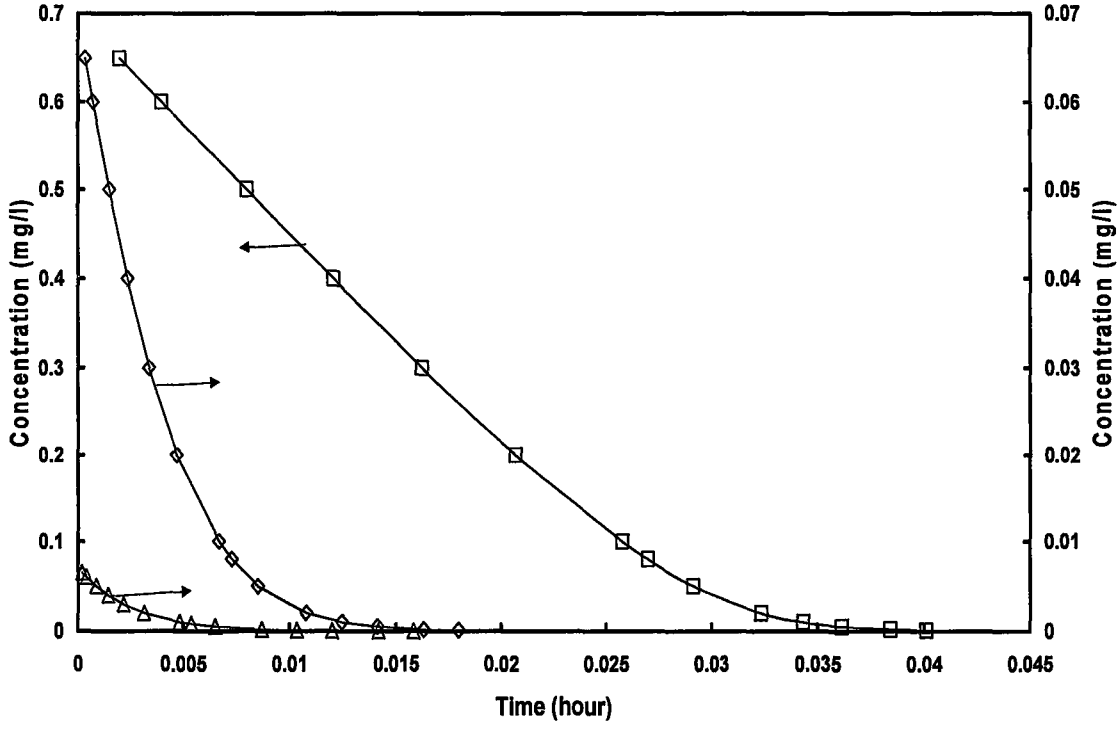

Fig. 4.4 The numerical solutions of concentration versus time of Eq. (4.7). □ 0.7 mg/l, ◊ 0.07 mg/l, Δ 0.007 mg/l.

while the others associated with low initial substrate concentrations (200 mg/l of case A and all the concentrations of case B) are concave. For clarity, we define the dimensionless (or relative) concentration S^* and dimensionless (or relative) time t^* by

$$S^* = \frac{S}{S_0} \tag{4.16}$$

$$t^* = \frac{t}{t_m} \tag{4.17}$$

where t_m is the maximum retention time. Using S^* and t^*, Eq. (4.7) becomes

$$K_S \ln\frac{1}{S^*} + S_0\left(1 - S^*\right) + S_0^2 \frac{1 - S^{*2}}{2K_I} = \frac{\mu_m}{Y_{X/S}} X_0 t^* t_m \tag{4.18}$$

Figs. 4.5 and 4.6, which use dimensionless units, are more perspicuous than Figs. 4.3 and 4.4.

2. Sensitivity Coefficients of the Andrews model (Solutions of Eqs. (4.9)-(4.12))

Substituting the data for substrate concentration against time obtained in step 1) into Eqs. (4.9)-(4.12), the values of four sensitivity coefficients for the parameters μ_m, K_S, K_I, and $Y_{X/S}$ were obtained. It was found that the values of the sensitivity coefficients often differed by several magnitudes. Some investigators used a method in which these sensitivity coefficients were multiplied by a factor to make their curves closer for comparison [Seagren, et al., 2003]. However, this method is still not clear enough, because the criterion for parameter identification in a graph is based on the subjective assessment of the separation of the curves of the sensitivity coefficients [Ellis et al., 1996; Seagren et al., 2003]. If two such curves are separated, their parameters are identifiable.

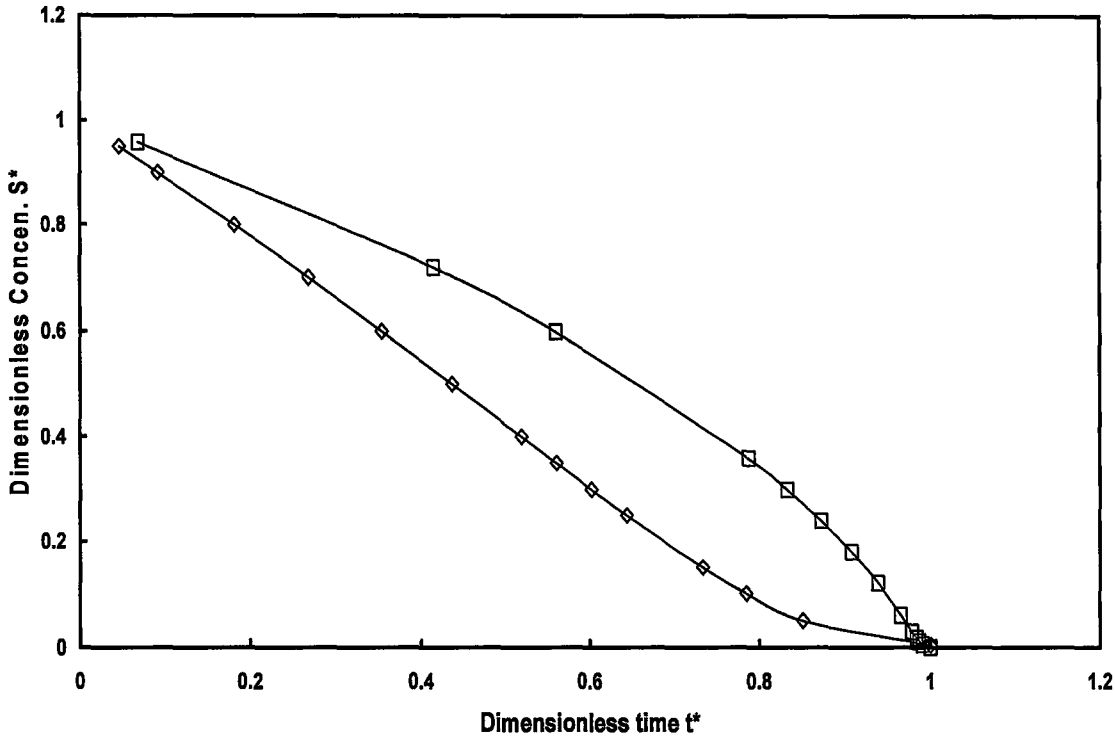

Fig. 4.5 The numerical solutions of dimensionless concentration versus time of Eq. (4.7). □ 1670 mg/l, ◊ 200 mg/l.

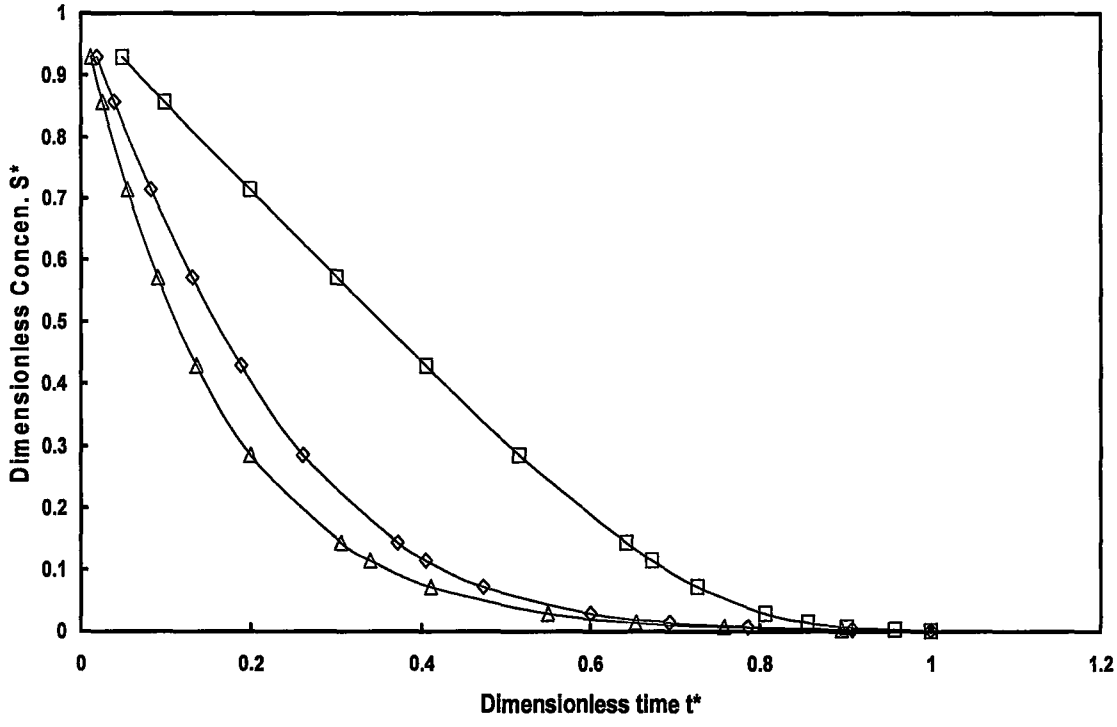

Fig. 4.6 The numerical solutions of dimensionless concentration versus time of Eq. (4.7). □ 0.7 mg/l, ◊ 0.07 mg/l, Δ 0.007 mg/l.

But it is often difficult to find a suitable multiplying factor to make these curves approach each other for a comparison. Furthermore, these sensitivity coefficient curves are often partly separated. Both these factor make judgment difficult. Therefore, we propose a new method, the dimensionless sensitivity coefficient (DSC), as follows.

4.5 Dimensionless Sensitivity Coefficient for Parameter Identification

The dimensionless sensitivity coefficient is defined as

$$DSC = \left(\frac{\partial S}{\partial p_i}\right)^* = \frac{SC}{SCM} = \frac{\left(\frac{\partial S}{\partial p_i}\right)}{\left(\frac{\partial S}{\partial p_i}\right)_m} \tag{4.19}$$

where SC is the sensitivity coefficient at any time t, SCM is the maximum sensitivity coefficient in a variable range, and the symbol * denotes a dimensionless quantity. Under this definition, the maximum dimensionless sensitivity coefficient is 1.

For n parameters of the model, Eq. (4.5) is divided throughout by the n maximum dimensionless sensitivity coefficients ($\prod_{k=1}^{n}\left(\frac{\partial S}{\partial p_k}\right)_m$), to yield

$$C_1'\left(\frac{\partial S}{\partial p_1}\right)^* + C_2'\left(\frac{\partial S}{\partial p_2}\right)^* + \ldots\ldots + C_j'\left(\frac{\partial S}{\partial p_j}\right)^* + \ldots\ldots + C_n'\left(\frac{\partial S}{\partial p_n}\right)^* = 0 \tag{4.20}$$

where

$$C_j' = \frac{C_j}{\prod_{k=1,k\neq j}^{n}\left(\partial S / \partial p_k\right)_m} \tag{4.21}$$

If we consider the identification of two parameters p_i and p_j, Eq. (4.20) reduces to

$$C_i'\left(\frac{\partial S}{\partial p_i}\right)^* + C_j'\left(\frac{\partial S}{\partial p_j}\right)^* = 0 \tag{4.22}$$

If the parameters p_i and p_j are linearly dependent, then at least one of the constants C_i' or C_j' is not zero. Furthermore, because both dimensionless sensitivity coefficients of the parameters p_i and p_j have the maximum value 1 at the same dimensionless time, if they are linearly dependent, we have

$$C_i' = -C_j' \tag{4.23}$$

and

$$\left(\frac{\partial S}{\partial p_i}\right)^* - \left(\frac{\partial S}{\partial p_j}\right)^* = 0. \tag{4.24}$$

Eq. (4.24) indicates that both dimensionless sensitivity coefficients of the parameters p_i and p_j overlap if they are linearly dependent. On the other hand, if the parameters p_i and p_j are linearly independent, then the terms $(\partial S/\partial p_i)^*$ and $(\partial S/\partial p_j)^*$ are less than or equal to one. Therefore, the terms $(\partial S/\partial p_i)^*$ and $(\partial S/\partial p_j)^*$ are easily comparable for their identification by a plot of dimensionless sensitivity coefficients. Two criteria have been suggested to examine the parameter identification of a model and the parameter identification degree (easy or difficult) in a variable range.

1) If two curves of dimensionless sensitivity coefficient overlap, two parameters represented by these curves are not theoretically identifiable.

2) The degree of separation between the two curves of dimensionless sensitivity coefficients indicates the identification degree of the corresponding two parameters. The bigger the separation is, the easier the identification of the corresponding two parameters is from a theoretic point of view.

According to criterion 2, the parameters of a model are theoretically identifiable if the two sensitivity coefficients do not overlap. However, when the two dimensionless sensitivity coefficient curves have a slight separation, and there is an inherent level of noise and error in the experimental data, the noise and errors may make some points or entire curves of the two dimensionless sensitivity coefficients overlap, resulting in lack of practical identification of the parameters. Thus we produce criterion 3:

3) The half vertical distance between the two curves of dimensionless sensitivity coefficient at a given dimensionless time can be a base for the calculation of the allowable level of noise, which is the maximum value of level of noise that does not make two points of the dimensionless sensitivity coefficient overlap. The half distance is adopted by consideration of the opposite situation, in which the deviations of the two dimensionless sensitivity coefficients are added. From this condition, the allowable noise level can be calculated.

Applying the method of dimensionless sensitivity coefficient to the parameters μ_m, K_S, K_I, and $Y_{X/S}$ of the integrated Andrews model, Eqs. (4.9)-(4.12) become

$$\left(\frac{\partial S}{\partial \mu_m}\right)^* = -\frac{X_0 t^* t_m}{Y_{X/S}\left(\frac{K_S}{S}+1+\frac{S}{K_I}\right)\left(\frac{\partial S}{\partial \mu_m}\right)_m} \tag{4.25}$$

$$\left(\frac{\partial S}{\partial K_S}\right)^* = \frac{\ln\frac{S_0}{S}}{\left(\frac{K_S}{S}+1+\frac{S}{K_I}\right)\left(\frac{\partial S}{\partial K_S}\right)_m} \tag{4.26}$$

$$\left(\frac{\partial S}{\partial K_I}\right)^* = -\frac{S_0^2 - S^2}{2K_I^2\left(\frac{K_S}{S}+1+\frac{S}{K_I}\right)\left(\frac{\partial S}{\partial K_I}\right)_m} \tag{4.27}$$

$$\left(\frac{\partial S}{\partial Y_{X/S}}\right)^{*} = \frac{\mu_m X_0 t^{*} t_m}{Y_{X/S}^2\left(\frac{K_S}{S}+1+\frac{S}{K_I}\right)\left(\frac{\partial S}{\partial Y_{X/S}}\right)_m} \tag{4.28}$$

where the maximum dimensionless sensitivity coefficients of Eq. (4.25)-(4.28) are

$$\left(\frac{\partial S}{\partial \mu_m}\right)_m = -\frac{X_0 t^{*}_{scm,\mu} t_m}{Y_{X/S}\left(\frac{K_S}{S_0 S^{*}_{scm,\mu}}+1+\frac{S_0 S^{*}_{scm,\mu}}{K_I}\right)} \tag{4.29}$$

$$\left(\frac{\partial S}{\partial K_S}\right)_m = \frac{-\ln S^{*}_{scm,S}}{\left(\frac{K_S}{S_0 S^{*}_{scm,S}}+1+\frac{S_0 S^{*}_{scm,S}}{K_I}\right)} \tag{4.30}$$

$$\left(\frac{\partial S}{\partial K_I}\right)_m = -\frac{S_0^2\left(1-S^{*2}_{scm,I}\right)}{2K_I^2\left(\frac{K_S}{S_0 S^{*}_{scm,I}}+1+\frac{S_0 S^{*}_{scm,I}}{K_I}\right)} \tag{4.31}$$

$$\left(\frac{\partial S}{\partial Y_{X/S}}\right)_m = \frac{\mu_m X_0 t^{*}_{scm,Y} t_m}{Y_{X/S}^2\left(\frac{K_S}{S_0 S^{*}_{scm,Y}}+1+\frac{S_0 S^{*}_{scm,Y}}{K_I}\right)} \tag{4.32}$$

The subscripts scm, μ, S, I, and Y denote the maximum dimensionless sensitivity coefficient, the specific growth rate, the saturation coefficient, the inhibition coefficient, and the yield coefficient, respectively.

1. Effect of the initial concentration on dimensionless sensitivity coefficients

The four dimensionless sensitivity coefficients for the parameters μ_m, K_S, K_I, and $Y_{X/S}$ (Eqs. (4.25)-(4.28)) are shown in Figs. 4.7 (1670 mg/l in case A), 4.8 (200 mg/l in case A), 4.9 (0.7 mg/l in case B), 4.10 (0.07 mg/l in case B), and 4.11 (0.007 mg/l in case B). All of the dimensionless sensitivity coefficients in Figs (4.7)-(4.11) first increase, reach a maximum point, and then decrease with increasing dimensionless time.

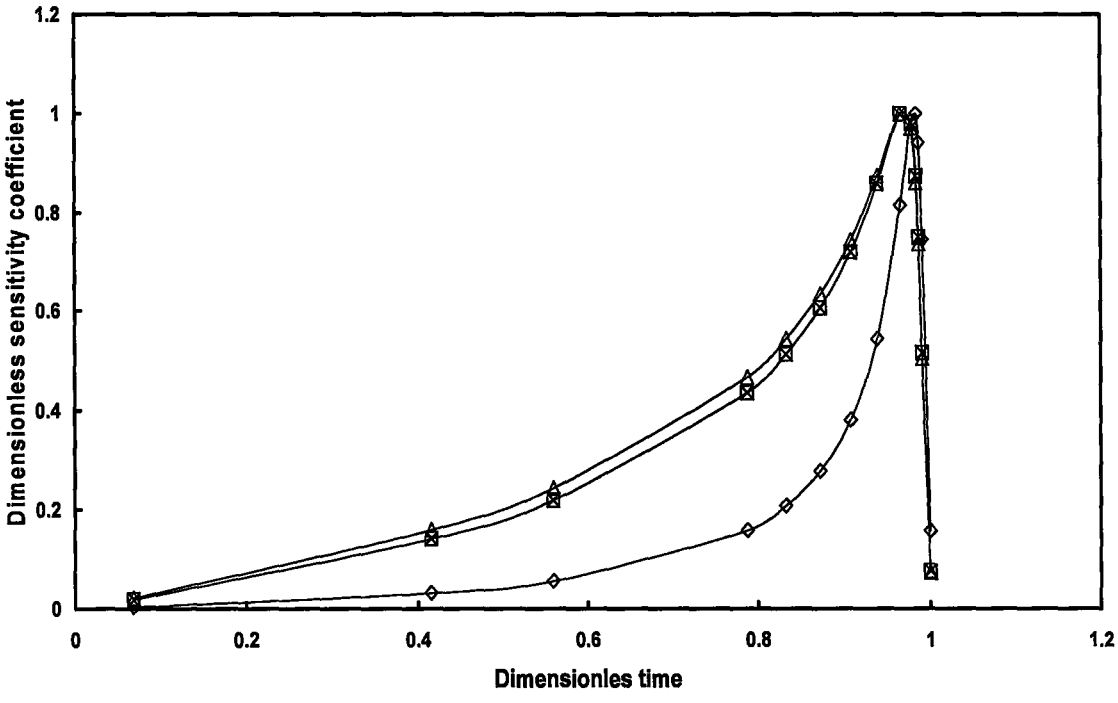

Fig. 4.7 Dimensionless sensitivity coefficients for substrate concentration 1670 mg/l, S_0/K_S 87, and the other conditions same as case A. □ $(\partial S/\partial \mu_m)^*$, ◊ $(\partial S/\partial K_S)^*$, Δ $(\partial S/\partial K_I)^*$, × $(\partial S/\partial Y_{X/S})^*$.

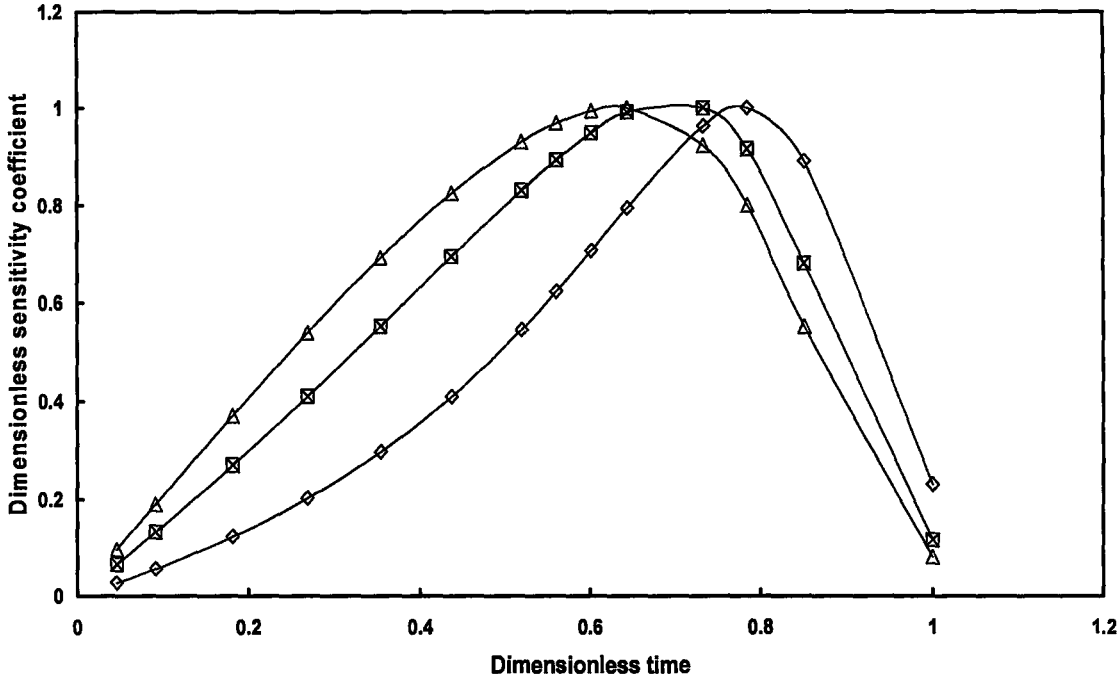

Fig. 4.8 Dimensionless sensitivity coefficients for substrate concentration 200 mg/l, S_0/K_S 10.4, and the other conditions same as case A. □ $(\partial S/\partial \mu_m)^*$, ◊ $(\partial S/\partial K_S)^*$, Δ $(\partial S/\partial K_I)^*$, × $(\partial S/\partial Y_{X/S})^*$.

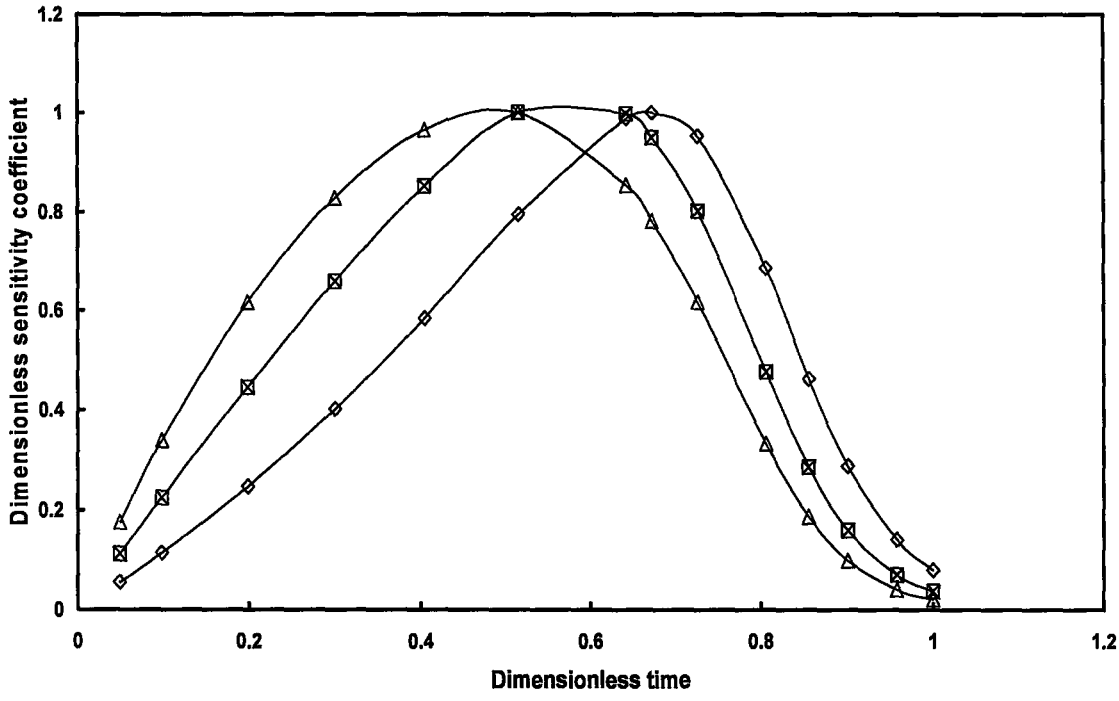

Fig. 4.9 Dimensionless sensitivity coefficients for substrate concentration 0.7 mg/l, S_0/K_S 10, and the other conditions same as case B. □ $(\partial S/\partial \mu_m)^*$, ◊ $(\partial S/\partial K_S)^*$, Δ $(\partial S/\partial K_I)^*$, × $(\partial S/\partial Y_{X/S})^*$.

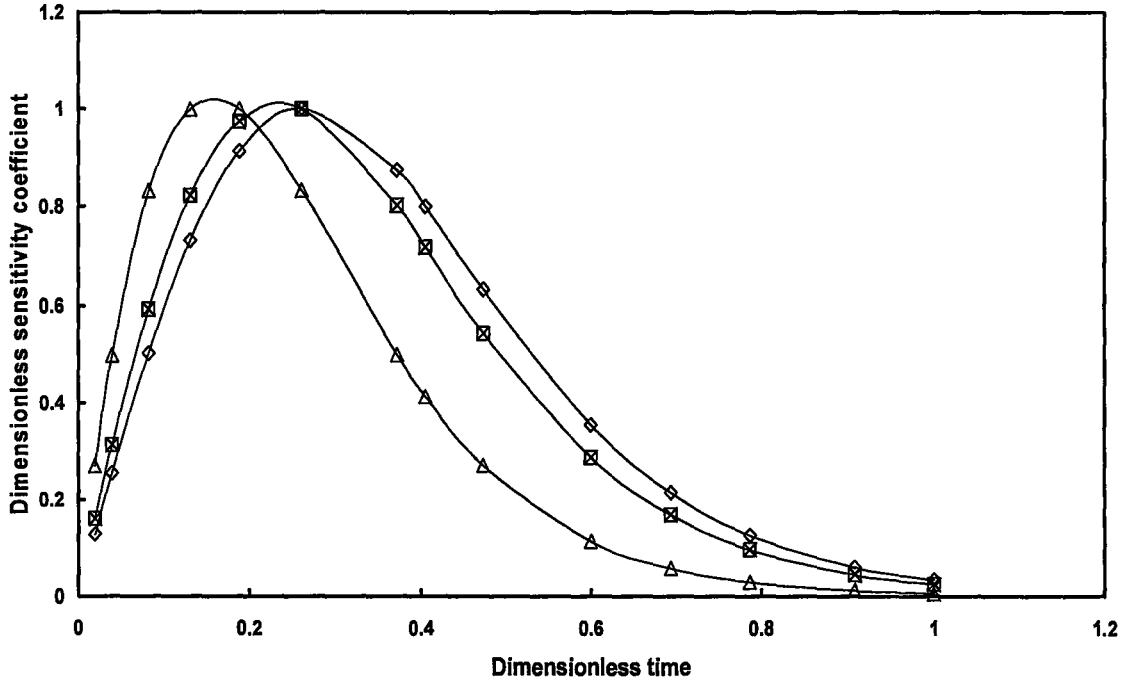

Fig. 4.10 Dimensionless sensitivity coefficients for substrate concentration 0.07 mg/l, S_0/K_S 1, and the other conditions same as case B. □ $(\partial S/\partial \mu_m)^*$, ◊ $(\partial S/\partial K_S)^*$, Δ $(\partial S/\partial K_I)^*$, × $(\partial S/\partial Y_{X/S})^*$.

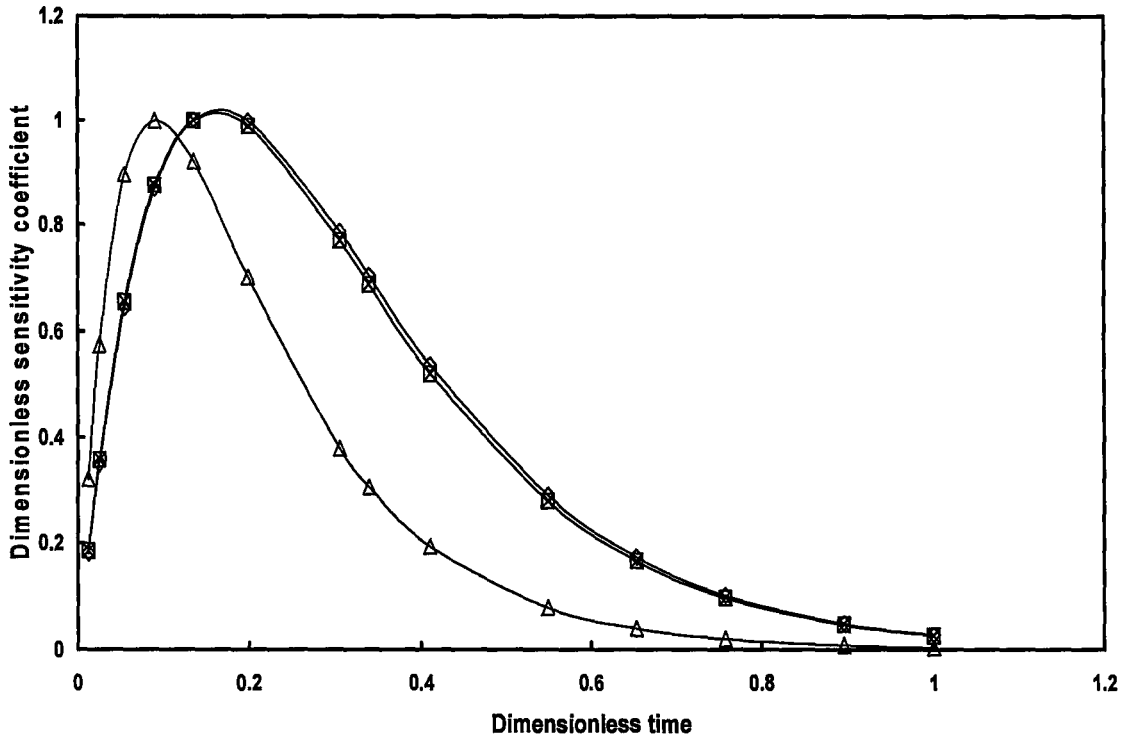

Fig. 4.11 Dimensionless sensitivity coefficients for substrate concentration 0.007 mg/l, S_0/K_S 0.1, and the other conditions same as case B. □ $(\partial S/\partial \mu_m)^*$, ◊ $(\partial S/\partial K_S)^*$, Δ $(\partial S/\partial K_I)^*$, × $(\partial S/\partial Y_{X/S})^*$.

With a decrease of the ratio S_0/K_S of the initial substrate concentration and the saturation coefficient, the peaks in the figures become wider from the ratio S_0/K_S 87 in Fig. 4.7 to 10.4 in Fig. 4.8 (Case A), and narrower from S_0/K_S 10 in Fig. 4.9 to 1 in Fig. 4.10 and 0.1 in Fig. 4.11 (Case B). It is found that the curves of $(\partial S/\partial \mu_m)^*$ in all the figures 4.7-4.11 overlap with those of $(\partial S/\partial Y_{X/S})^*$, which means that both parameters μ_m and $Y_{X/S}$ are not identifiable, and confirms the conclusion in the previous section.

2. Effect of the saturation coefficient on dimensionless sensitivity coefficients

The four dimensionless sensitivity coefficients for the parameters μ_m, K_S, K_I, and $Y_{X/S}$ (Eqs. (4.25)-(4.28)) with varying saturation coefficients are shown in Figs. 4.12 (S_0/K_S 87, S_0 200 mg/l, and K_S 2.3 mg/l in Case A), 4.13 (S_0/K_S 10.4, S_0 1670 mg/l, and K_S 160 mg/l in Case A), 4.14 (S_0/K_S 0.1, S_0 0.07 mg/l, and K_S 0.7 mg/l in Case B), and 4.15 (S_0/K_S 10, S_0 0.07 mg/l, and K_S 0.007 mg/l in Case B). It was found that if the ratios of S_0/K_S are equal in case B, the curves of the dimensionless sensitivity coefficients are almost equal (comparing Fig. 4.14 with Fig. 4.11, and Fig. 4.15 with Fig. 4.9) with either the initial substrate concentration or the saturation coefficient varying. But in case A the curves with the same ratio of S_0/K_S 10.4 in Figs. 4.13 and 4.8 are very different.

The peaks in Fig. 4.13 are narrower than those in Fig. 4.8, and the dimensionless sensitivity coefficients $(\partial S/\partial K_I)^*$ and $(\partial S/\partial \mu_m)^*$ almost overlap in Fig. 4.13 when the dimensionless time becomes large. In addition, when the saturation coefficient decreases from 160 mg/l to 2.3 mg/l at the initial substrate concentration of 1670 mg/l in Figs. 4.13-4.12, the four curves for the dimensionless sensitivity coefficients overlap in part when the dimensionless time approaches 1, which suggests that parameter identification becomes difficult at a smaller saturation coefficient.

To examine the cause of these phenomena, we note that the right-hand terms of Eqs. (4.25)-(4.28) become dimensionless by substituting Eqs. (4.16) and (4.17), resulting in

$$\left(\frac{\partial S}{\partial \mu_m}\right)^* = \frac{t^*\left(\frac{K_S}{S^*_{scm,\mu}S_0}+1+\frac{S^*_{scm,\mu}S_0}{K_I}\right)}{t^*_{scm,\mu}\left(\frac{K_S}{S^*S_0}+1+\frac{S^*S_0}{K_I}\right)} \tag{4.33}$$

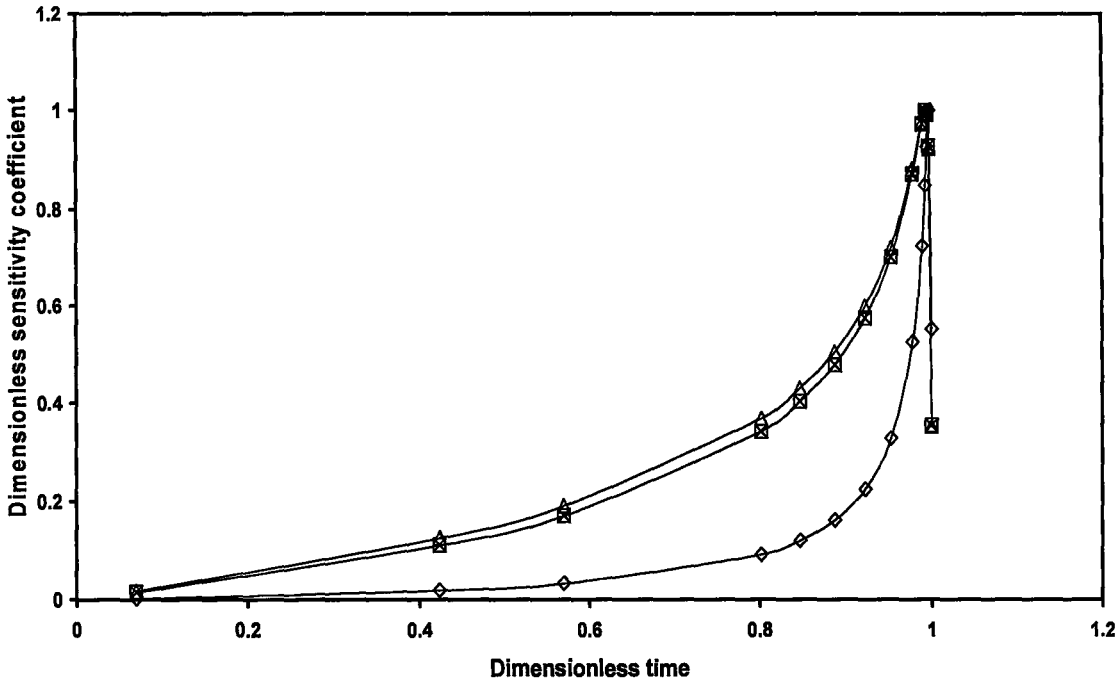

Fig. 4.12 Dimensionless sensitivity coefficients for substrate concentration 1670 mg/l, K_S 2.3 mg/l, S_0/K_S 726, with the other conditions the same as case A. □ $(\partial S/\partial \mu_m)^*$, ◊ $(\partial S/\partial K_S)^*$, Δ $(\partial S/\partial K_I)^*$, × $(\partial S/\partial Y_{X/S})^*$.

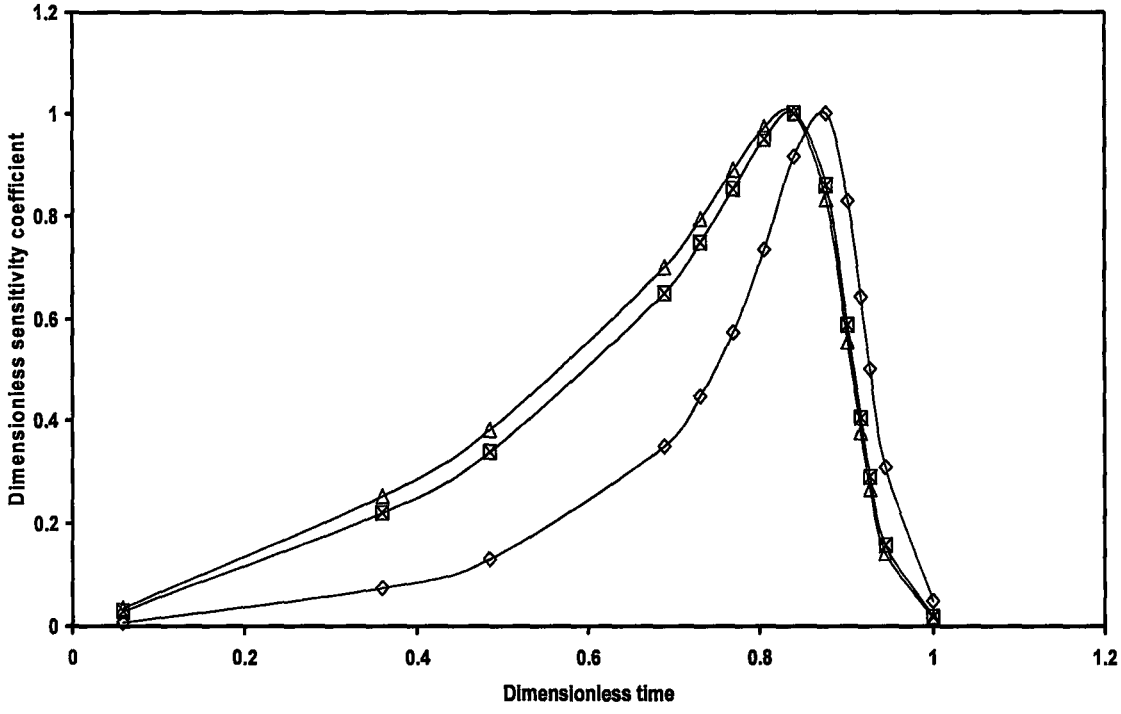

Fig. 4.13 Dimensionless sensitivity coefficients for substrate concentration 1670 mg/l, K_S 160 mg/l, S_0/K_S 10.4, with the other conditions the same as case A. □ $(\partial S/\partial \mu_m)^*$, ◊ $(\partial S/\partial K_S)^*$, Δ $(\partial S/\partial K_I)^*$, × $(\partial S/\partial Y_{X/S})^*$.

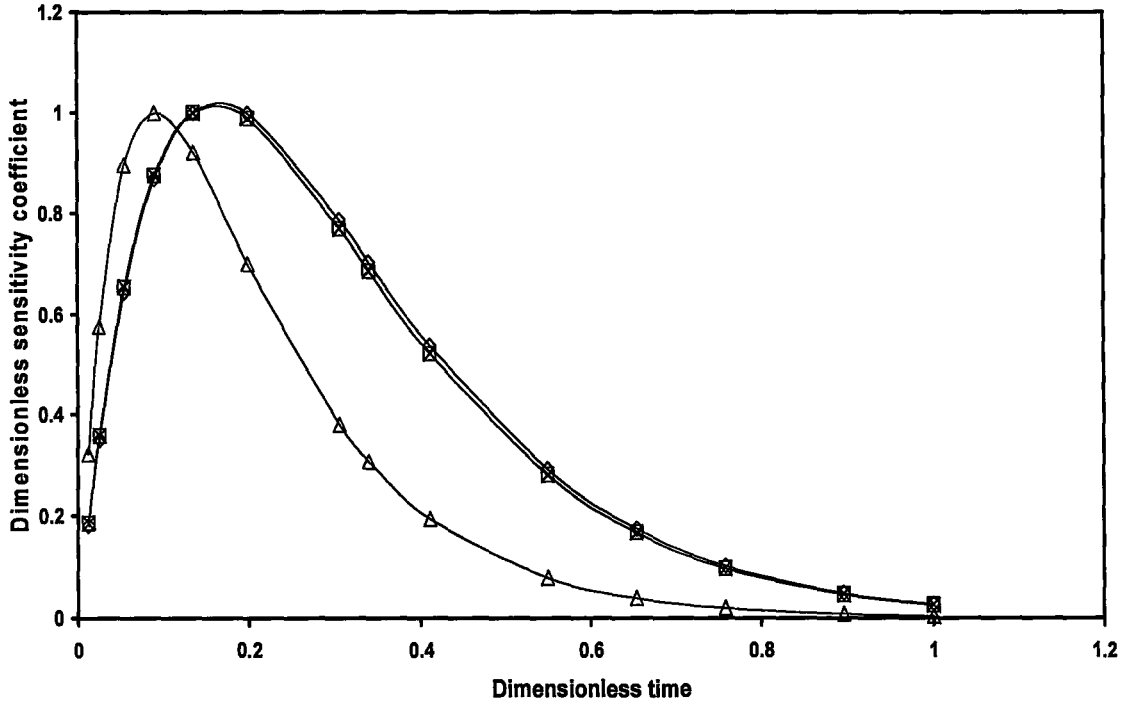

Fig. 4.14 Dimensionless sensitivity coefficients for substrate concentration 0.07 mg/l, K_S 0.7 mg/l, S_0/K_S 0.1, with the other conditions the same as case B.□ $(\partial S/\partial \mu_m)^*$, ◊ $(\partial S/\partial K_S)^*$, Δ $(\partial S/\partial K_I)^*$, × $(\partial S/\partial Y_{X/S})^*$.

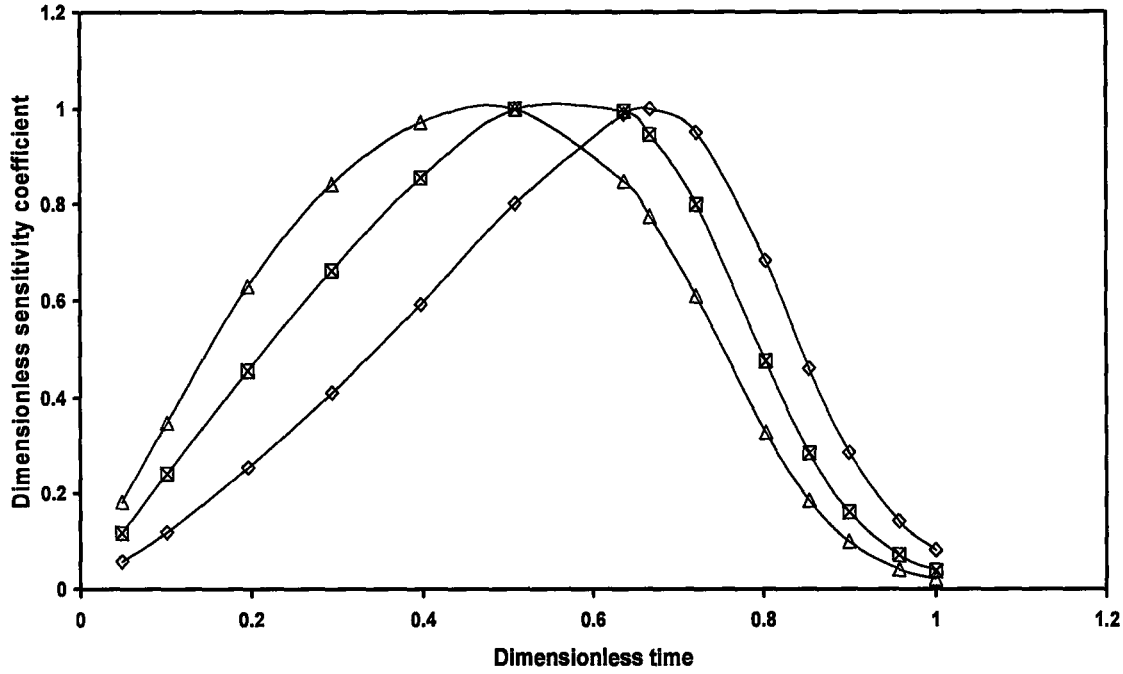

Fig. 4.15 Dimensionless sensitivity coefficients for substrate concentration 0.07 mg/l, K_S 0.007 mg/l, S_0/K_S 10, with the other conditions the same as case B. □ $(\partial S/\partial \mu_m)^*$, ◊ $(\partial S/\partial K_S)^*$, Δ $(\partial S/\partial K_I)^*$, × $(\partial S/\partial Y_{X/S})^*$.

$$\left(\frac{\partial S}{\partial K_S}\right)^* = \frac{\left(\frac{K_S}{S^*_{scm,S}S_0} + 1 + \frac{S^*_{scm,S}S_0}{K_I}\right)\ln S^*}{\left(\frac{K_S}{S_0S^*} + 1 + \frac{S_0S^*}{K_I}\right)\ln S^*_{scm,S}} \tag{4.34}$$

$$\left(\frac{\partial S}{\partial K_I}\right)^* = \frac{\left(\frac{K_S}{S^*_{scm,I}S_0} + 1 + \frac{S^*_{scm,I}S_0}{K_I}\right)\left(1 - S^{*2}\right)}{\left(\frac{K_S}{S_0S^*} + 1 + \frac{S_0S^*}{K_I}\right)\left(1 - S^{*2}_{scm,I}\right)} \tag{4.35}$$

$$\left(\frac{\partial S}{\partial Y_{X/S}}\right)^* = \frac{\left(\frac{K_S}{S^*_{scm,Y}S_0} + 1 + \frac{S^*_{scm,Y}S_0}{K_I}\right)t^*}{\left(\frac{K_S}{S_0S^*} + 1 + \frac{S_0S^*}{K_I}\right)t^*_{scm,Y}}. \tag{4.36}$$

It is found that because the initial substrate concentration S_0 is very low in case B, this means that the contribution of the initial substrate concentration is small compared to the term $(K_S/(S_0S^*) +1 + S_0S^*/K_I)$ in the denominator of Eqs. (4.33)-(4.36), and at a constant ratio of S_0/K_S, the effect of increasing K_S is the same as that of decreasing S_0 in Eqs. (4.33)-(4.36). Therefore, the curves at a constant ratio of S_0/K_S are almost the same with either K_S or S_0 varying. However, at high substrate concentrations (Case A), the initial substrate concentration makes a greater contribution to the term $(K_S/(S_0S^*) +1+ S_0S^*/K_I)$ in the denominator of Eqs. (4.33)-(4.36). Therefore, the curves in Figs. 4.8 and 4.13 are very different.

3. Effect of the inhibition coefficient on dimensionless sensitivity coefficients

In the same manner, when the inhibition coefficient becomes 111, 11.1 and 1.11 mg/l, respectively, the four dimensionless sensitivity coefficients for the parameters μ_m, K_S, K_I,

and $Y_{X/S}$ (Eqs. (4.25)-(4.28)) with varying the inhibition coefficient (Case B) (Figs. 4.16, 4.10, and 4.17) differ only slightly because of the low substrate concentration 0.07 mg/l. However, at a high substrate concentration, 1670 mg/l in case A, and the decrease of the inhibition coefficient from 2872 mg/l in Fig. 4.19 to 344 mg/l in Fig. 4.7 and 34.4 mg/l in Fig. 4.18, the four dimensionless sensitivity coefficients increase sharply, resulting in partial overlap when the dimensionless time is approximately equal to one. This indicates a decreasing identification between these parameters with a decrease of the inhibition coefficient.

4. Effect of the initial biomass concentration on dimensionless sensitivity coefficients

From the right-hand term in Eq. (4.7), the product of initial biomass concentration and time should be constant, because the left-hand term of Eq. (4.7) is constant at the same initial substrate concentration, *i.e.* X_0 and t vary inversely to each other. Therefore, the change of initial biomass concentration will not affect the curve shape of the dimensionless sensitivity coefficient.

4.6 Parameter Identification Using Noisy Data

As discussed in section 4.5, when the dependent variables have some noise associated with them, the model parameters may become practically un-identifiable, even though the model parameters are theoretically identifiable. This situation can be illustrated by the following expression [Arthur, et. al., 1998]:

Response variable = Mechanistic model + Variance model (4.37)

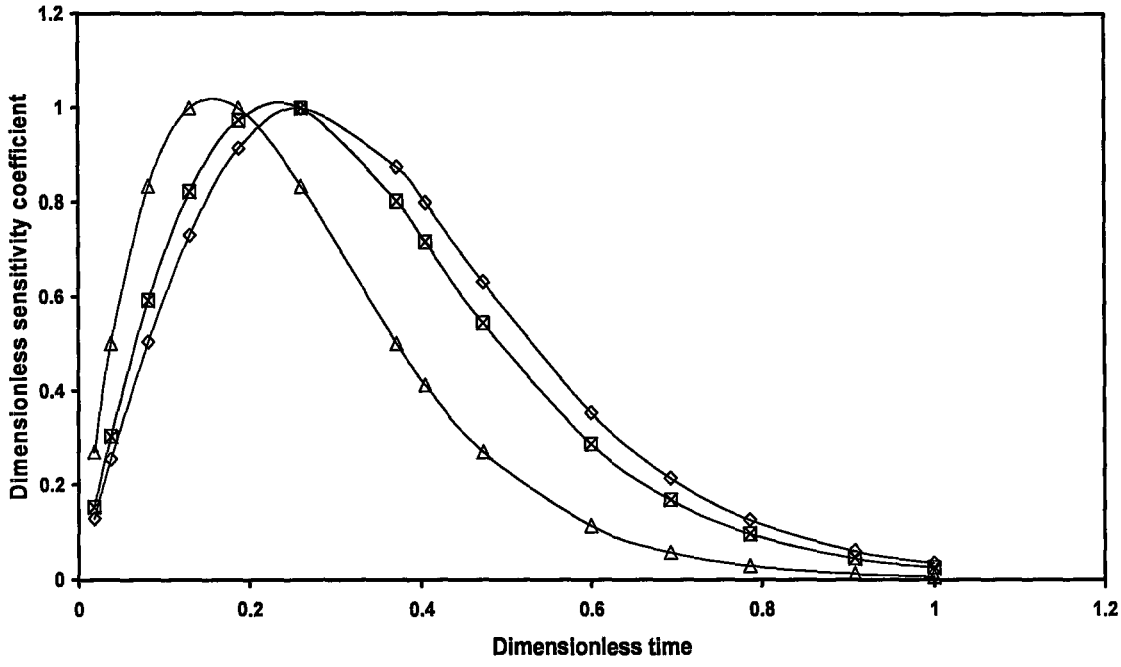

Fig. 4.16 Dimensionless sensitivity coefficients for substrate concentration 0.07 mg/l, K_I 111 mg/l, with the other conditions the same as case B. □ $(\partial S/\partial \mu_m)^*$, ◊ $(\partial S/\partial K_S)^*$, Δ $(\partial S/\partial K_I)^*$, × $(\partial S/\partial Y_{X/S})^*$.

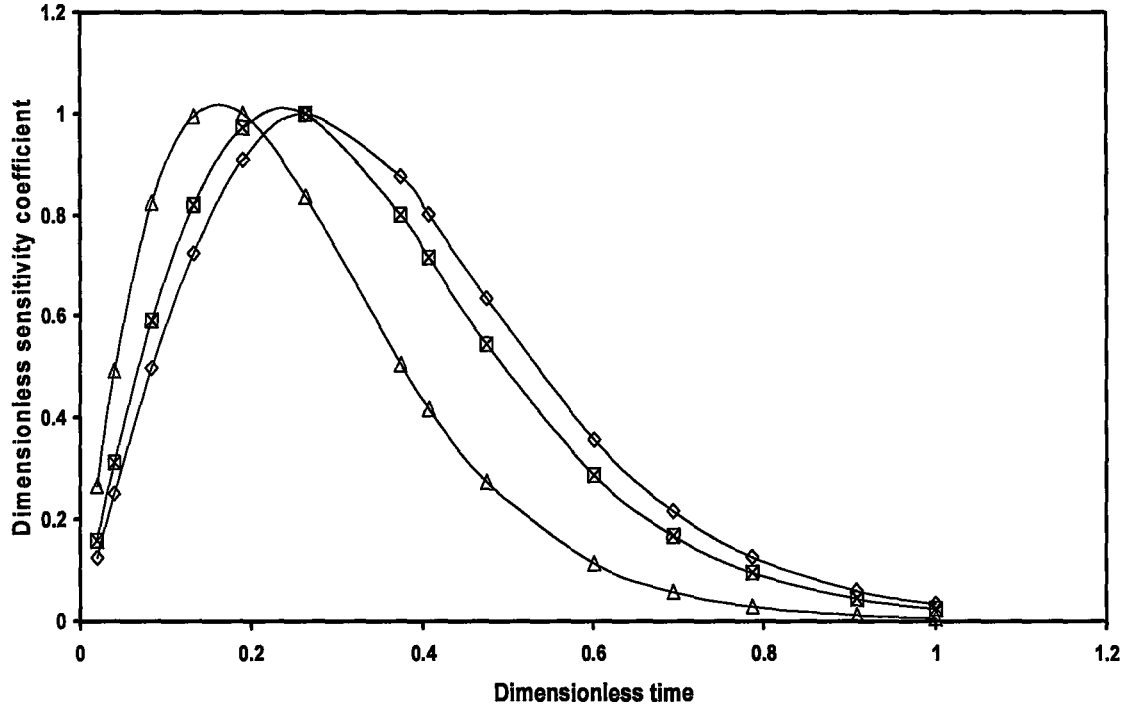

Fig. 4.17 Dimensionless sensitivity coefficients for substrate concentration 0.07 mg/l, K_I 1.11 mg/l, with the other conditions the same as case B. □ $(\partial S/\partial \mu_m)^*$, ◊ $(\partial S/\partial K_S)^*$, Δ $(\partial S/\partial K_I)^*$, × $(\partial S/\partial Y_{X/S})^*$.

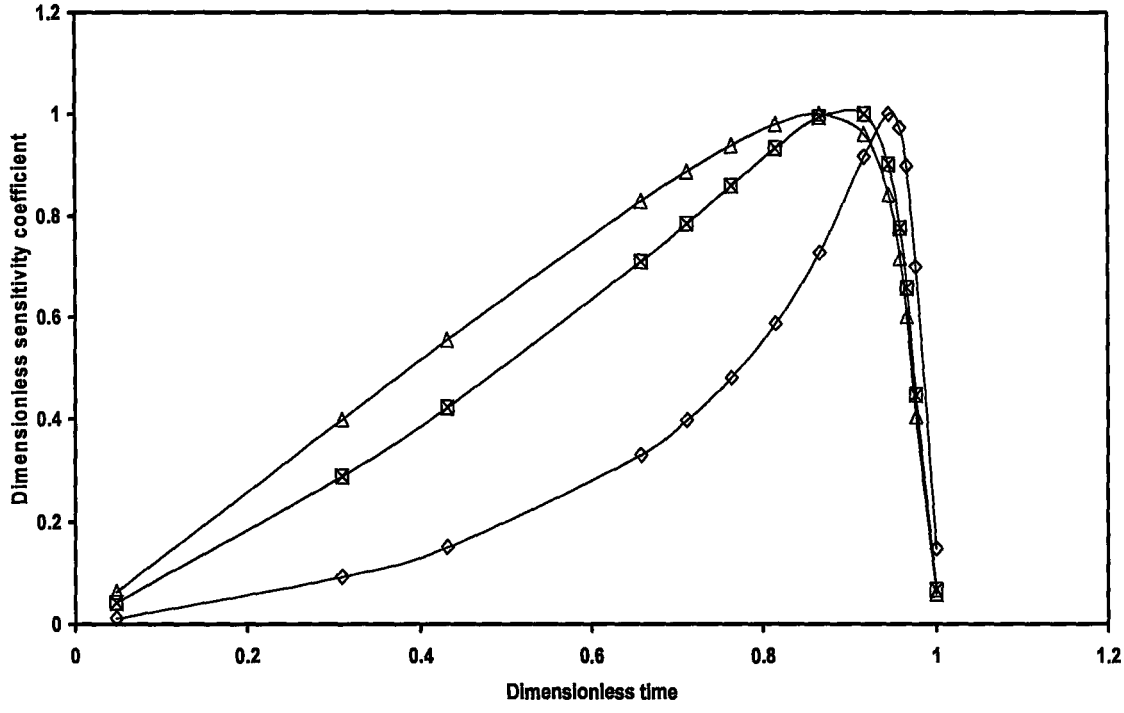

Fig. 4.18 Dimensionless sensitivity coefficients for substrate concentration 1670 mg/l, K_I 2872 mg/l, with the other conditions the same as case A. □ $(\partial S/\partial \mu_m)^*$, ◊ $(\partial S/\partial K_S)^*$, Δ $(\partial S/\partial K_I)^*$, × $(\partial S/\partial Y_{X/S})^*$.

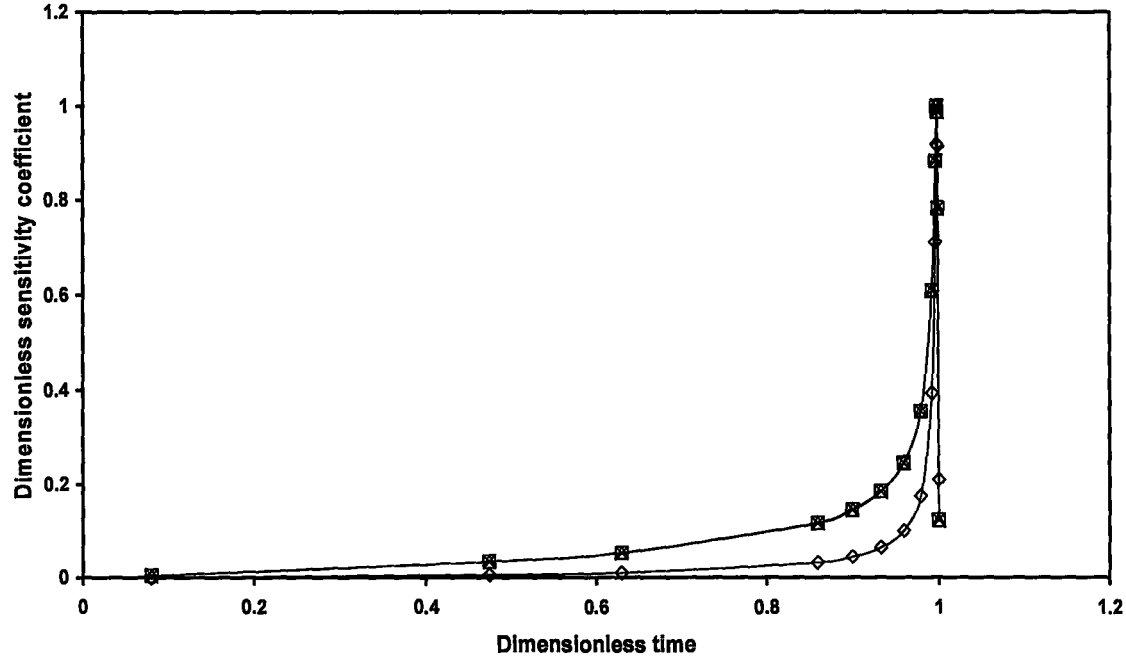

Fig. 4.19 Dimensionless sensitivity coefficients for substrate concentration 1670 mg/l, K_I 34.4 mg/l, with the other conditions the same as the case A. □ $(\partial S/\partial \mu_m)^*$, ◊ $(\partial S/\partial K_S)^*$, Δ $(\partial S/\partial K_I)^*$, × $(\partial S/\partial Y_{X/S})^*$.

where the response variable is the measured quantity, such as substrate or biomass concentration, the mechanistic model could be (e.g) Eq. (4.7), and the variance model is generally unknown and practically impossible to identify. If the variance model dominates the mechanistic model, then the parameters of the mechanistic model cannot be uniquely estimated regardless of whether they are identifiable theoretically.

According to criterion 3 in the previous section and Eq. (4.7), the allowable noise level for a variable can be calculated. Supposing that two parameters p_i and p_j are linearly dependent on their sensitivity coefficients, from Eq. (4.7) we have

$$C_i \frac{\partial S}{\partial p_i} + C_j \frac{\partial S}{\partial p_j} = 0 \tag{4.38}$$

where C_i and C_j are not both zero. For definiteness, supposing that $C_i \neq 0$, this yields

$$\frac{\partial S}{\partial p_i} = C_{i,j} \frac{\partial S}{\partial p_j} \tag{4.39}$$

where the constant $C_{i,j} = -C_j/C_i$. Eq. (4.39) shows that the sensitivity coefficient of the parameter p_j is proportional to that of the parameter p_i. To eliminate the constant $C_{i,j}$, two time points t_1 and t_2 are taken. Eq. (4.39) is applied to t_1 and t_2, respectively. The ratio of the resulting equation is taken. This yields

$$\frac{(\partial S / \partial p_i)_1}{(\partial S / \partial p_i)_2} = \frac{(\partial S / \partial p_j)_1}{(\partial S / \partial p_j)_2} \tag{4.40}$$

where the subscripts 1 and 2 denote the sensitivity coefficient at times t_1 and t_2, respectively. Eq. (4.40) is a basic equation to calculate the allowable level of noise. Some examples are given below. Assuming that the initial substrate concentration is S_0, the substrate concentrations are S_1 and S_2 in the dimensionless sensitivity coefficient of

parameter p_i at times t_1 and t_2, Eqs. (4.9) and (4.10) are substituted into Eq. (4.40) in order to examine parameter identification between K_S and μ_m. We have:

$$\frac{\ln\frac{S_0}{S_1}}{t_1} = \frac{\ln\frac{S_0}{S_2}}{t_2} \tag{4.41}$$

or

$$S_2 = \frac{S_0}{(S_0/S_1)^{t_2/t_1}} \tag{4.42}$$

Using the same procedure for Eqs. (4.9) and (4.11) to examine parameter identification between K_I and μ_m, we have

$$S_2 = \left[S_0^2 - \frac{t_2}{t_1}\left(S_0^2 - S_1^2\right)\right]^{0.5} \tag{4.43}$$

The relative allowable level of noise (E) to allow identification of the parameters of the Andrews model is given by:

$$E\% = \left|\frac{S_2' - S_2}{S_2'}\right|\% \tag{4.44}$$

where S_2' denotes the substrate concentration of the dimensionless sensitivity coefficient of parameter p_j at time t_2. The calculated results and conditions are shown in Tables 4.2 and 4.3. It is found that for identification of K_S and μ_m in the integrated Andrews model, the allowable noise level for substrate concentration decreases with a decrease of substrate concentration. For an initial substrate concentration of 0.007 mg/l in case B, the maximum allowable level of noise is very small (0.591 %). Such a small deviation is not often met in experiments, indicating that the parameters K_S and μ_m are not identifiable in practice, even thought they are theoretically identifiable. This quantitative result advances

Ellis's qualitative conclusion [1996]. It also extends Holmberg's conclusion for the Monod model to the Andrews model: although the parameters K_S and μ_m are theoretically identifiable, the measured errors will affect their practical identification [1982]. For the identification of the parameters K_I and μ_m, the values of the maximum allowable level of noise decreases with increasing substrate concentration. For the initial concentration 1670 mg/l in case A, the maximum allowable level of noise is as low as 0.72 %, which means that the parameters K_I and μ_m are not practically identifiable in this situation.

Table 4.2 The maximum allowable levels of noise to identify K_S and μ_m of the integrated Andrews model for cases A and B

S_0 (mg/l)	S_1 (mg/l)	S_2 (mg/l)	S_2' (mg/l)	t_1 (h)	t_2 (h)	E %
1670	1	1600	1002	0.4831	0.03324	37.4
200	1	190	156.4	0.02956	0.001372	17.7
0.7	0.001	0.65	0.5066	0.04011	0.00198	22.1
0.07	0.0001	0.065	0.06168	0.01798	0.000347	5.11
0.007	0.00001	0.0065	0.006462	0.01583	0.000193	0.591

Table 4.3 The maximum allowable levels of noise to identify K_I and μ_m of the integrated Andrews model for cases A and B

S_0 (mg/l)	S_1 (mg/l)	S_2 (mg/l)	S_2' (mg/l)	t_1 (h)	t_2 (h)	E %
1670	1	1600	1612	0.4831	0.03324	0.72
200	1	190	195.3	0.02956	0.001372	2.79
0.7	0.001	0.65	0.6825	0.04011	0.00198	5.00
0.07	0.0001	0.065	0.06932	0.01798	0.000347	6.65
0.007	0.00001	0.0065	0.006957	0.01583	0.000193	7.03

4.7 The Causes of Parameter Non-identification of the Integrated Andrews Model

As mentioned in section 4.6, the parameters of the integrated Andrews model become un-identifiable at either a low or a high substrate concentration if there is noise in the experimental data. Both situations can be attributed to an indirect cause (linearization of the Andrews equation (Eq. (4.3)) as well as due to a direct cause (the integrated Andrews equation (Eq. (4.7)) reduces to two simpler equations, respectively, at a low or high substrate concentration. Furthermore, the experimental data containing measured noises can make the curves of the integrated Andrews model more approach the those of its two simpler equations at a low or high substrate concentration, respectively, than those data free of measured noises.

1. The indirect cause

At a low substrate concentration ($K_S >> S$), the Andrews equation reduces to a first order (*i.e.* a linear equation) kinetics:

$$\mu = \frac{\mu_m S}{K_S} \tag{4.45}$$

in which the parameters μ_m and K_S can be combined as a constant. They are, therefore, not identifiable. At a high substrate concentration ($K_S << S$ in a certain concentration range), the Andrews equation becomes

$$\mu = \frac{\mu_m K_I}{K_I + S} \tag{4.46}$$

in which the parameters μ_m and K_I also can be combined as a constant. They are, therefore, cannot be directly identifiable. Eq. (4.46) can be linearized to

$$\frac{1}{\mu} = \frac{S}{K_I \mu_m} + \frac{1}{\mu_m}. \tag{4.47}$$

Figs. 4.20 (case B) and 4.21 (case A) indicate the relationships between the specific growth rate and the substrate concentration. When the initial substrate concentration is decreased from 0.7 mg/l to 0.007 mg/l, the curves in Fig. 4.20 become more linear, resulting in non-identification of the parameter K_S and μ_m. On the other hand, at a high substrate concentration (1670 mg/l in case A in Fig. 4.21) the curves of Eqs. (4.3) and (4.46) approach each other at points of the substrate concentration greater than 100 mg/l, and from Eq. (4.47) the latter has a linear correlation coefficient R = 0.999 for these points. Both figures show that the cause of non-identification of parameters of the Andrews model is the linearization of the curve of specific growth rate versus substrate concentration.

2. The direct cause

The integrated Andrews model reduces to the two simpler equations, respectively, at a low or high substrate concentration.

$$\ln\frac{S_0}{S} = \frac{\mu_m}{K_S Y_{X/S}} X_0 t \tag{4.48}$$

and

$$2K_I(S_0 - S) + S_0^2 - S^2 = \frac{2K_I\mu_m}{Y_{X/S}} X_0 t \tag{4.49}$$

in which the parameters K_S and μ_m in Eq. (4.48) and K_I and μ_m in Eq. (4.49) are not estimated uniquely because they can be combined a constant, respectively.

As discussed in the previous section, the presence of noise in experimental data may result in parameter non-identification. This effect can be examined by the following method. Using Eq. (4.42) a series of substrate concentrations S_2 in the allowable noise level range at a low initial concentration (for example, 0.007 mg/l in case B) can be

calculated. The set of data (S_2) are in turn substituted into Eq. (4.48) and a set of time t', for which the quantities containing noise levels are the function of t', can be obtained. The set of obtained time t' are substituted into Eq. (4.7) and a set of concentrations (S_2') can be recalculated. At this point there are two curves (S_2 versus t', and S_2' versus t'). The residual sum of squares between S_2 and S_2' with respect to t' can then be calculated. Using the same series of time values as used in section 1 "Solution of Eq. (4.7) for the initial substrate concentrations" in Chapter 4.4 to Eqs. (4.48) and (4.7), we get the other curves (S_2 versus t, and S_2' versus t). The residual sum of squares (RSS) between S_2 and S_2' with respect to t also can be calculated. The similar procedure can be applied to Eqs. (4.49) and (4.7) for two set of times t' and t. If the residual sum of squares of the former ($S_2(t') - S_2'(t')$) is less than that of the latter ($S_2(t) - S_2'(t)$), it is demonstrated that due to the presence of noise, the integrated Andrews equation approaches its reduced equations (Eqs. (4.48) and (4.49)). In this case, the parameters K_S and μ_m, or K_I and μ_m are not identifiable at either a low or high substrate concentration. The calculated residual sums of squares for four curves, for an initial substrate concentration of 0.007 mg/l in case B, and an initial substrate concentration of 1670 mg/l in case A, are presented in Table 4.3. The corresponding curves are shown in Figs. 4.22 and 4.23. The results show that the residual sums of squares of ($S_2(t') - S_2'(t')$) (1.0753×10^{-7} for the initial substrate concentration 0.007 mg/l in case B, and 35638 for 1670 mg/l in case A) are smaller than the corresponding residual sums of squares for ($S_2(t) - S_2'(t)$) (1.1802×10^{-7} and 75095), respectively, demonstrating that the presence of noise does make the parameter un-identifiable.

Table 4.4 A comparison of the residual sums of squares of Eqs. (4.48), (4.49), and (4.9) under the presence of noise

No.*	1	2	3	4
RSS	1.1802×10^{-7}	1.0753×10^{-7}	75095	35638

*

No. 1 denotes the residual sum of squares between Eqs. (4.48) and (4.7) (S_2 and S_2' with respect to t) for 0.007 mg/l in case B.

No. 2 denotes the residual sum of squares between Eqs. (4.48) and (4.7 (S_2 and S_2' with respect to t') for 0.007 mg/l in case B.

No. 3 denotes the residual sum of squares between Eqs. (4.49) and (4.7) (S_2 and S_2' with respect to t) for 1670 mg/l in case A.

No. 4 denotes the residual sum of squares between Eqs. (4.49) and (4.7) (S_2 and S_2' with respect to t') for 1670 mg/l in case A.

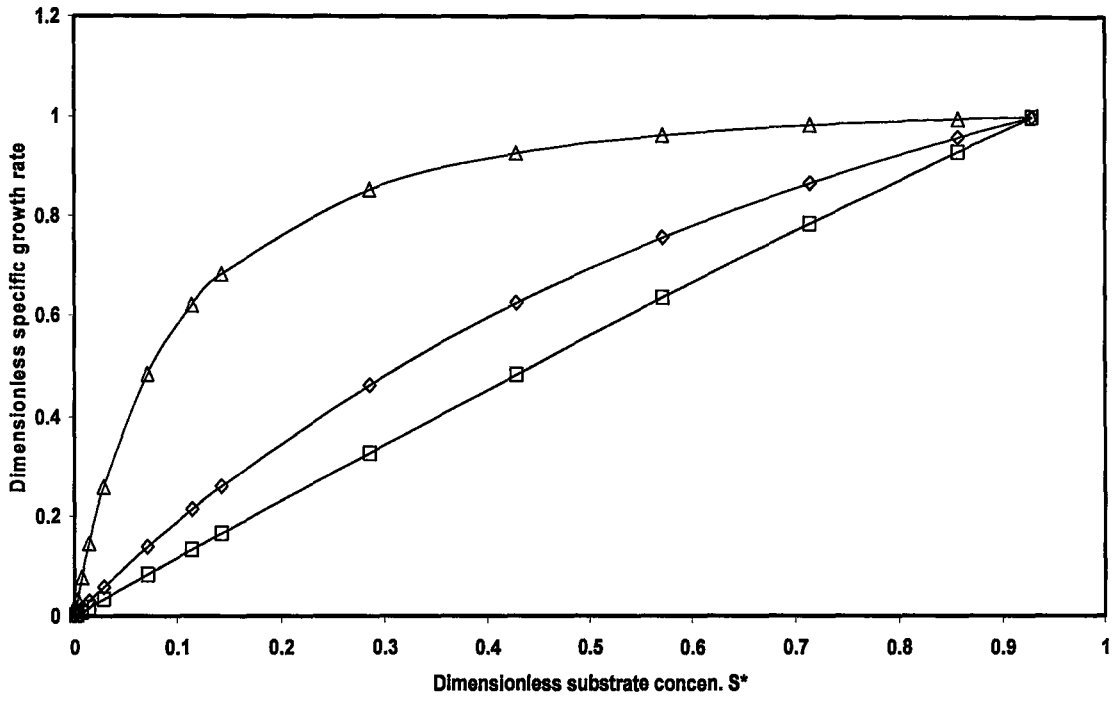

Fig. 4.20 Cause of parameter non-identification (Case B). The curves denote Eq. (4.3). □ Initial substrate concentration 0.007 mg/l, ◊ 0.07 mg/l, Δ 0.7 mg/l.

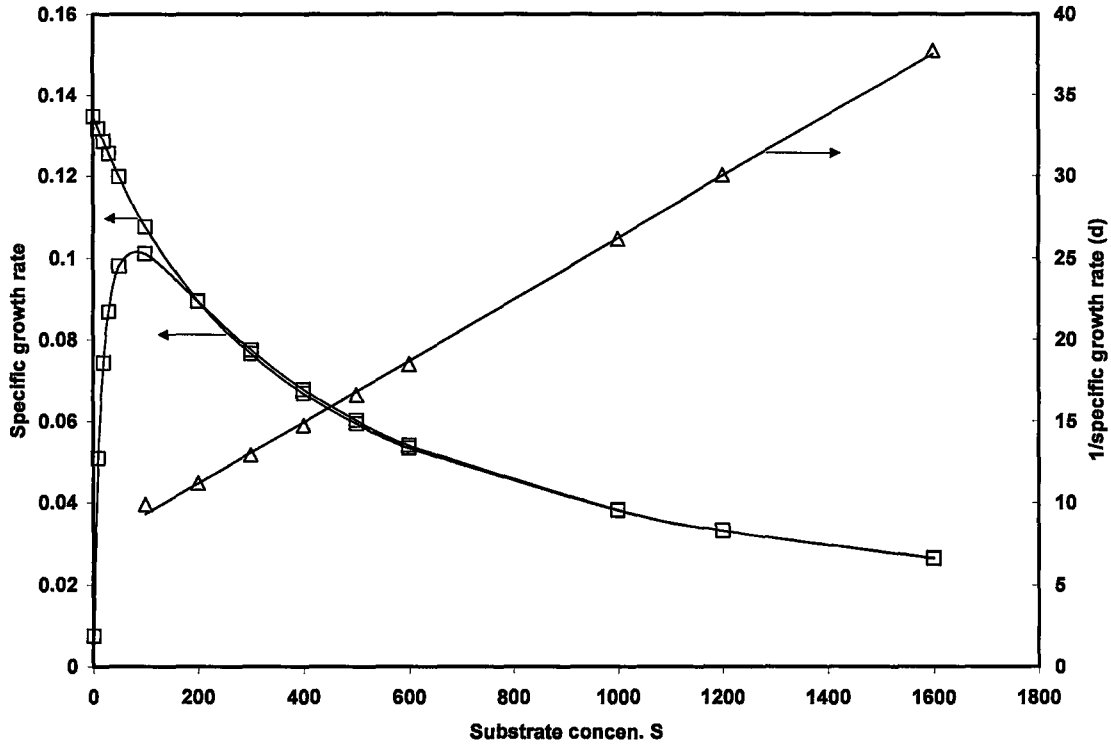

Fig. 4.21 Cause of parameter non-identification (Initial substrate concentration 1670 mg/l in Case A). □ Eq. (4.7), ◊ Eq. (4.46), Δ Eq. (4.47).

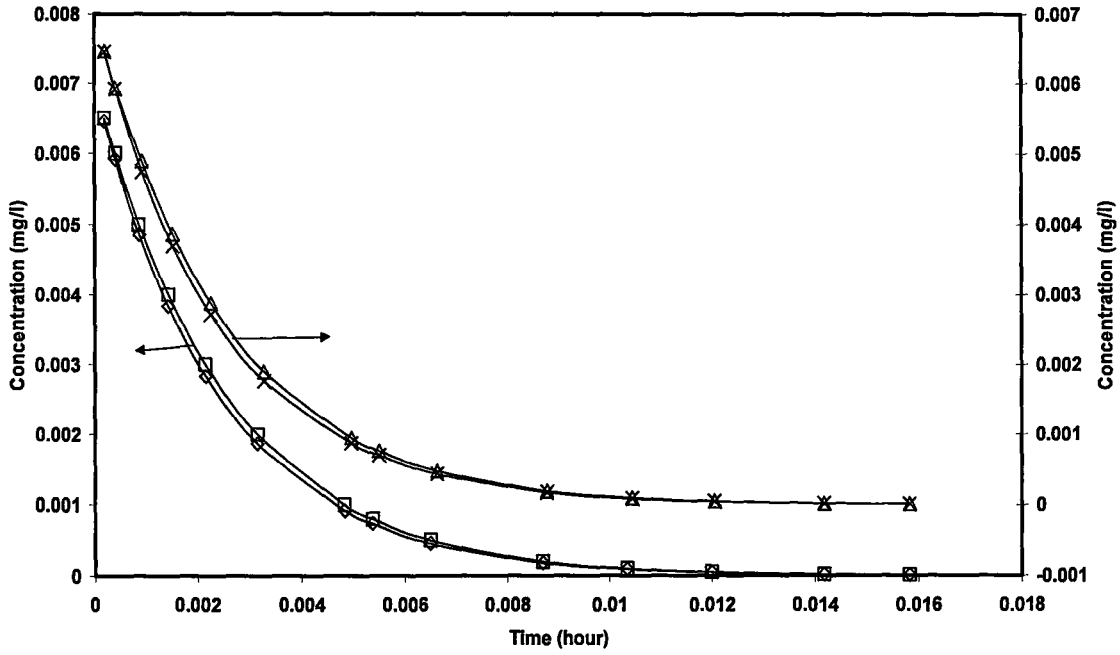

Fig. 4.22 A comparison of the effect of noise for an experiment with an initial substrate concentration equal to 0.007 mg/l in case B. □ Eq. (4.7) (S_2' versus t), ◊ Eq. (4.48) (S_2 versus t), Δ Eq. (4.7) (S_2' versus t'), × Eq. (4.48) (S_2 versus t').

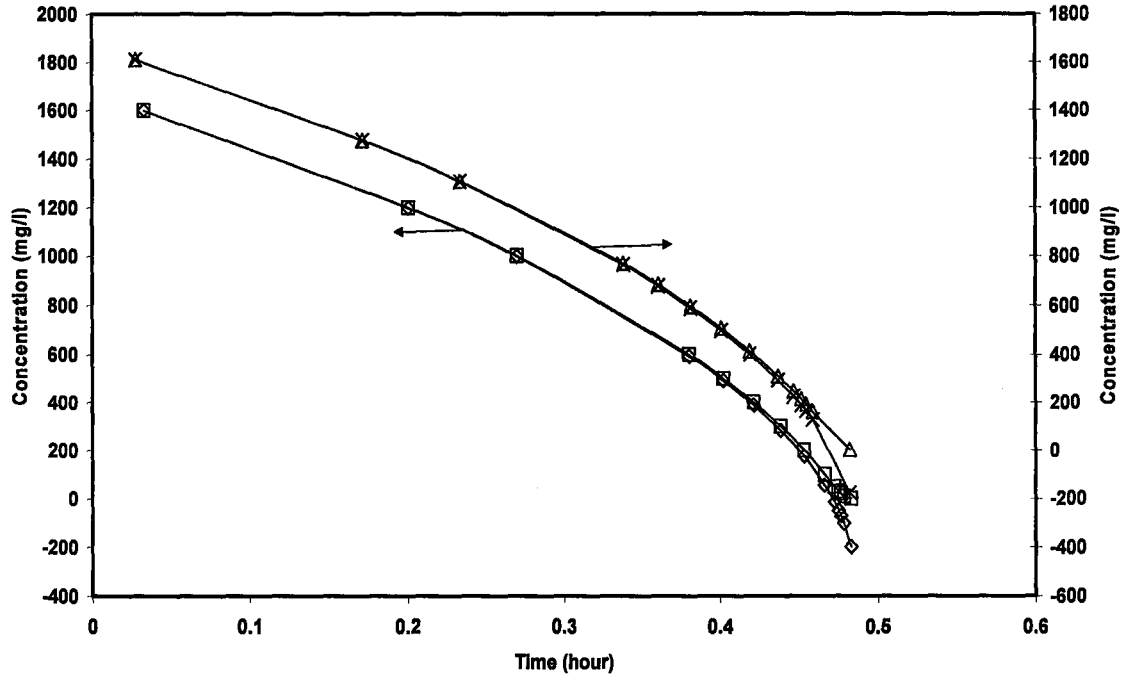

Fig. 4.23 A comparison of the effect of noise for an experiment with an initial substrate concentration equal to 1670 mg/l in case A. □ Eq. (4.7) (S_2' versus t), ◊ Eq. (4.49) (S_2 versus t), Δ Eq. (4.7) (S_2' versus t'), × Eq. (4.49) (S_2 versus t').

Chapter Five

Conclusions

The effectiveness factor in biofilms and bioflocs including the effect of cell density was estimated based on a new developed model. A gradual decrease of the cell density in biofilms and bioflocs, resulting from a gradual decrease of the substrate concentration along its diffusion route in the interior of these bioparticles because of cell's metabolism and mass transfer resistance of substrate, was considered in this model. A parameter, $\alpha = \frac{Y_{X/S} S_0}{X_0}$, represents the effect of cell density on the effectiveness factor. The effectiveness factors were calculated using numerical methods for three reaction rate expressions: Monod, Andrews (substrate inhibition), and multiple-Monod (two-limiting substrates). It was found that the effectiveness factors decrease with increasing values of α, due to a decrease of cell density in these bioparticles. It was also found that the effectiveness factors can be greater than 1 in the narrow range of the Thiele modulus in the case of substrate inhibition when the parameter $\alpha < 1$. However, if $\alpha > 1$, the effectiveness factors will continuously decrease with increasing Thiele modulus without attaining a value greater than 1. Analytical solutions and approximate analytic versions of the effectiveness factor were derived for biofilms for two different kinetic models: Monod and Andrews. The results from the approximate analytic solutions are in agreement with those by the numerical method when the Thiele modulus is greater than five.

A comparison of the effect of random noise on the estimates of the PRAMUS and arithmetic mean parameters in the Andrews model was conducted. It was found that the

fitted curve from the PRAMUS parameters has smaller deviations than those from the arithmetic mean parameters. This is because PRAMUS parameters are optimized once more than the arithmetic mean parameters.

It was proved that the parameters of the integrated Andrews model can be estimated uniquely if the experimental data are free of noise, based on a criterion proposed by Beck and Arnold [1977]. A novel method has been developed for parameter identification examination, referred to as dimensionless sensitivity coefficient method, which is based on plotting the dimensionless sensitivity coefficients against dimensionless time. Three criteria for parameter identification and degree of identification have been proposed. The curves produced by this method are clearer than those used previously for assessing parameter identification. This method was also used to evaluate the effect of the presence of noise on parameter identification. Using a new derived equation, the allowable levels of noise, in whose range the parameters of the integrated Andrews model could be identified, were calculated for several examples. It was found that the allowable levels of noise decreases for the parameters K_S and μ_m, and increases for the parameters K_I and μ_m, with decreasing initial substrate concentration. At either very low or very high initial concentrations, either K_S and μ_m, or K_I and μ_m, are not practically identifiable even though they are theoretically identifiable. It was also shown that the non-identification of the Andrews parameters stems indirectly from the linearization of the curve of specific growth rate versus substrate concentration, and directly from the collapse of the integrated Andrews equation to two simpler equations, in which the parameters K_S and μ_m, or K_I and μ_m, are not identifiable.

BIBLIOGRAPHY

Andrews, J.F. A mathematical model for the continuous culture of microorganisms utilizing inhibitory substrates. Biotechnol. Bioeng. 10: 707-723, 1968.

Atkinson, A. Biochemical Reactor. London: Pion Limited. p 68-88, 1974.

Atkinson, A., and Manchester, I.S.D. Microbial flocs and flocculation in fermentation process engineering. Advances in Biochemical Engineering Edited by Ghose, T.K., Fiechter, A., and Blakebrough, N. Vol. 4, p42. 1976.

Atkinson, A., and Rahman, F. Diffusion limitations and floc size distributions. Biotech. Bioeng. Vol. XXI, 221-251, 1979.

Bailey, J.E, Ollis, D.F. Biochemical Engineering Fundamentals. 2ed. McGraw-Hill, Inc. p386, 1986.

Beck, J.V., and Arnold, K.J. Parameter Estimation in Engineering and Science. John Wiley & Sons, Inc. p17-23, 1977.

Berthouex, P.M., Brown L.C. Statistics for environmental engineers. Lewis, Boca Raton, Fla. 1994.

Cano, G.V., and Cabanes, A.L. A generalized analysis of internal diffusion of immobilized enzyme in multi-enzyme reactions. Chemical Engineering J. 56: B61-B67, 1994.

Chang, H.N. Numerical calculation of effectiveness factors for the Michaelis-Menten type kinetics with high Thiele Moduli. AIChJ 26(6): 1030-1032, 1982.

Chou, Hsin-Hsien, and Huang, Ju-Sheng. Role of mass transfer resistance in overall substrate removal rate in upflow anaerobic sludge bed reactors. Journal of Environmental Engineering 548-556, April 2005.

Costerton, J.W., Lewandowski, Z., Caldwell, D.E., Korber, D.R., and LappinScott, H.M. Microbial biofilms. Annu. Rev. Microbial. 49: 711-745, 1995.

Ellis, T.G., Barbeau, D.S., Smets, B.F., and Grady, C.P.L. Jr. Respirometric technique for determination of extant kinetic parameters describing biodegradation. Water Environ Res 68:917–926, 1996

Fink, D.J., Na, T., and Schultz, J.S. Effectiveness factor calculations for immobilized enzyme catalysts. Biotechnol. Bioeng. XV: 879-888, 1973.

Gheewala, S.H., and Annachhatre, A.P. Efficacy of biofilm under toxic conditions. J. Envir. Engr. June: 576-579, 2003.

Grady, C.P.L. Jr., Daigger, G.T., and Lim, H.C. Biological Wastewater Treatment. 2ed, New York: Marcel Dekker, Inc. p84, 1999.

Haggard, Paul W. Basic Linear Algebra. Allyn and Bacon, Inc. Boston. p106, 1972.

Hill, C.G, Jr. An Introduction to Chemical Engineering Kinetics & Reactor Design. John Wiley & Sons Inc. p440, 1977.

Holmberg, A. On the practical identification of microbial growth models incorporating Michaelis-Menten type non-linearities. Math. Biosci. 62: 23-43, 1982.

Lettinga, G., Van Velsen A.F.M., Hobma, S.W., de Zeeuw, W.J., and Klapwijk, A. Use of the upflow sludge blanket (USB) reactor concept for biological wastewater treatment. Biotech. Bioeng. 22: 699-734, 1980.

Liu, Yu, Xu, Hai-Lou, Yang, Shu-Fang, and Yay, Joo-Hwa. Mechanisms and models for anaerobic granulation in upflow anaerobic sludge blanket reactor. Water Research 37: 661-673, 2003.

Magbanua B.S., Lu Y.T., Grady C.P.L. A technique for obtaining representative biokinetic parameter values from replicate sets of parameter estimates. Water Research 32 (3): 849-855, 1998.

Mahoney, E.M., Varangu, L.K., Cairns, W.L., Kosaric, N., and Murray, R.G.E. The effect of calcium on microbial aggregation during UASB reactor start-up. Water Sci Technol p249-260, 1987.

MATLAB 13. The MathWorks, Inc, 2002.

Metcalf & Eddy Inc. Wastewater Engineering Treatment and Reuse. 4th ed. McGraw-Hill Inc. New York, NY p1005-1016, 2003.

Moo-Young, M., and Kobayashi, T. Effectiveness factors for immobilized-enzyme reactions. Can. J. Chem. Engr. 50: 162-167, 1972.

Petersen, E.E. Chemical Reaction Analysis. N. J: Prentice-Hall, Inc. p64, 1965.

Robinson, J.A. Determining microbial kinetic parameters using nonlinear regression analysis: advantages and limitations in microbial ecology. In: Marshall, KC. (Ed) Advances in microbial ecology, Vol. 8. Plenum, New York, p61–114, 1985.

Seagren, E.A., Kim, H., and Smets, B.F. Identification and retrievability of unique parameters describing intrinsic Andrews kinetics. Applied Microbiology and Biotechnology 61 (4): 314-322, 2003.

Shuler, M.L., and Kargi, F. Bioprocess Engineering. 2ed NJ: Prentice Hall PTR. p245-280, 2002.

Smith, J.M. Chemical Engineering Kinetics. McGraw-Hill, Inc. p428-430, 1970.

Koch, Arthur L., Robinson, Joseph A., and Milliken, George A. Mathematical Modeling in Microbial Ecology. Chapman & Hall, USA. 1998. p20, 1970.

Tay, J.H., Xu, H.L., and Teo, K.C. Molecular mechanism of granulation. I:H^+ translocation-dehydration theory. J Environ Eng 403-410, 2000.

Teo, K.C., Xu, H.L., and Tay, J.H. Molecular mechanism of granulation—II: proton translocating activity. J Environ Eng 411-418, 2000.

Van Loosdrecht, M.C.M., Lyklema, J., Norde, W., Schraa, G., and Zehnder, A.J.B. Electrophoretic mobility and hydrophobicity as a measure to predict the initial steps of bacterial adhesion. Appl Environ Microbiol 1898-1901, 1987.